REVIEW

of the

TRICAL COMMUNICATION LABORATORY

PPON TELEGRAPH AND TELEPHONE PUBLIC CORPORATION

Former Reports of the Electrical Communication Laboratory
Nippon Telegraph and Telephone Public Corporation
from Vol.1, No.1, Sept. 1953 to Vol. 7, No. 12, Dec. 1959

Published Bimonthly by
HE ELECTRICAL COMMUNICATION LABORATORY
NIPPON TELEGRAPH AND TELEPHONE PUBLIC CORPORATION
1551, Kitizyôzi, Musasino-si, Tôkyô, Japan

VOLUME 8
NUMBERS 9-10

September-October
1960

Review of the Electrical Communication Laboratory

EDITORIAL COMMITTEE

Susumu OKAMURA *Chairman*

Tadasu FUKAMI
Giichi ITO
Hideo KAWASAKI
Yukio NAKAMURA
Tatsuya SHIMBORI
Takuzo SHINDO
Toyotaro SHIRAMATSU
Takakichi UZAWA
Ginsaku YASAKI

Koji MAEDA
Nobukazu NIIZEKI
Osamu TUKIZI

EDITORIAL STAFF

Susumu HIRANO *Editor*
Tutomu SAITO *Assistant Editor*
Masao HIROSE 〃

The Review of the Electrical Communication Laboratory is published six times a year (bimonthly) by the Electrical Communication Laboratory, Nippon Telegraph Telephone Public Corporation, 1551, Kitizyôzi, Musasino-si, Tôkyô, Japan. Telephone: Tôkyô (391) 2261 and 2271.

All rights of republication, including translation into foreign languages, are reserved by the Electrical Communication Laboratory, NTT.

Subscriptions are accepted at ¥1,200 per year. Single copy ¥300 each. Foreign postage is ¥300 per year or ¥50 per copy. Remittance should be made in check payable to the Electrical Communication Laboratory and mail to the Director.

Printed by Aoyama Printing Co., Tokyo, Japan

R E V I E W
of the
ELECTRICAL COMMUNICATION LABORATORY

NIPPON TELEGRAPH AND TELEPHONE PUBLIC CORPORATION

Volume 8, Numbers 9-10 September-October 1960

U.D.C. 534.1:621

The Analysis of Frame Vibrating Systems*

Motonobu YONEKAWA†

Free and forced vibration problems of a portal frame composed of uniform beams are analyzed by making use of both the stiffness matrix of beams and electrical network analogies. The natural frequencies and normal functions of the frame are calculated, and frequency responses of displacement at the tip of the frame under external concentrated force are obtained by the method of normal function expansion.

Introduction

As a model of a vibrating system which serves the purpose of research on the transfer characteristics of mechanical vibration transmitted from one point to another, a frame structure was devised where two cantilevers are arranged in parallel and their free ends are rigidly connected with a connecting beam.

The analysis of the vibration of structures composed of uniform beams has been carried out by many authors: Veletsos and Newmark (1) described a method of calculating the natural frequencies of the undamped vibration of continuous beams and of rigid-jointed frames, and defined the "dynamic flexural stiffness" of the uniform beam; R.E.D. Bishop(2) analyzed the natural frequencies of structures, such as portal frames, by using the "receptance" of the beam; and A: Okumura(3) established a general method to analyze vibration and stability problems of linear mechanical structures by using the "stiffness matrix" and the "transfer matrix."

In these papers, a single beam is regarded as the unit-system of the structures, and the whole system is represented by connecting the unit-systems, concerning each of which the relations among displacements, rotations, bending moments and shearing forces at both ends are known.

These methods are analogous to those adopted in electrical network theory, and therefore network analogy is effective. The papers mentioned above are lacking in such analogous consideration.

On the other hand, by regarding a beam as a multiterminal transmission line, G. Kron (4) has derived the equivalent circuits of a beam by assuming forces to represent currents and displacements to voltages. His method of consideration, however, is quite different from that of the other authors'. The purpose of this paper is to analyze the vibration problems of frames, such as natural frequencies and normal functions, by using the stiffness matrix of beams and the methods of network analysis. The stiffness matrix of a beam is derived in Section ②, network analogy is given in

---

* MS in Japanese received by the Electrical Communication Laboratory, July 22, 1960. Originally published in the *Kenkyû Zituyôka Hôkoku* (*Electrical Communication Laboratory Technical Journal*), N.T.T., Vol. 9, No. 6, pp. 653-680, 1960.

† Station Apparatus Research Section.

Section ③, and free and forced vibration problems are described in Section ④ and ⑤.

The forced vibration problems, such as the frequency characteristics of displacement at any point of the frame when the system is driven by an external force, are analyzed using the normal functions of the system.

Definition of Symbols

A, B, C: Beams which compose the frame.
D: Generalized displacement.
E: Young's modulus.
F_1–F_6: Elements of dimensionless stiffness matrix.
$[F]$: Stiffness matrix.
$[\overline{F}]$: Dimensionless stiffness matrix.
I: Second moment of sectional area around neutral axis.
l: Length of beam.
M: Bending moment.
$n=\alpha_B/\alpha_A=\sqrt[4]{\rho_B E_A I_A/\rho_A E_B I_B}(l_B/l_A)$.
P: External force.
Q: Generalized force.
S: Shearing force.
T: Axial force.
$X=x/1$: Dimensionless coordinate along the beam.
x: x-coordinate.
$\alpha=\sqrt[4]{\rho\omega^2/EI}\cdot l$.
$\alpha_m=\sqrt[4]{\rho\omega_m/EI}\cdot l$: m-th eigenvalue of the system.
$\beta=(E_B I_B/l_B)/(E_A I_A/l_A)$: Ratio of the bending rigidity of beam B to beam A.
η: Transverse displacement of beam.
$\bar{\eta}=\eta/l$: Dimensionless form of η.
$\eta', \eta'', \eta'''=d\eta/dX,\ d^2\eta/dX^2,\ d^3\eta/dX^3$, respectively.
θ: Angular rotation $(\fallingdotseq d\eta/dx)$.
μ: Mass ratio of beam B to beam A.
ξ: Displacement in the axial direction of beam.
Ξ_m: m-th normal function of the system.
ρ: Mass of beam per unit length.
ω: Angular frequency of oscillation.
ω_m: m-th natural angular frequency.
$\overline{M}, \overline{S}$: Dimensionless forms of M and S respectively.
$\overline{Q}, \overline{D}$: Dimensionless forms of Q and D respectively.
$E_A, I_A, \rho_A, \alpha_A$: Values for beam A.
$E_B, I_B, \rho_B, \alpha_B$: Values for beam B.

1. The Stiffness Matrix of Beams

A complicated framework becomes a set of isolated beams when the junction points of the system are disconnected. The individual beam, therefore, is considered as the unit system of the complete framework.

When the vibration characteristics of a beam are known, those of the whole system composed of the beams can be found by the theory of connections.

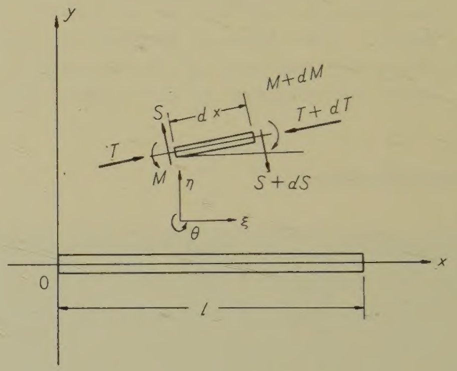

Fig. 1—Relations between section-forces, displacements and co-ordniates for the uniform beam.

In this section, the relations between forces and displacements at both ends of a uniform beam subject to transverse vibration are derived. Referring to the coordinates illustrated in Fig. 1, the stationary free vibration of a uniform beam is represented by the following fourth order differential equation:

$$d^4\eta/dX^4-\alpha^4\eta=0. \tag{1}$$

The general solution of Eq. (1) is

$$\eta=a\sin\alpha X+b\cos\alpha X+c\sinh\alpha X+d\cosh\alpha X \tag{2}$$

where a, b, c and d are arbitrary constant.

The time factor is assumed to have the form $e^{j\omega t}$, but has been omitted for simplicity.

The arbitrary constants in Eq. (2), which are determined by the boundary conditions of the beam, have no direct physical meaning. As a result, they should be replaced by quantities with physical meaning (physical quantities). The physical quantities adopted are displacement, rotation, bending moment, and shearing force, and the positive directions of these quantities are chosen as indicated in Fig. 1. Then the following relation exists:

$$\begin{pmatrix} \eta \\ \theta \\ M \\ S \end{pmatrix} = \begin{pmatrix} \eta \\ (1/l)d\eta/dX \\ -(EI/l^2)d^2\eta/dX^2 \\ (EI/l^2)d^3\eta/dX^3 \end{pmatrix} = \begin{pmatrix} l\bar{\eta} \\ \bar{\eta}' \\ -(EI/l)\bar{\eta}'' \\ (EI/l^2)\bar{\eta}''' \end{pmatrix} \tag{3}$$

where $\bar{\eta}$, $\bar{\eta}'$, $-\bar{\eta}''$, and $\bar{\eta}'''$ are considered as dimensionless forms of η, θ, M, and S respectively. Therefore, the following expression may be obtained:

$$\begin{pmatrix} \bar{\eta} \\ \bar{\theta} \\ \bar{M} \\ \bar{S} \end{pmatrix} = \begin{pmatrix} \bar{\eta} \\ \bar{\eta}' \\ -\bar{\eta}'' \\ \bar{\eta}''' \end{pmatrix} \tag{4}$$

The suffixes 1 and 2 are used for the quantities at $X=0$ and 1 respectively. From Eq. (2), the following relation is obtained as a relation connecting both ends of a beam.

$$\begin{pmatrix} \bar{\eta}_2 \\ \bar{\theta}_2 \\ \bar{S}_2 \\ \bar{M}_2 \end{pmatrix} = \left(\begin{array}{cc|cc} c^+ & s^+/\alpha & s^-/\alpha^3 & -c^-/\alpha^2 \\ \alpha s^- & c^+ & c^-/\alpha^2 & -s^+/\alpha \\ \hline \alpha^3 s^+ & \alpha^2 c^- & c^+ & -\alpha s^- \\ -\alpha^2 c^- & -\alpha s^- & -s^+/\alpha & c^+ \end{array}\right) \begin{pmatrix} \bar{\eta}_1 \\ \bar{\theta}_1 \\ \bar{S}_1 \\ \bar{M}_1 \end{pmatrix} \tag{5}$$

where

$$c^+ = (1/2)(\cosh\alpha + \cos\alpha),$$

$$c^- = (1/2)(\cosh\alpha - \cos\alpha),$$

$$S^+ = (1/2)(\sinh\alpha + \sin\alpha),$$

$$S^- = (1/2)(\sinh\alpha - \sin\alpha).$$

Eq. (5) shows that the quantities at $X=1$ can be given by those at $X=0$. If the beam is considered as a vibration-transmission element, the coefficient matrix of Eq. (5) corresponds to the transfer parameter. Inversely, when it is desired to show quantities at $X=0$ by those at $X=1$, these quantities are obtained by calculating the inverse relation of Eq. (5).

Now, generalized force and generalized displacement of dimensionless form are defined as

$$Q_i = \begin{pmatrix} \bar{S}_i \\ \bar{M}_i \end{pmatrix} \quad D_i = \begin{pmatrix} \bar{\eta}_i \\ \bar{\theta}_i \end{pmatrix} \quad (i=1, 2).$$

Eq. (5) is simplified to

$$\begin{pmatrix} \bar{D}_2 \\ \bar{Q}_2 \end{pmatrix} = \left(\begin{array}{c|c} A & B \\ \hline C & D \end{array}\right) \begin{pmatrix} \bar{D}_1 \\ \bar{Q}_1 \end{pmatrix} \tag{5a}$$

where A, B, C, and D are the submatrices of the coefficients of Eq. (5). From this, the relation between generalized force and generalized displacement is obtained as

$$\begin{pmatrix} \bar{Q}_1 \\ \bar{Q}_2 \end{pmatrix} = \left(\begin{array}{c|c} -B^{-1}A & B^{-1} \\ \hline C-DB^{-1}A & DB^{-1} \end{array}\right) \begin{pmatrix} \bar{D}_1 \\ \bar{D}_2 \end{pmatrix}$$

or

$$\begin{pmatrix} \bar{S}_1 \\ \bar{M}_1 \\ \bar{S}_2 \\ \bar{M}_2 \end{pmatrix} = \left(\begin{array}{cc|cc} F_5 & F_3 & -F_6 & F_4 \\ F_3 & F_1 & -F_4 & F_2 \\ \hline F_6 & F_4 & -F_5 & F_3 \\ -F_4 & -F_2 & F_3 & -F_1 \end{array}\right) \begin{pmatrix} \bar{\eta}_1 \\ \bar{\theta}_1 \\ \bar{\eta}_2 \\ \bar{\theta}_2 \end{pmatrix} \tag{6}$$

where

$$F_1 = \frac{\alpha(\sin\alpha\cosh\alpha - \cos\alpha\sinh\alpha)}{1-\cos\alpha\cosh\alpha}$$

$$F_2 = \frac{\alpha(\sinh\alpha - \sin\alpha)}{1-\cos\alpha\cosh\alpha}$$

$$F_3 = \frac{\alpha^2\sin\alpha\sinh\alpha}{1-\cos\alpha\cosh\alpha}$$

$$F_4 = \frac{\alpha^2(\cosh\alpha - \cos\alpha)}{1-\cos\alpha\cosh\alpha}$$

$$F_5=\frac{\alpha^3(\sin\alpha\cosh\alpha+\cos\alpha\sinh\alpha)}{1-\cos\alpha\cosh\alpha}$$

$$F_6=\frac{\alpha_3(\sinh\alpha+\sin\alpha)}{1-\cos\alpha\cosh\alpha}.$$

Eq. (6) can be simplified to

$$[\bar{Q}]=[\bar{F}][\bar{D}]. \tag{6a}$$

Here, the coefficient matrix $[\bar{F}]$ on the right side of Eq. (6a) is called the dimensionless stiffness matrix of a beam.

Eq. (6) is shown in dimensionless form. If the connection of beams is considered, quantities with dimensions must be used. The stiffness matrix $[F]$ is related to the dimensionless stiffness matrix $[\bar{F}]$ as[(3)]

$$[F]=\frac{EI}{l^2}\left(\begin{array}{cc:cc} 1/l & 1 & 1/l & 1 \\ 1 & l & 1 & l \\ \hdashline 1/l & 1 & 1/l & 1 \\ 1 & l & 1 & l \end{array}\right)\dot{\times}[\bar{F}] \tag{7}$$

where × is the notation used for the overlap-multiplication of matrices of the same form; for example

$$A\dot{\times}B=\begin{pmatrix} a_{11} & a_{12} \\ a_{21} & a_{22}\end{pmatrix}\dot{\times}\begin{pmatrix} b_{11} & b_{12} \\ b_{21} & b_{22}\end{pmatrix}$$

$$=\begin{pmatrix} a_{11} & b_{12} & a_{12} & b_{12} \\ a_{21} & b_{21} & a_{22} & b_{22}\end{pmatrix}.$$

The matrix $[F]$ is called the stiffness matrix of a beam. The relation between generalized force $[Q]$ and generalized displacement $[D]$ is represented as

$$[Q]=[F][D]. \tag{8}$$

$[F]$ corresponds to the admittance matrix or the impedance matrix in electrical network theory. This correspondence will be described in the next section.

Next the case when a concentrated mass is attached to an arbitrary point of a beam will be considered.

When an external force $Pe^{j\omega t}$ is applied to the concentrated mass m, the followiug relation is obtained:

$$P=m\frac{d^2\xi}{dt^2}=-m\omega^2\xi \tag{9}$$

where ξ is the displacement of the mass. Now ω^2 can be described by the constants of the lateral vibrating beam as

$$\omega^2=\frac{EI\alpha^4}{m_r}\cdot l^3$$

where m_r: mass of the beam.

Therefore, Eq. (9) is rewritten as

$$P=-\frac{m}{m_r}\frac{EI\alpha^4}{l^3}\xi=-\frac{EI}{l^3}\mu\alpha^4\xi,\quad \mu=\frac{m}{m_r}.$$

The stiffness F_m of the concentrated mass is shown by

$$F_m=\frac{P}{\xi}=-\frac{EI}{l^3}\mu\alpha^4 \tag{10}$$

or, in dimensionless form, by

$$\bar{F}_m=\frac{l^3}{EI}F_m=-\mu\alpha^4. \tag{10a}$$

3. A Study of Lateral Vibrating Beams Using Network Analogies

By the relations derived in the previous section, the characteristics of a uniform beam subject to lateral vibration has become obvious; the transfer function connecting the end quantities is shown by Eq. (5), and the stiffness function by Eq. (8). These representations in matrix form show that beam systems may be treated in a manner analogous to that used in electric network theory.

As correspondence between mechanical and electrical quantities, forces are assumed to represent currents, and displacements voltages, according to Kron's beam analogies.[(4)]

Of course, the opposite correspondence is possible, but the former is more convenient, because fixed ends (zero displacement) correspond to earth points (zero voltage) of the network and free ends (zero force) to open points (zero currents), and as a resnlt, corresponding points can be described by the same symbols for both systems in the illustration.

As for lateral vibrating beams, there appear two pairs of quantity at an end, i.e. shearing force (S) and displacement (η), bending moment (M) and angular rotation (θ), so that if a beam is regarded as a multiterminal transmission line, two pairs of terminal are required for each end of the transmission line.

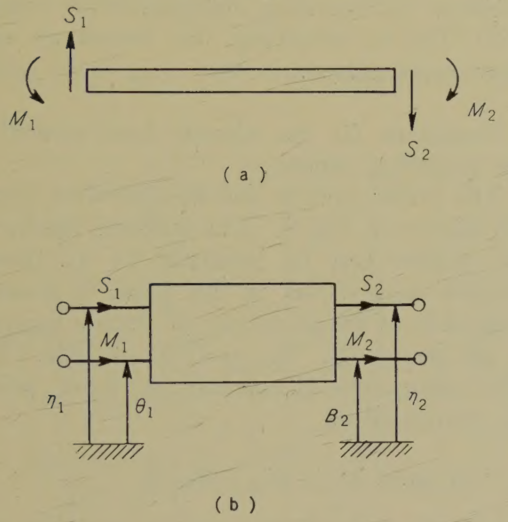

Fig. 2—Uniform beam (a) and its equivalent circuit (b).

The electrical network corresponding to the beam shown in Fig. 2 (a) can de shown by Fig. 2 (b), where the beam is represented by a box and only the terminals at both ends are shown. The interior of the box, which will not be considered at this time, represents a circuit with an admittance matrix equal to $[F]$ in Eq. (8). S_i and M_i $(i=1,2)$ correspond to the currents flowing into or out of the circuit, and η_i and θ_i correspond to the voltages at doth ends, respectively,

Next, the equivalent circuit of a cantilever shown in Fig. 3 (a) is considered, where end (1) is fixed and end (2) is free. The electrical network is shown in Fig. 3 (b), where terminal (1) is earthed, and terminal (2) is open.

From Eqs. (6) and (7), the relations between currents and voltages at terminal (2) are obtained as

$$\begin{pmatrix} S_{A2} \\ M_{A2} \end{pmatrix} = \frac{EI}{l^2}\begin{pmatrix} 1/l & 1 \\ 1 & l \end{pmatrix} \overset{\cdot}{\times} \begin{pmatrix} -F_5 & F_3 \\ F_3 & -F_1 \end{pmatrix}\begin{pmatrix} \eta_{A2} \\ \theta_{A2} \end{pmatrix}. \tag{11}$$

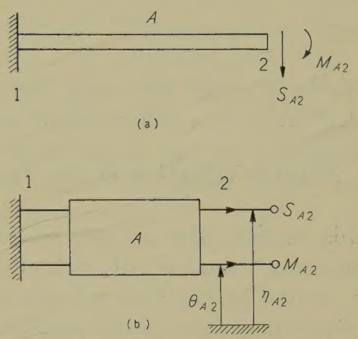

Fig. 3—Cantilever (a) and its equivalent circuit (b).

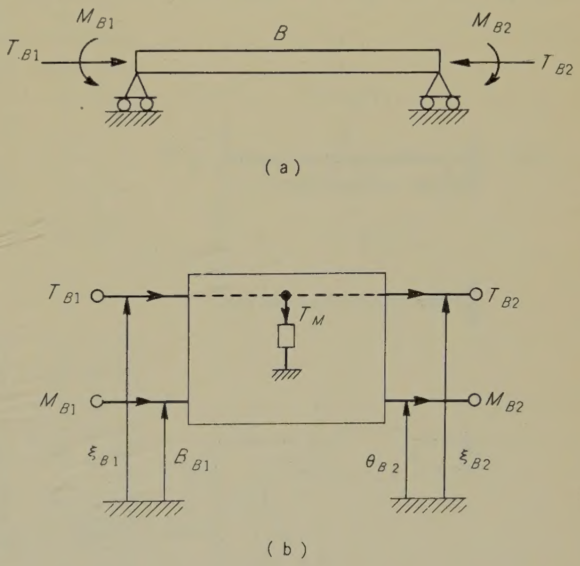

Fig. 4—Roller-roller beam (a) and its equivalent circuit (b).

The equivalent circuit of a vibrating system shown in Fig. 4 (a) is shown by Fig. 4 (b), where the S-terminal may be omitted because lateral displacements at both ends are zero, and only the M- and the T-terminals are shown. If the extension or contraction in the axial direction of the beam is neglected, the circuit between the T-terminals becomes as shown by Fig. 4 (b), where the admittance attached to the circuit is due to the mass inertial of the beam.

Relations between currents and voltages are

$$T_M = T_{B2} - T_{B1} = -m\omega^2\xi, \quad \xi_{B1} = \xi_{B2} = \xi,$$

$$\begin{pmatrix} M_{B1} \\ M_{B2} \end{pmatrix} = \frac{EI}{l} \begin{pmatrix} F_1 & F_2 \\ -F_2 & -F_1 \end{pmatrix} \begin{pmatrix} \theta_{B1} \\ \theta_{B2} \end{pmatrix}. \tag{12}$$

4. Natural Vibration of the Frame

In this section, the natural frequencies and corresponding modes of vibration of the system shown in Fig. 5 (a) are calculated using the equivalent circuits in the preceding section.

In the analysis, henceforce, it is assumed that the extensions or contractions of beams in the axial direction are neglected and that only plane vibration is taken into account.

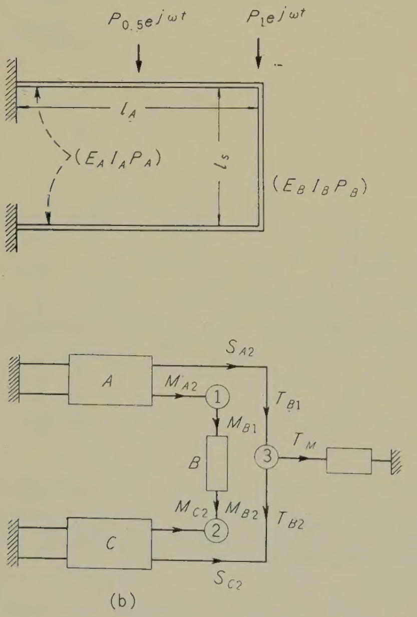

Fig. 5—Model of a vibrating system (a) and its equivalent circuit (b).

4.1. Natural Frequencies of the Frame

The eigenvalues of the natural vibration of frames can be found by the following procedures:

(i) The stiffness matrices of the unit-system of which the whole system is composed are found, and they are shown by the equivalent circuits.

(ii) The equivalent circuit of the composite system is constructed, and ifs stiffness matrix $[F]$ is obtained. The formula det $[F]=0$ becomes the frequency equation of the system.

(iii) The α_m satisfying the frequency equation is calculated.

Procedure (i) has already been treated in the preceding section.

The entire system and its equivalent circuit are shown in Fig. 5. The stiffness matrix of the system can be obtained by G. Kron's general method, but in this paper it is easily derived from the continuity of electric currents at the points ①, ②, and ③ in Fig. 5 (b). The continuities of currents at those points are expressed as

$$\left.\begin{array}{ll} \text{at point ①} & -M_{A2}+M_{B1}=0 \\ \text{at point ②} & -M_{B2}-M_{C2}=0 \\ \text{at point ③} & -S_{A2}-S_{C2}+T_M=0. \end{array}\right\} \tag{13}$$

By substituting Eqs. (11) and (12) into Eq. (13), and letting $\eta_{A2}=\xi$, $\theta_{A2}=\theta^B{}_1$, the homogeneous equations of generalized displacements ξ, $\theta^B{}_1$, and $\theta^B{}_2$ at connecting points are obtained. The stiffness matrix is the coefficient matrix of Eq. (13), and it is denoted by $[F]$.

The frequency equation is given by det $[F]=0$, which can be divided into two independent equations as

$$F_1(A)+\beta\{F_1(B)-F_2(B)\}=0 \tag{14}$$

$$\begin{vmatrix} F_3(A)-\mu\alpha^4 A & -F_3(A) \\ -F_3(A) & F_1(A)+\beta\{F_1(B)+F_2(B)\} \end{vmatrix}=0 \tag{15}$$

where $F_i(A)$ and $F_i(B)$ are elements of the beam stiffness matrix and A and B indicate that α in F_i should be replaced by α or $\alpha_B = n\alpha_A$.

In general, α_A satisfying Eq. (14) or (15) take an infinite number of discrete values, which are shown as $\alpha_1, \alpha_2 \cdots\cdots\cdots \alpha_m \cdots\cdots\cdots$ in ascending order of value.

The natural angular frequency ω_m corresponding to m-th eigenvalue α_m is calculated from

$$\omega_m = \frac{\alpha^2_m}{l_{A2}} \sqrt{\frac{E_A I_A}{\rho_A}}. \tag{16}$$

Eqs. (14) and (15) are respectively the frequency equations referring to symmetric and antisymmetric modes of vibration about the symmetric axis of the frame.

The values of α_m calculated with an electronic digital computer, illustrated in Fig. 6, are shown as functions of β (the flexural rigidity ratio of beam B to A) with parameter μ when $n=0.2$. The Figs. (a)-(d) are the eigenvalues for antisymmetric modes, and Figs. 6 (e)-(h) are the eigenvalues for symmetric modes. It is noteworthy that these are the values when the beam B is extremely close to the static region ($n=0.2$) and that therefore, these values can be considered as applying to beam A when it is statically constrained at one end.

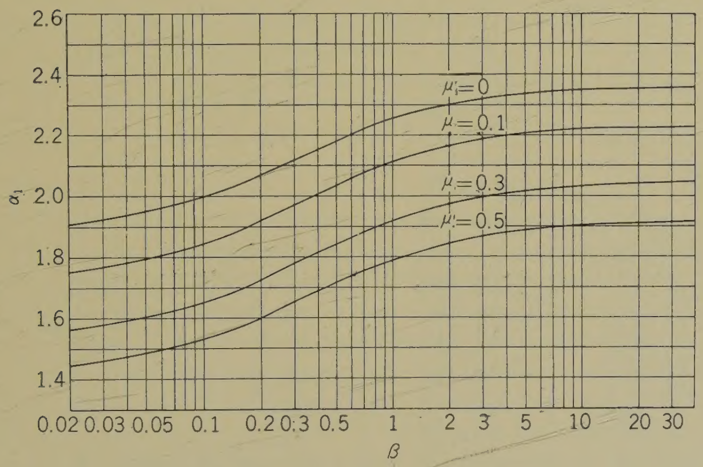

Fig. 6 (a)—1st eigenvalues for antisymmetric mode.

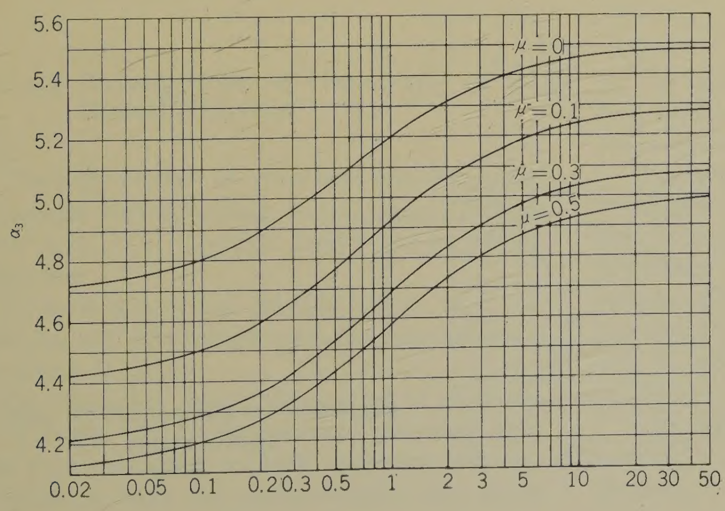

Fig. 6 (b)—2nd eigenvalues for antisymmetric mode.

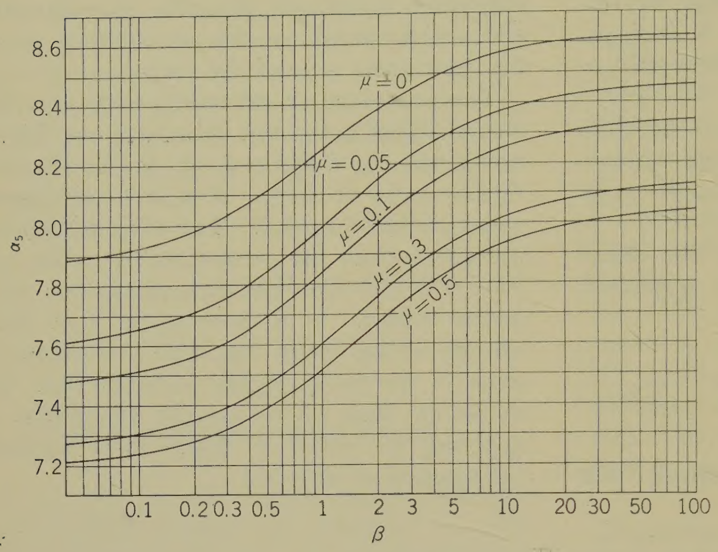

Fig. 6 (**c**)—3rd eigenvalues for anti-symmetric mode.

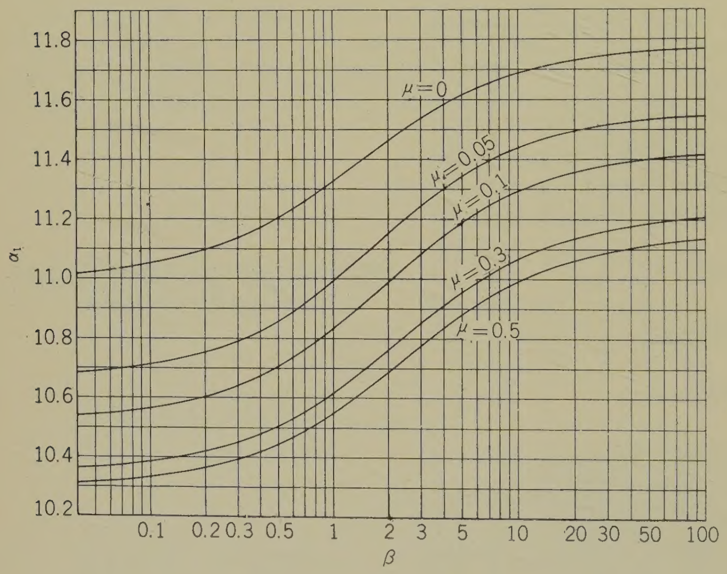

Fig. 6 (**d**)—4th eigenvalues for anti-symmetric mode.

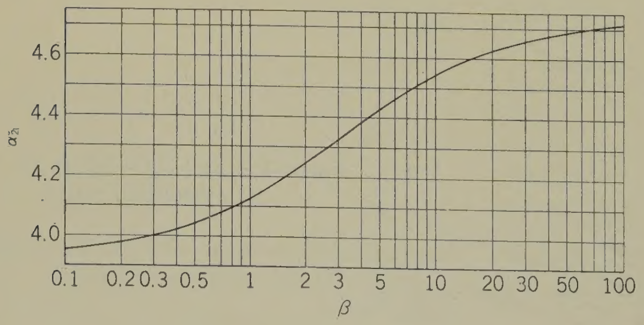

Fig. 6 (**e**)—1st eigenvalues for symmetric mode.

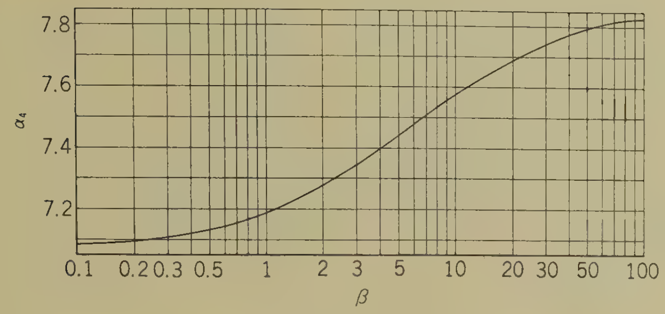

Fig. 6 (**f**)—2nd eigenvalues for symmetric mode.

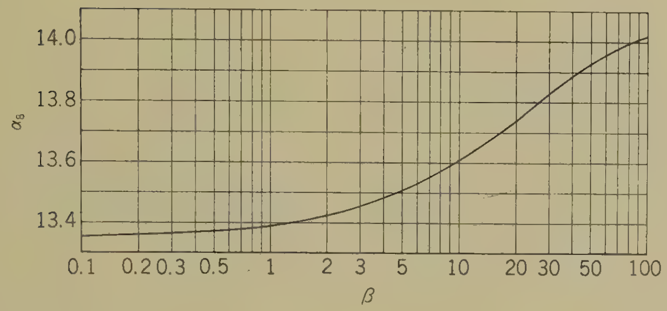

Fig. 6 (**g**)—3rd eigenvalues for symmetric mode.

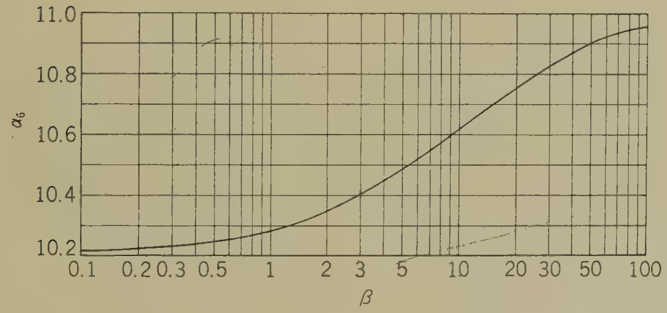

Fig. 6 (**h**)—4th eigenvalues for symmetric mode.

4.2 Natural Modes of Vibration; Normal Functions

Natural modes of vibration are the eigenfunctions corresponding to the eigenvalues α_m $(m=1, 2, \cdots\cdots)$ which satisfy the frequency equation.

If α_m is given, the relative values of ξ, θ_{B1} and θ_{B2} are determined from the homogeneous equation (13).

On the other hand, the modes of vibration of a beam can be determined, provided that the four quantities as both ends are known. Therefore, from the displacements and slopes at the connecting points obtained through the homogeneous equation, the relative displacement at any point of beam can be calculated.

The modes of vibration can be divided into symmetric and antisymmetric modes about the symmetry axis of the frame, just as the frequency equation can be divided into two independent equations. The equivalent vibrating systems for both modes are shown in Fig. 7, which are the upper half of the whole structure.

The calculations of modes of vibration were carried out for these equivalent vibrating systems.

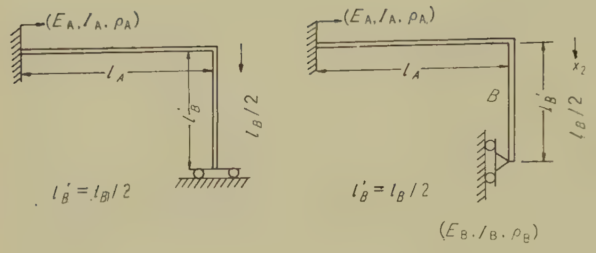

Fig. 7—The equivalent vibrating systems for symmetric mode (a), and for antisymmetric mode (b).

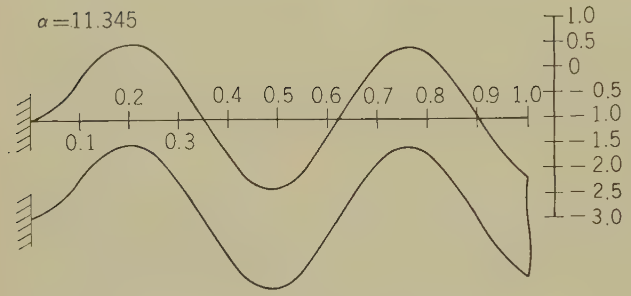

Fig. 8 (a)—The normal functions of antisymmetric mode; ($l_B/l_A=0.5$, $E_BI_B/E_AI_A=0.5$, $\rho_B/\rho_A=0.5$).

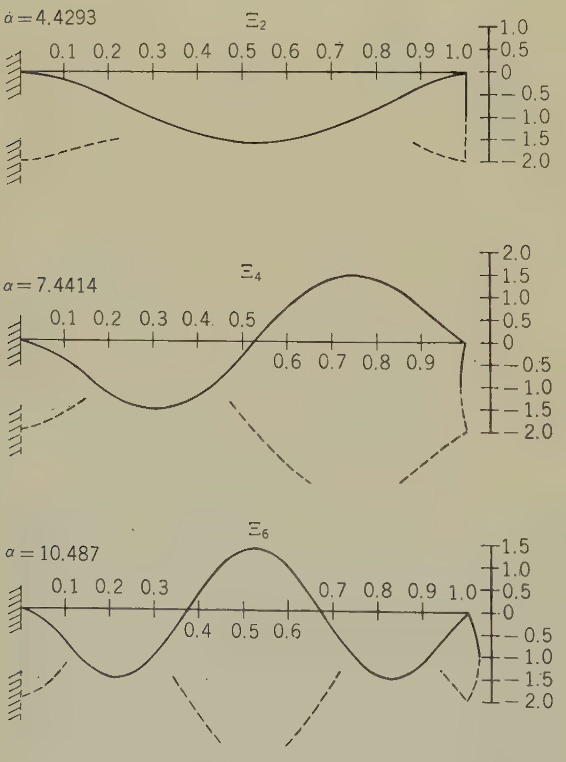

Fig. 8 (b)—The normal functions of symmetric mode; ($l_B/l_A=0.2$, $E_BI_B/E_AI_A=0.5$, $\rho_B/\rho_A=0.5$).

Here, the m-th natural mode of vibration of the system is denoted by η_m. The amplitudes of η_m can be chosen at will, but it is most favorable, especially for the analysis of forced vibration, to normalize them. The density integration of η_m^2 over the whole framework is normalized to M, the mass of the system.

These functions are called the m-th normal functions of the system and written as Ξ_m.

Fig. 8 shows one example of Ξ_m of the system with the following dimensions:

$$\frac{l_B}{l_A}=0.2, \quad \frac{E_B I_B}{E_A I_A}=0.5, \quad \mu=0.05.$$

These results were calculated with an electronic digital computer.

5. The Analysis of Forced Vibration

The analysis of forced vibration is possible by a method analogous to that of solving network problems through equivalent circuits previously derived. In this case, the Ho-Thevenin theorem is also available.

This method is suitable for direct analysis of the problems of forced vibration, when the characteristics of free vibration are unknown. When they are already known, i.e., when the eigenvalues and the normal functions of the system are already given, forced vibration can be calculated more easily by making use of them.

This section treats the methods to analyze vibration of the frame by the characteristics of free vibration calculated in the preceding section, and also the results of analysis. The driving force is assumed to have the form $Pe^{j\omega t}$. In general, the response of the vibrating system driven by this external force is represented as the sum of a transient term and a steady term.

But, here, only the steady term is considered.

The steady component of displacement ξ_y of the system driven by the concentrated force $P_x e^{j\omega t}$ is given by

$$\xi_y=\frac{P_x}{M}\sum_{m=1}^{\infty}\frac{\Xi_m(X)}{\omega_m{}^2-\omega^2}\cdot\Xi_m(Y)e^{j\omega t} \tag{17}$$

where X and Y represent respectively the driving point and the point under consideration, M the total mass and Ξ_m the normal function of the system.

Forced vibration of the frame structure can also be analyzed through Eq. (17) by using Ξ_m of the structure. It should be noticed that there exist two types of vibration modes, symmetric and antisymmetric. If the displacement at the tip of the frame is desired, it is sufficient to consider the antisymmetric mode only, because the symmetric mode at this point vanishes. But in other cases, both modes must be considered.

As a simple example, a calculation will be applied to the driving point displacement at the tip of the frame on which the concentrated force $Pe^{j\omega t}$ is imposed as indicated in Fig. 9.

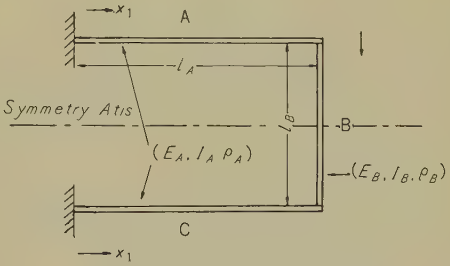

Fig. 9—The forced vibration of the frame when an external force $(P_1 e^{j\omega t})$ is imposed on the tip of the frame, or $(P_{0.5}e^{j\omega t})$ on the middle point of the frame.

By substituting $X=Y=1$ into Eq. (17), the following equation is obtained.

$$\xi_1=\frac{P_1}{M}\sum_{m=1}^{\infty}\frac{\Xi_m{}^2(1)}{\omega_m{}^2-\omega^2}e^{j\omega t}. \tag{18}$$

For the vibrating system, the values calculated in the previous section are used. In this case, it is sufficient to consider only the antisymmetric components of the normal functions. These constants are given in Table 1, where α_m shows the eigenvalue, $\Xi_m(1)$ the normal function at the tip of the frame and $\Xi_m(0.5)$ normal the function at the middle point.

Table 1

THE CONSTANTS OF THE VIBRATING SYSTEMS, CORRESPONDING TO THE ANTISYMMETRIC MODE OF VIBRATION

m	α_m	$\Xi_m(1)$	$\Xi_m(0.5)$
1	2.2662	1.5680	0.8127
3	5.2831	−1.3301	1.4392
5	8.3088	1.2779	−0.3062
7	11.3426	−1.2099	−1.4005

In Fig. 10, relative displacements at the tip are plotted by plotting ω/ω_1 on the axis of abscissas, where ω_1 is the first natural angular frequency. The displacement when $\omega=1$ is $\xi_1=4.568\times10^{-2}\cdot P_1l_A^3/E_AI_A$.

Fig. 11 shows the displacement at the tip when the middle point is driven, calculated by Eq. (17). Displacement when $\omega=0$ is $\xi_1=2.184\times10^{-2}\cdot P_{0.5}l_A^3/E_AI_A$ in this case.

Those calculations were made taking into account the normalized functions of up to the fourth-order of the antisymmetric mode.

The modes of vibration when the system is driven by an external force can also be calculated easily using Eq. (17).

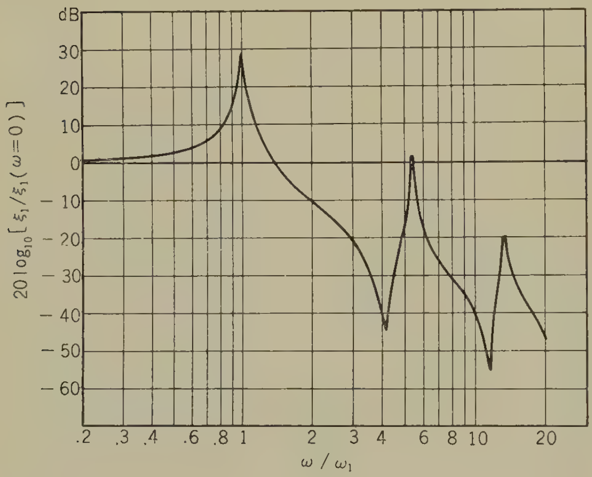

Fig. 10—Frequency characteristics of driving point displacement at the tip of the frame when an external force $P_1e^{j\omega t}$ is applied at that point; $(E_AI_A/P_1l_A^3)\xi_1(\omega=0)=4.568\times10^{-2}$, $l_B/l_A=0.2$, $E_BI_B/E_AI_A=0.5$, $\mu=0.05$.

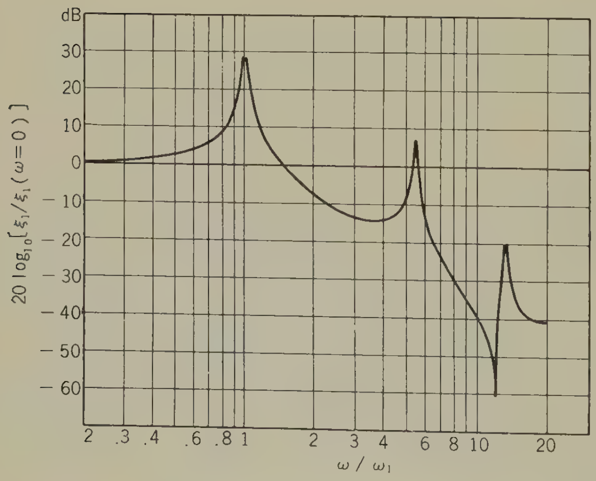

Fig. 11—Frequency characteristics of displacement at the tip of the frame when an external force $P_{0.5}e^{j\omega t}$ is imposed on middle point of the frame; $(E_AI_A/P_{0.5}l_A^3)\xi_1(\omega=0)=2.184\times10^{-2}$, $l_B/l_A=0.2$, $E_BI_B/E_AI_A=0.5$, $\mu=0.05$.

Conclusion

The methods of analysis for free and forced vibration problems of frames composed of uniform beams have been shown with numerical examples.

In sections 2 and 3, the fundamental relations necessary for dealing with such problems where given. The transfer matrix of a uniform beam subject to lateral vibration are derived, and one example of the methods of treating beams by multiterminal transmission lines is shown.

In free vibration problems, frequency equation has been derived with an aid of equivalent circuits, the eigenvalues have been obtained by calculating the equation with an electronic digital computer, and one example of the normal functions of the frame has been shown. It may be thought that the eigenvalues shown in Fig. 6 are those of cantilevers, whose free ends are constrained almost statically, for the beam *B* is in almost static range in this case.

The frequency equation is given by det $[F]=0$. Complex systems have many connecting points and the order of the matrix becomes very large, therefore the calculations become difficult. In these cases, a simpler equation is obtained by decreasing the independent points, for the purpose of which transfer matrix is used to convert the values at one point to those at another point instead of making the stiffness matrices at all connecting points.

For the complex structures, the calculation of normal function can not be easily accomplished, but this difficulty can be overcome by the use of an electronic digital computer.

In forced vibration problems, frequency characteristics of displacement at the tip of the frame were calculated by using normal functions of the frame, when concentrated sinusoidal force was imposed on that tip or on the middle point of the frame. In this case normal functions of first four antisymmetric modes were taken into account.

Of course, there is a direct method of analysis of forced vibration as is used in network analysis, but the method described in this paper seems more convenient for problems of this kind. For example, when the characteristics for the frequency range up to the first natural frequency are discussed, it will be sufficient to consider the normal functions in the first mode or in the first two modes.

It is obvious that the method of normal function expansion is applicable to the calculation of transient response, but this is not described in this paper.

References

(1) A. S. Veletsos & N. M. Newmark. "Natural Frequencies of Continuous Flexural Members" *Proc. A.S.C.A.* 81,735,1955. "Determination of the Natural Frequencies of Continuous Beams on Flexible Supports" *Proc. 2nd U.S. National Congress of Appl. Mech.* p. 147, June, 1954.

(2) R. E. D. Bishop: "The Analysis of Vibrating Systems which embody beams in flexure" *Proc. I. Mech. Eng.* 169, 51, 1955. "The Vibration of Frames" *Proc. I. Mech. Eng.* 170, 29, p. 955, 1956.

(3) A. Okumura: "On a Method of Analysis for Vibration and Stability Problems of Linear Mechanical Systems or Structures" *Memoirs of the School of the Science & Engineering, Waseda Univ.* No. 21, 1957.

(4) G. Kron: "Tensorial Analysis and Equivalent Circuits of Elastic Structures" *Jour. of Franklin Inst.* 238, 6, p. 399, Dec., 1944. "Numerical Example for Interconnecting Piecewise Solutions of Elastic Structures" *Memoirs of the Unifying Study of the Basic Problems in Engineering Science by means of Geometry*, Vol. 2, F-3, p. 51, Gakujutsu Bunken Fukyukai, Tokyo.

* * * *

U.D.C. 534.78 : 495.6] : 621.391

On Fundamental Qualities of Vowel Sounds in Speech Communication*

Yosiyuki OCHIAI† and *Teruo FUKUMURA*†

Basing upon phonemic and vocal qualities put in question for the first time as fundamental timbre qualities of vowel sounds in speech communication, we observe in detail the correspondence between timbre signals as stimuli in the communication system and timbre qualities as responses to these stimuli. Further, by means of detailed analysis of timbre confusion, we can clarify the mechanism of not only the deterioration of quality but also the formation of quality in the dimension of frequency. From an exhaustive study of incoming and outgoing confusions, it is evident that as the basis of quality theory, there is both positive importance and negative importance. Finally, there are several modes of quality distribution according to the difference of qualities: for phonemic quality, there are some narrow bands of quality concentration; for vocal quality, there are wide bands of quality dispersion.

Introduction

Significance of Quality in Speech Study

Although the interpretation of speech waves from physical and physiological viewpoints is of course necessary (1) (2) (3), yet one of the most important factors in the fundamental theory of Communication Science should be the interpretation of speech sound waves viewed from the leading conception of "transmission quality" or "speech quality", as this is connected with the fundamental problem of communication. From the technological viewpoint in speech communication, what part of the speech wave or the speech pattern is contributing to what kind of qualities and to what degree in the consideration of speech-effect transmission? This problem is rather an old one, still full of attraction as the theory of quality develops. In the course of historical development there have been changing emphases on the importance of certain qualities, for example loudness was once considered to be very important. Then "articulation" in telephone and radio-broadcasting engineering became the most important quality. But this is not the only quality to emphasize for communication, particularly for speech communication. Taking a view of future technology, we realize that there will exist other qualities as necessary or more necessary than articulation. In short, the final target of our transmission technique will not be set, until the mechanism of formation of the various qualities attributable to speech patterns is clarified.

From the above point of view, speech study will be made hereafter in a more concrete way. As has already been noticed in papers (3) (4) & (5), the idea of "fidelity" as a target of transmission technique by which we are required to reproduce at the output terminals just the same acoustical figure as given at the input terminals is rather classical, and judging from the standpoint of fidelity transmission, it is of no significance to study "speech" itself. But from the actual circumstances which result in unfaithful transmission,

---

* MS in Japanese received by the Electrical Communcation Laboratory, Aug. 18, 1960. Originally published in the *Kenkyû Zituyoka Hokoku* (*Electrical Communication Laboratory Technical Journal*), N.T.T., Vol. 9, No. 12, pp. 1469–1549, 1960.

† Nagoya University.

arises technical consideration about the transmission of speech-effect and accordingly real scientific research of "speech" itself.

We can consider of course speech signals as having a physical side as those given for vibrational and acoustical substances at the input terminal of the communication system. However, we should not neglect the other side of signals as being impressed upon the mind, through sensorium, of the recipient situated at the output terminal, other side which is a highly qualified subjective or psychological side. Furthermore, this side of recipient impression should exactly correspond to the expression side of the transmitter situated at the input terminal of the communication system. It is in this sense that the communication circuit is closed in the subjective meaning.

Now, take vowel signals, for instance, and we are able to feel various elements from the same and sole stimulus of vowels, such as pitch, loudness, vocality and voice quality of the calling subject. That is to say, in response to a single vibrational signal, the recipient is aware of pitch, loudness, phoneme, voice and other elements. This is because the communicants carry out subjectively such multi-qualified operations. Speech quality is a concept anticipating a qualifying operation of subjectivity. The concept of speech quality or transmission quality neither exists nor can be defined without the premise of communication subjectivity and this is the very place where our quality theory does stand up.

Next we will approach more closely our vowel-sound problem. If regarded as timbre base, the vowel sounds may be considered a series of spectrum components or a series of harmonic components (in case of timbre with pitch). If we use the traditional term "formant" given by L. Hermann about a hundred years ago, it will be possible to give formant numbers F_1, F_2, F_3,. . . . to describe a timbre structure of vowels, numerating the order of the conspicuous parts of its construction, as clarified in the latest minute analysis. It is too hasty, however, to conclude that all the formants will contribute to phonemic quality only. As will be seen later in our quality analysis, some of the formants contribute not only to phonemic quality but also to voice quality, and some are found to affect remarkably the formation of loudness in addition to phonemic and voice qualities. There is a reason to assume that there may possibly exist other formants connected with qualities still unknown. Thus the first mistake we should avoid making is to consider hastily that physically and apparently conspicuous formant structure is an element contributing to phonemic quality. Verifying by subjective measurement is indispensable before making a conclusion. Phonemic-quality contributing formant and voice-quality contributing formant respectively require proof. There also may exist formant structure contributing to establishment of subjective loudness, and probably to formation of subjective pitch. When studies on quality theory are further advanced, these mechanisms will be clarified. In short, in order to strictly interpret wave-forms of speech sounds, we may stress at the beginning that we should be fully prudent to make a sufficient quality study.

Timbre Quality

If we interpret, as stated above, the quality of the speech which is to be transmitted subjectively, we inevitably face the problem of the complex construction of speech, which makes the study of speech quality very complicated. There must be some unification of all these different qualities, which in itself is a kind of interpretation. One interpretation is that of the Bell school represented by H. Fletcher and R. H. Galt (6). They consider that the first aspect of speech perception is that of "interpretation", which leads to the articulation quality as shown by the "articulation index" method. Then follows in order the "loudness" aspect, the "pitch" aspect, and the "quality" aspect.

The view of the authors is that there are only two qualities in speech; one is the "phoneme" aspect and the other the "voice" aspect. But, there are three acoustic attributes in a general sense; pitch, loudness and timbre. These three acoustic attributes, which are the foundation of the two quality aspects and their interrelations, are not parallel on a plane as considered by the Bell school, but correlative in a solid as shown in the following:

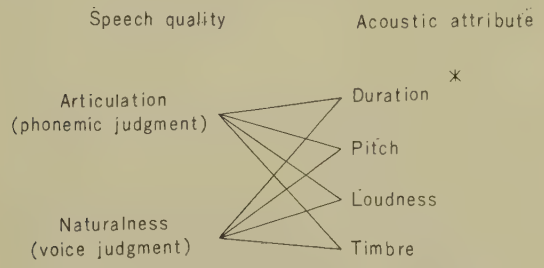
Speech quality
Acoustic attribute
Articulation (phonemic judgment)
Naturalness (voice judgment)
Duration
*
Pitch
Loudness
Timbre

The authors consider that articulation (phonemic quality) as well as naturalness (voice quality) find themselves on the base of unification of three attributes; pitch (height of the base), loudness (stress or intensity) and timbre (color or nuance). With regard to vowel and consonant articulations, it is clear that conditional restriction found in pitch and loudness in the phonetical meaning in addition to the timbre element can contribute to articulation. In the same way, it is very easily seen that intonation and stress in the phonetical sense play a major role in identification of voice and discrimination of individuality.

When, however, the mechanism of formation of the phoneme and the voice qualities are to be considered, there is no argument to the fact that the greatest element is timbre (particularly in Japanese). Aside from the relation between timbre and pitch, or that between timbre and loudness, it is most important, to begin with, to clarify the establishing mechanism of phoneme and voice qualities on the bases of the main attribute of timbre. In a view of timbre quality taken up in this sense, the vowel signal of stationary and static timbres is made the objective of our present study, in order both to check and re-examine the so-called "formant" theory of the vowels and to prove definitively that voice quality is quite different from phonemic quality.

Transmission Quality and System Rating

"Transmission Quality", an abstract idea in the transmission technique of telecommunication, is intimately connected with the problem of evaluation or rating of the transmission system. To trace the historical development of system evaluation and ration is to follow the growth, development, and change of the communication concept of "transmission quality". To show what the quality study means, reference will be made to the principal quality studies appearing in the literature, centering around the problem of system rating.

The "Standard Cable-Mile" system early introduced and adopted in England was later improved and replaced by the attenuator pad (dB) system, specified loudness quality as its standard quality and means system rating by "transmission equivalent". The transmission equivalent system has long been adopted for its convenience, and there is a series of detailed studies (8) (9) (10) of so-called "Bezugsdämpfung" by K. Braun in Germany. Now in the U. S., the revised method by P. W. Blye has been advanced by the Bell school.

On the other hand, along with the tendency of the times when "transmission efficiency" has been gradually transformed into "transmission quality", it is found insufficient to relay upon loudness representation, though quantitatively convenient, in order to show quality.

Articulation has then been pointed out as a standard quality. This corresponds exactly to the period of "Nutzdämpfung". Being shown by the same dB as in the case of transmission equivalent, the meaning has changed from being quantitative to being qualitative (13) (14).

In the history of communication England and the United States, and then most other countries began early the study of articulation using its own language. The articulation index method was first completed in the U. S.; and then in Japan (16), the Soviet Union (17)-(21), and other countries. Articulation may

---

[*] Duration is shown parallel here for convenience, though it is by its nature essentially correlated to the other three acoustic attributes.

well be said to be the standard quality for evaluating a telephone transmission circuit, so far as the primary objective of the telephone is "intelligibility". This method is connected with the calculation of articulation quality, which is fairly complicated to handle. Moreover, when evaluating a sufficiently high-quality system, it is difficult to duly evaluate the system by articulation, as was found by a series of studies of J. Collard (22)-(24).

To break the deadlock of the articulation evaluation method, K. Küpfmüller proposed another method (25), based on experimental research by E. Schäfer (26). It was called "naturalness" (Natürlichkeit) as against "articulation" (Verständlichkeit). The naturalness of Küpfmüller and Schäfer, as if pertains to speech, can be defined only by an experimental process; that is, by manipulating the bandwidth of the system in question. Thus, having speech as the objective of observation and being considered a quality other than articulation, this naturalness of Küpfmüller and Schäfer could not really clarify the following important point: what part of speech and what content in speech are really utilized in the experiment as the basis of the naturalness judgement? Furthermore, we pose the following question: judging from the fact that the experimental operation limiting bandwidth is relied upon as the foundation for defining this quality, how should the naturalness be defined in case of distortion other than band-elimination distortion? In fact, it is extremely difficult to define naturalness in the most general sense. It may be that the insufficiency and difficulty are not limited to the definition of naturalness by Küpfmüller and Schäfer. For example, the new idea in the early "Standard of Performance" proposed by J. Collard, which was the origin of the articulation index method in later years, may be considered the concept proposal made at the ultimate stage of formant theory in the direction from "sound articulation" to "band articulation". Insofar as it has speech as the objective of transmission, it seems, however, still ambiguous what part of speech has been really and concretely aimed at in this quality. As a result, the way of calculation in the standard of performance has been finally utilized in a minute calculation of articulation quality of the articulation index method, contrary to the expectation of the early proposal that there might be another quality.

In short, the history of system evaluation shows that much work has been done trying to find the most suitable quality, going from loudness evaluation to articulation evaluation and further seeking after some standard still unknown. One of the reasons may be that there was something lacking in making studies of quality. In full consideration of this point the authors have always made major efforts to examine the relation between timbre patterns and quality responses. This was quite natural for both quality studies and for interpretation of signal patterns, and further this was connected with the initial problem as to whether the timbre pattern was properly represented or not.

This report is mainly a summary, reexamimed and reconsidered, of the researches (29)-(33) conducted at Nagoya University, during the five years from 1953 to 1957, as contracted research for the Electrical Communication Laboratory, Nippon Telegraph and Telephone Public Corporation. In this report, general items are described in the first part and followed by more specialized items.
The order of description, however, does not necessarily correspond to that of the experiments.

1. Study of Pattern Representation of Timbre Stracture

It is preliminarily necessary to study and check up the phoneme kind change and individual voice (speaker) change found in the mode of frequency or harmonic spectra which are obtained by physical process of perfect and exact analysis, before entering into our quality study. If once we can discover some hidden tendencies and establish certain exact rules concerning spectra-configuration due to phoneme change and voice change, only a carefull preparation of timbre pattern based upon spectra material will do for our purpose, because formal and mechanical process of spectra-data will lead us to determine the respective qualities and even to predict the existence of these quality elements. According to our study on quality conceptions (34) (35), the phonemic element (exclusively dependent of phoneme kind) is almost invariable in regard to pitch and loudness, and varies, within some limits and conditionally, in regard to variation of the individual; while the voice elements (exclusively dependent of variation of individual) depends to some measure upon pitch and loudness, and is almost independent of the variation of the phoneme). Therefore, it is possible to find out proper quality elements, if a given spectrum is duly processed according to these quality definitions, which will further help us in interpreting the experimental results gained by the subjective measurements, as will be described hereafter.

1.1. Experimental Methods

Speech analysis (36) from the above standpoint was first carried out in 1953. The calling subjects comprised two males, two females and one child, picked in consideration of the sex factor in regard to individual difference. The vowels were limited to the five Japanese oral vowels ア, イ, ウ, エ, オ, designated "A", "I", "U", "E", "O". These vowels were spoken successively, each one being held for five or six seconds in a sustained state without vibrato as in the speaking mode instead of the singing one. The vocal intensity in emission was first maintained at *mezzo forte* in consideration of pattern modification of voice quality. Pitch was varied in view of the aim of our study stated above within an octave interval in the voice register of the individual. As loudness is closely connected with the speech level, it is of course better to make loudness constant instead variable for our data treatment. But loudness matching was much complicated in process, level matching (in VU) was adopted as a temporary substitute. The analyzer was of the hetrodyne type, using a magnetostriction resonator. The band width of the resonator at the 3 dB attenuation point was 30 c/s. The output was recorded with an electromagnetic oscillograph. A type MR 101 capacitor microphone was used, the speaking subject was placed about 25 cm in front of it. The mean level of speech at the microphone was about 75 dB re. 0.0002 dyne/cm^2. As the vowel spectrum was of large fluctuation, five to ten oscillograms were prepared for each vowel sound to obtain the mean value of all the spectra.

1.2. Data-Processing Method and Timbre Pattern.

Since vowel spectra are determined by vibration mode of a vocal cord itself, and then by acoustic transfer characteristics of the throat cavity, buccal cavity, nassal cavity, etc., it is impossible to infer directly from the forms of spectra the transfer characteristics of articulatory organs as an element to determine phoneme. The method adopted to infer what corresponds to the qualities aimed at in the spectra thus obtained was the data-treatment method, as stated before, complying with the general definition of qualities. That is, with regard to phonemic quality, the pattern of a vowel spoken in different pitches shows different spectrum intervals and spectrum envelopes. However, judging from the fact that they have the same phonemic value, it is conceivable that some kind of averaging operation can be conducted to obtain things common out of different diagrams. One method adopted is the component enveloping method, or juxtaposition method, as shown in the Fig. 1.

This is a method to juxtapose the spectra of all patterns in all pitches on the frequency axis and to obtain the envelope of component-amplitudes drawn. Those processed according to the general definition of phonemic quality are called "vowel patterns in a broad sense". The vowel patterns individually obtained for the five calling subjects selected are shown in Fig. 2.

Those marked with vowels in the upper part of the Fig. 2 for each calling subject are the vowel patterns. The vertical axis shows the deflection of the oscillograph, in linear scale. After finding the difference in phoneme

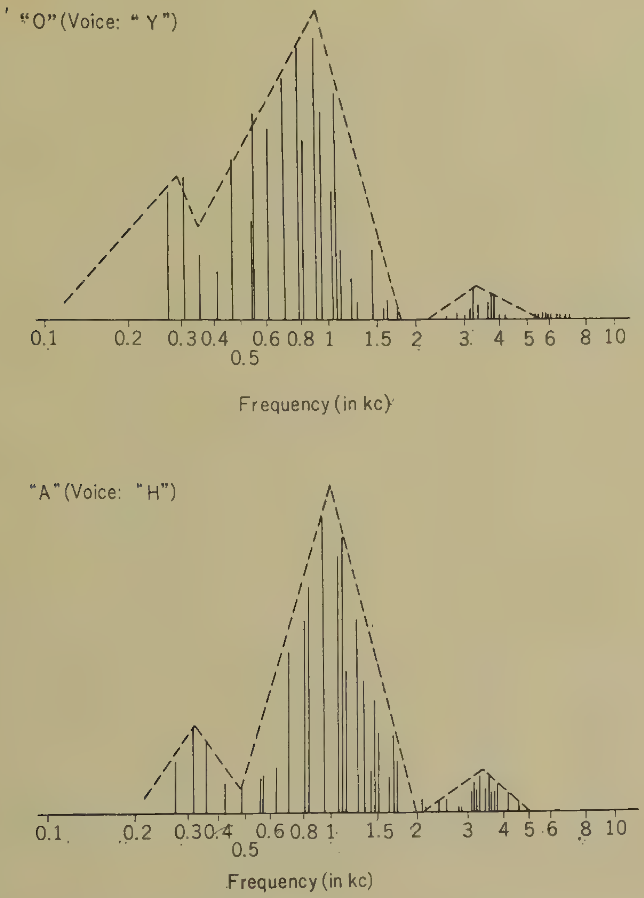

Fig. 1—Timbre pattern representation by juxtaposition method.

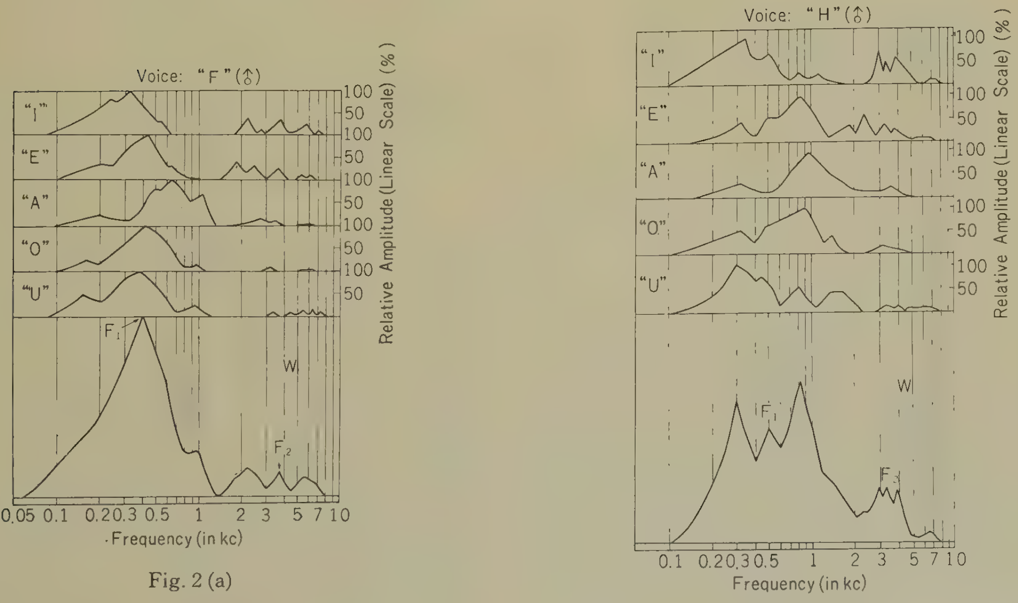

Fig. 2 (a)

Fig. 2 (b)

Fig. 2—Representation of timbre and voice patterns of five vowels of five calling subjects.

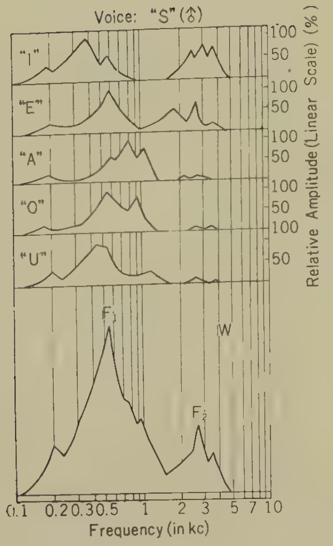

Fig. 2 (c)

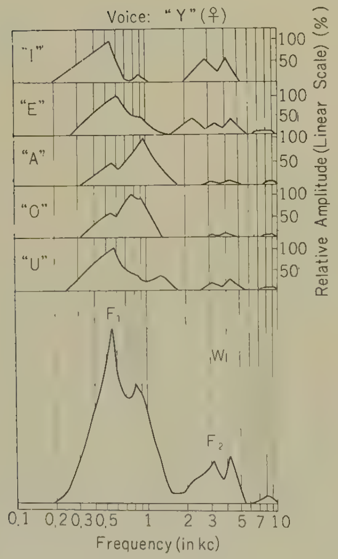

Fig. 2 (d)

for the form of the vowel patterns, it is possible to read the spectrum part corresponding to phonemic quality. Though with some individual difference in the position of frequency, it almost completely coincides with a vowel formant already known.

What we are now most concerned with is whether or not it is possible to find things

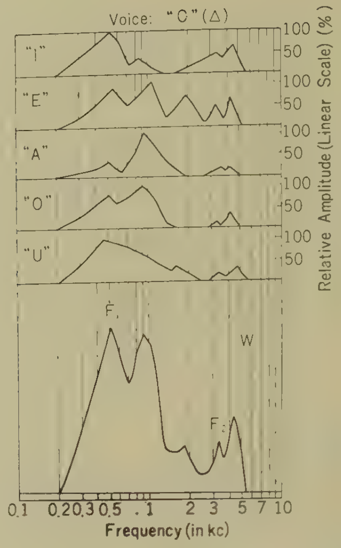

Fig. 2 (e)

Fig. 2—Representation of timbre and voice patterns of five vowels of five calling subjects.

invariable in phoneme, namely corresponding to voice quality, from the vowel patterns. For this purpose, an averaging method is taken as follows. To the vertical axis of each vowel pattern, linear compression or expansion is given, so as to make the maximum amplitude 100 %, and then each vowel pattern is averaged for each frequency within each calling subject. The patterns thus made are shown in the bottom part of the graph for each calling subject. For the sake of convenience, they are expanded as a component sum, representing the average form of patterns for vowels spoken by each calling subject. These graphs at the bottom may be further regarded as devocalized patterns obtained after counter-balancing the effects of phonemic quality, and are called "vocal patterns" or "voice patterns" The patterns made from frequency spectra, according to the general definition of quality, are called the "timbre patterns of voice in general." They naturally take fairly different forms for each calling subject, but it is understood that peaks are the frequency parts in which the strongest element in the average sense for each vowel pattern exists. If peaks or formants are looked for as corresponding to voice quality, in voice patterns, it is assumed from pattern forms that they may exist in two parts····upper and lower ones, with a demarcation point of about 1.5 kc. These demarcation regions of about 1.5 kc are called "vocal glens" (36), which are very important when the relation between the results of quality measurement and patterns is to be established. The part above the glen frequency is called an upper part, and that below a lower part. Even if voice patterns are evaluated in upper and lower parts, there are found plural peaks in each frequency region for some calling subjects, and the one to be related to voice quality is still unknown. If, however, formants are to be required as voice-quality elements, the formants as found in voice patterns should also appear in each part of pattern. If, from this standpoint, the relation between the peak in voice pattern and that in each vowel is taken up, rather completely for calling subjects "C" and "S", and not so conspicuously for other subjects. Thus formants are pointed out as corresponding to voice quality for the lower and the upper parts respectively, and are marked with F_1 and F_2 in the Fig. 2. The formant, being independent of phoneme, can be called an "invariant" formant. It is interesting to note that the frequency of the geometric mean for these two fixed formants in the upper and the lower parts is found to be the same, about 1.3 kc, for all calling subjects.

2. Study of Fundamental Qualities Based upon Subjective Measurement

The concept of voice quality originates from the problem of discrimination of individuality in speech. Because of the diversity and complexity of individual speech quality, the detection of the voice difference is inherently difficult. The principle of the method adopted here for our measurements was exclusively based upon the so-called "identification" method, considering "voice quality" in connection with "phoneme quality" on the same basis as the timbre aspect. The "identification" method was selected because the so-called "comparison" method as adopted in Schäfer's experiment gave results which are short of concreteness in the content of quality judgment.

The experimental procedure was to make the listeners who have received the stimulus of vowel sounds arranged at random identify individuality of voices and at the same time phonemes. With regard to phonemic quality, the number of phonemes is limited to five as far as Japanese vowels are concerned. However, the finite number represented in samples in the voice ensemble was not known to us. The first consideration to follow when planning an experiment was to what extent it is possible for listeners to classify voice qualities. If rules and system can be found in voice-quality classification by listeners, not only the content of perceptional response will be grasped more concretely, but also the base of selection upon which the kind of voices is determined will be orientated. Thus the measurement experiment according to the above course had to be repeated several times and finally in this experiment different subjective measurements were carried out six times, as will be stated herein.

2.1. Contents of Experimental Program and Illustration of Procedure

2.1.1. Contents

The contents of six experiments are summed up in Table 1.

2.1.2. Experimental Procedure

The fundamental scheme of experiment followed throughout for six times is shown in Fig. 3. Speech sounds of five vowels by five calling subjects selected were recorded according to the order specified in the test list where voice and phoneme were placed so as to occur at random. A number of tape lists thus prepared were used arbitrarily in each distorting condition.

Reproduced signals from a recorder were given to listeners through a distortion system,

Table 1

TIME SCHEME OF SIGNAL PRESENTATION (SIGNAL-PAUSE)

Test Number	Year of Test	Calling Pitch	Voice Ensemble	Vocal Intensity	Vowel Ensembl	Presentation of Signal Signal-Pause	Listner Group	Transducer	Number of Observation (per 1 Point)	Kinds of Distortion
1	1953	280∼	5 F°(♂) S°(♂) C°(△) Y°(♀) H°(♀)	mezzo-forte	5 I, E, A, O, U	4 sec–4 sec	4 Fu (♂) Fa (♂) Na (♂) Ha (♂)	Loud-Speaker	2000	BED
2	1954	140∼	4 K (♂) Y (♂) N (♂) F (♂)	mezzo-forte	5 I, E, A, O, U	4 sec–4 sec	4 K (♂) Y (♂) N (♀) S (♀)	Loud-Speaker	1200	BED RSD
3	1954	240∼	5 K (♂) Y (♂) S (♀) N (♂) F (♂)	mezzo-forte	5 I, E, A, O, U	4 sec–4 sec	4 K (♂) Y (♂) N (♂) S (♀)	Loud-Speaker	1500	BED RSD
4	1955	240∼	5 K (♂) Y (♂) F°(♂) C (♀) S (♀)	Piano torte	5 I, E, A, O, U	4 sec–4 sec	4 K (♂) Y (♂) C (♀) S (♀)	Loud-Speaker	1500	BED
5	1956	220∼	4 K′(♂) M (♂) C′(♀) S (♀)	mezzo-forte	5 I, E, A, O, U	3 sec–3 sec	4 K′(♂) M (♂) C′(♀) S (♀)	Loud-Speaker	1200	BED TD
6	1957	150∼	4 T (♂) S′(♂) M′(♂) H (♂)	mezzo-forte	5 I, E, A, O, U	2 sec–3 sec	4 T (♂) S′(♂) H (♂) D (♀)	Receiver	2000	BED AD

(N.B.) (♂): Male, (♀): Female, (△): Children. BED: Band-eliminating distortion. RSD: Rotational synchronous distortion.
TD: Time-cutting distortion. AD: Attenuation distortion.
A capacitor microphone and a magnetic tape recorder were used throughout all of these experiments.

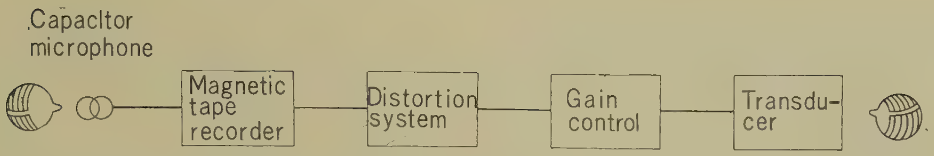

Fig. 3—Block diagram of the experimental setup for these experiments.

a gain control and finally a transducer. For voice, four or five calling subjects were given suitable symbols, for example, "KA" would be recorded if the vowel of a calling subject "K" is identified as "A". In case where signal loudness diminishes considerably as in attenuation distortion, listeners were notified in advance that signals would be sent out so as to synchronize with the turning on and off of the lamp placed in front of them.

The gain control was prepared so that diminution of loudness due to component elimination of signals would not contaminate quality evaluation when investigating frequency construction of qualities by BED. It was not used at all or used as little as possible, at elimination points such as LC: 4.0, 6.0 kc, as band elimination was meaningless, if loudness was recovered to a great extent. It was of course not used in No. 6 test where comparison between BED and AD was intended. All voice signals were carefully recorded only for 2-4 seconds during middle part of sustained vowels to avoid the subsiduary effect of the transient part in build-up and in decay of vowel waves for quality judgment of individuality identification.

2.2. Illustration of Experimental Results

In all the six subjective measurements, great effort was made to obtain frequency construction of voice quality, in comparison with that of phonemic quality. The following illustration of the results is limited only to those due to BED and those due to other distortion will be considered in a separate paragraph on cutting distortion.

2.2.1. Listeners' Capacity to Identify Voice Quality

Voice quality in a concrete sense as it will now be taken up may be said to be completely unknown up to the present. The response which comes from listeners for voice quality must be clarified, as was done in the preliminary experiment prior to the No. 1 experiment, in which the listeners consisted of three male students and a member of the laboratory staff, and the calling subjects were the five who had been used in the analytical study in Section 1.

The three students were unknown to the calling subjects but the other listener had been in contact with them during the period of the analytical experiment (about six months). Prior to the experiment each listener was confirmed by measuring the minimum auditory threshold of pure tones of his hearing acuity, and then trained by loudness comparison between pure tones. In order to have them became acquainted with unknown voices, the listeners were told to compare the loudness of the vowels of the speakers to be used in the principal experiment. With these preliminary experiments over, the training of voice judgment was started. In the first place they were trained to discriminate five voice qualities in one vowel. This training was conducted using recordings on which voices were recorded at random with vowels kept constant. The learning curves obtained in the experiment for each listener are shown in Fig. 4 (A). One of the curves in the figure shows very high percentage of correct judgment from the begining of training. This was recorded by a member of the laboratory staff who had been acquainted before with the calling subjects. From this fact it clearly follows that the listeners' past experience has much to do with correct judgment. With the other listeners who has no contact with calling subjects, the first ratio of correct judg-

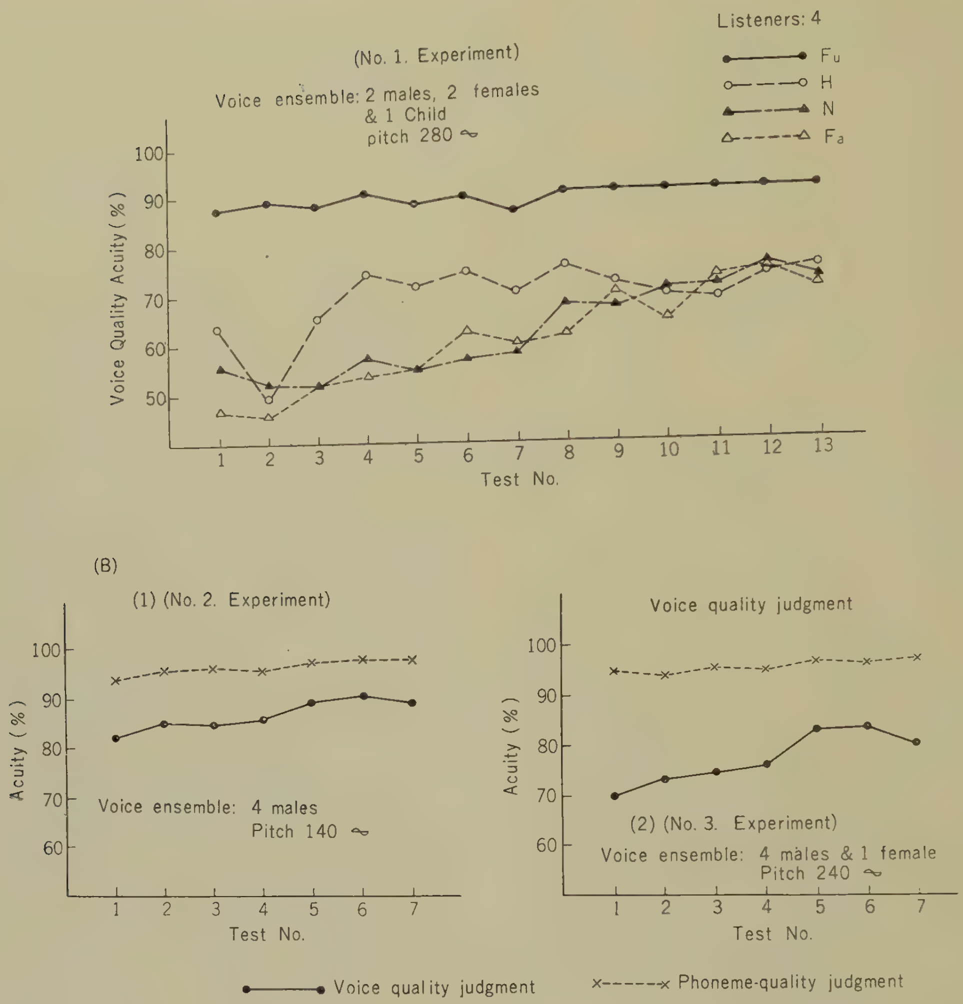

Fig. 4—Curves of learning effects in experiments Nos. 2 & 3.

ment reached about 50 %, showing that the timbre discrimination of stational vowel sounds is not easy. This ratio, however, rose, though gradually, to over 70 % in the final experiment. It may be said that during this training period each listener became able to discriminate the timbre difference of each voice, to catch and remember its characteristics, and to identify voice quality with fairly high percentage of correct judgment.

(B)-1 in the same figure shows an averaged learning curve obtained in an experiment preliminary to the No. 2 experiment. In this case each listener knew the calling subjects or hear his own voice, and the percentage of voice judgment, different from No. 1 experiment, reached over 80 % at the start, with further rise to 90 % after some training. (B)-2 shows a learning curve in the No. 3 experiment where the same calling subjects as the above raised their calling pitch by 100 c/s and a female voice was added from among the listeners. The first percentage of voice judgment went down to about 70 %. As the No. 3 experiment was conducted immediately following the No. 2 experiment, the fall in the ratio of voice judgment shows that the quality judgment in the No. 3 experiment had nothing to do with the listeners' past contact with the calling subjects, and further that when the calling pitch was changed unnaturally (compard with natural speaking pitch), voice quality changed considerably and timbre discrimination was a main clue to voice judgment.

Although there was considerable difference in individual capacity of discrimination, it was possible to obtain immediately stabilized and high judgment when listeners had been in contact with the calling subjects. Further, as will be stated later, not much difference in trend was found between experiments No. 1 and 2 regarding the fall in judgment due to BED. Thus in all the experiments that followed, the listeners were replaced by calling subjects, or the calling subjects acquainted with listeners were employed.

Fig. 4 (B) also shows training curves of phoneme judgment and it is of interest to note that there also appeared some learning effect. It is impossible to judge accurately the quality of phoneme from segments of sustained vowels as found in syllables, leaving a possibility of raising the judgment ratio.

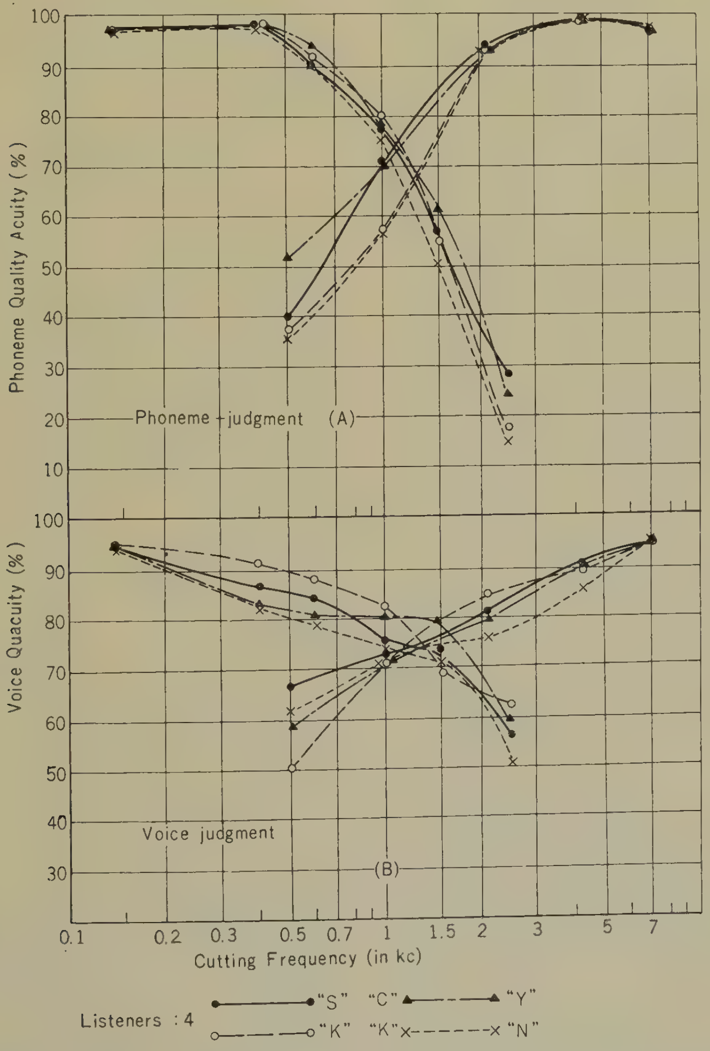

Fig. 5—Quality characteristics curve due to BED. (Experiment No. 2)

2.2.2. Individual Difference in Quality Judgment

When speech pattern is deformed due to BED, change in the phonemic and voice qualities is natural. It is quite conceivable that there should appear individual differences in the listeners' responses to such deformed patterns. All the experiments conducted were checked on this point and generally speaking, there was considerable individual difference in listeners' capacity of discrimination and memory of each voice quality in a given voice ensemble. The greatest difference reached as high as 20 %, but the individual difference in the falling of judgment ratio due to BED was not so remarkable, and the quality characteristic curves were fairly similar among individuals as shown in Fig. 5 (A) (B) for the experiment No. 2.

(A) is for phoneme judgment. (B) is voice judgment characteristics. In the curve for each individual, the percentage in reference (all pass) condition was adjusted to be the same, to compare the shape only.

Comparing (A) with (B), when distortion is small, individual difference in phoneme judgment is somewhat smaller. As, however, distortion becomes larger, individual differences in both quality judgments become comparable and in some cases, voice judgment shows a more stabilized trend. This is due to the fact, to be described later in detail under the item of auditory confusion, that quality modification due to BED is more remarkable in phonemic quality and a systematic individual trend exists in phoneme judgment of changed patterns. For example, some listeners tend to judge the higher cut-off (HC: 1 kc) vowel "I" as "U", while other listeners are liable still to judge it as "I". The fact that there is much individual difference in HC distortion, when judging phoneme, will easily be understood from the HC curve in Fig. 5 (A). The individual difference can not be so much detected in voice judgment as easily seen in (B).

Then, the clue to memory and discriminate the voice quality is a little different in individuals.

2.2.3. Interdependency of Vocal and Phonemic Qualities

How are the contents of voice quality discriminated and memorized by the listeners related to phonemic quality? This relation is to be considered here since voice quality and phoneme quality have, up to this point, been considered separately. To what extent is interdependency observed in these judgments successively conducted (voice quality judgment

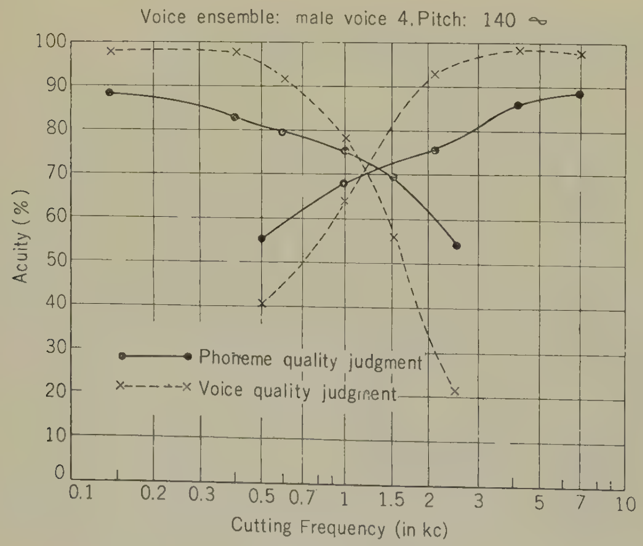

Fig. 6—Averaged characteristics curves in BED of phonemic and voice quality judgment.

preceded phonemic judgment throughout all the experiments)? This needs to be examined, statistically under the experimental design. For the present, it will be considered from the fall in judgment ratio, namely, from mutual comparison of shapes of quality characteristic curves. For example, in Fig. 6 is shown averaged curves of phonemic and voice quality judgment in the experiment No. 2. In the measurements, listeners were instructed to endeavor to record the most similar phoneme and voice, even when they found it difficult to judge phoneme or voice of signals due to changes of patterns by distortion. The fall of the curves in the figure shows not only the degree in which each signal pattern loses its own quality but also that in which it gains other qualities (for instance, "I" becomes like "U"). As an example, in one distorting condition the phonemic quality of a specific vowel is simply destroyed; while in another the quality of the vowel is changed into a different phonemic quality. There is naturally found a difference in correct judgment and the fall in ratio is more pronounced in the second case. Fig. 6 shows a distinct difference in the shapes of two judgment curves for phonemic and voice qualities and in the former a sharper curve slope takes place. This explains that in every step of BED, quality change occurs more rapidly in phonemic quality than in voice quality. The pattern change, as stated above, should be regarded as having both destruction and modification of qualities. Voice judgment curves do not show steep slopes, from which it may be interpreted that voice qualities of the whole spectrum do not change remarkably, even if a specific part of the spectrum is suddenly cut off by a filter having such an attenuation characteristics as was used in this measurement.

By comparing these curve shapes, it is assumed that the two qualities dealt with are of different natures having different structures. According to the concept of band quality, it may be said that quality element is more dispersed in voice quality than in phonemic quality on the frequency scale. This seems to contradict the existence of the voice quality element as formant, as discussed in Section 1. But the contents of voice quality (or the contents of listeners' judgment) are not simple and it is impossible to examine the quality contents and thus to explain properly the mechanism of quality formation, unless by perfect analysis of data including other experimental results.

2.2.4. Observation of Relation between Quality Judgment Curves and Vocal Patterns

1) Relation between Pitch and Quality Balancing Point

Sufficient quality study can not be said to have been made, unless the shapes of quality judgment curves obtained by subjective measurement are explained in relation to the shapes of vocal patterns obtained through physical analysis.

Of course, the relation between the physical wave forms at a listeners' input and the quality judgment as the output at his sensorium can not easily be found, but the tendency towards relation is expected to be read to some extent on the chart. For this purpose, the relation between the pattern change by pitch and balancing point of vocal quality is shown in Fig. 7. The judgment curves of experiment, 1, 2 & 5 are shown in the same figure. Vocal patterns shown in the lower part of the figure were obtained by averaging all the patterns of each voice and vowel in each ensemble. To obtain these spectra, the same frequency analyzer was used as that used for the studies reported in Section 1. Since pitch was adjusted to be the same for all the voices of the ensemble, the averaging calculation could be conducted by taking the mean amplitude for each of the higher harmonics. Judging from these vocal patterns, the movement of patterns begins distinctly as pitch is raised. Each voice-quality balancing-point corresponds to the vocal glen of each pattern, that is the frequency of distribution of voice quality is divided into two parts with demarcation

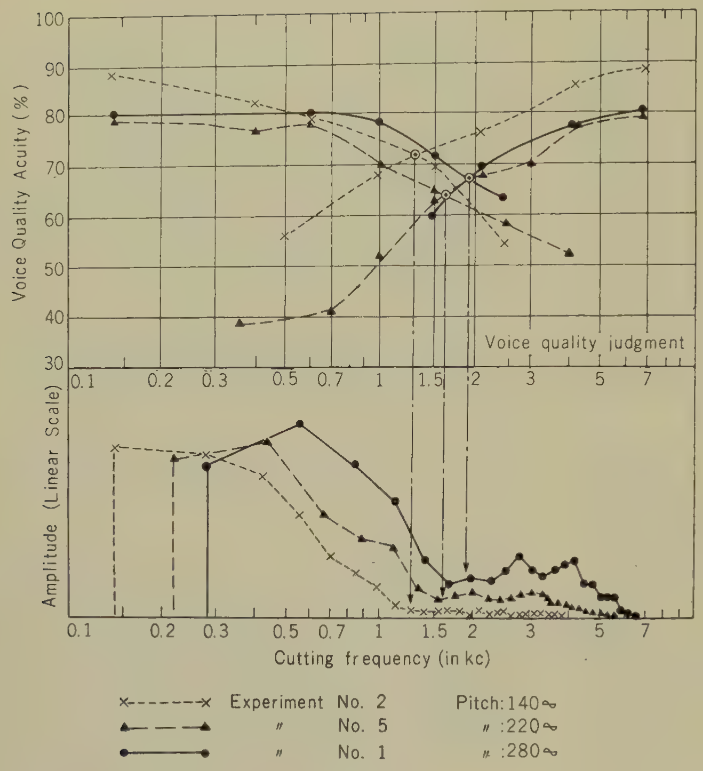

Fig. 7—Correlation between voice-quality judgment curves and vocal patterns—collelation between movement of quality balancing point by pitch and vocal glen.

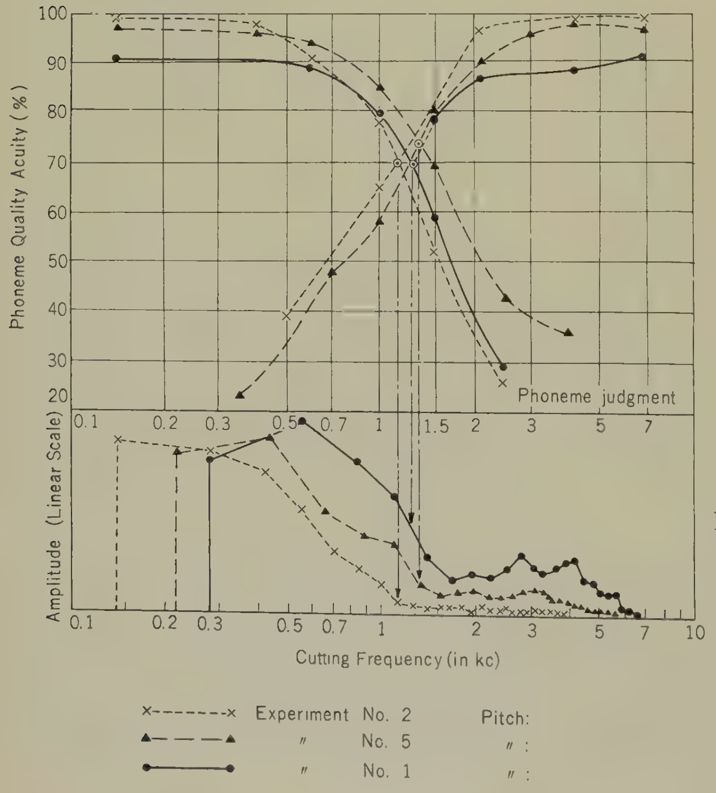

Fig. 8—Collelation between phoneme-quality judgment curves and vocal patterns—change of quality balancing points by pitch and movement of patterns.

point the vocal glen. This glen is situated in frequency considerably higher that the center of the energy distribution.

In order to emphasize characteristics of such voice-quality distribution, comparison is made in Fig. 8 between phonemic quality judgment curves and vocal patterns, both obtained in the same experiment. It is seen that judgment curves are a little different according to the pitch change.

It is too hasty to conclude from this, however, that the phonemic quality elements in spectrum move along the frequency axis, because a different modification (not destruction) occurs in the same distorting condition, if the spectrum structure changes by pitch. The difference which appears on the crossing points is neither so conspicuous as in voice quality, nor does its frequency position correspond to the order in pitch. With regard to frequency distribution of phonemic quality, the sex of the voice ensemble should be taken into consideration. As will be explained in the following item, the positions of phonemic element for female and children's voices are generally higher. Besides, the crossing points in experiment No. 1, which covers most of the female and children's voices, are not so different from those in experiment No. 2, having a male voice only. In short, frequency distribution of phonemic quality, is not much affected by calling pitch. If, therefore, voice quality is compared with phonemic quality from this point of view, it may be said that distribution of phonemic quality is stationary and stable in freqnency, while distribution of voice quality has a rather shifting nature according to pitch.

(*to be continued*)

* * * *

REVIEW OF THE ELECTRICAL COMMUNICATION LABORATORY
VOLUME 8, NUMBERS 9-10, SEPTEMBER-OCTOBER 1960

U.D.C. 621. 372. 8. 001. 2

Circular Electric Wave Transmission through Hybrid-Mode Waveguide*

***Ken-ichi NODA*†**

General formulae for mode generation from distributed sources are derived for hybrid-mode waveguides. Using the formulae, the mode conversion by irregular parts of the dielectric layer in a dielectric-coated waveguide is calculated. Coupling between modes at geometrical imperfections and in intentional bends are described as the relations between the normal hybrid-modes. The coupling coefficients between the TE_{01} and HY_{1m} modes in the curved helix waveguide are obtained as functions of the arbitrary wall impedance. Several other transmission characteristics in the hybrid-mode waveguide are also analysed.

1. Introduction

The circular electric mode in a circular waveguide is considered to be used for a long distance low loss transmission, but it is not easy to keep the mode pure through the transmission. Mode conversion to the TM_{11} mode is very serious problem at bends. But, if the degeneration is removed by proper methods, the converted power can be kept to less than the small value permissible even though the conversion is inevitable. The dielectric-coated waveguide is promising for use at intentional bends.(1) The thin dielectric layer coated on the inner wall of the waveguide changes the propagation constant of the TM_{11} by a larger amount than it changes that of the TE_{01} mode. To obtain a low loss bend with this kind of waveguide, attenuation increase due to dielectric loss must be kept as low as possible not only for the TE_{01} mode but also for the unwanted modes, for example, for the TM_{11} or TE_{12} modes. However, it was difficult to make the low loss dielectric material adhere tightly to the metal, but the development of a good primer and the improvement of the coating techniques of the plastics to the inner surface of the waveguide have made possible the manufacturing of such a type of waveguide.(2)

The thickness of the dielectric layer can not be made perfectly uniform, and the irregularity of the thickness causes mode conversion. The converted mode power is calculated by solving the problem of radiation in the hybrid-mode waveguide from the induced polarization of the irregular parts of the layer by the incident wave. Many papers treat the radiation problem of the plain waveguide.(3)(4)(5) The present paper extends the problem to the case of waveguides having an inhomogeneous material and an impedance wall. The amplitude of the converted mode power is represented by the equivalent current distribution and the field components of the normal modes of the dielectric-coated waveguide. Thus, the conversion losses are obtained in terms of the standard deviation of the thickness of the layer. Practical examples show that in many cases the mode conversion losses are very small compared with the heat loss.

At the junction of the dielectric-coated waveguide with the plain waveguide, a part of the incident TE_{01} wave is converted to the TE_{0m} modes. Unger made a rough

---

* MS in Japanese received by the Electrical Communication Laboratory, Apr. 15th, 1960. Originally published in the *Kenkyû Zituyoka Hôkoku* (*Electrical Communication Laboratory Technical Journal*), T.N.T., Vol. 9, No. 6, pp. 585–620, 1960.

† Hyper-frequency Research Section.

estimation of the conversion coefficients at the junction.(1) Exact conversion coefficients are derived from the continuity relationship of the electric and magnetic transverse fields at the junction.

Mode conversion losses due to slight deformations of the waveguide wall have been calculated already.(4) But when the waveguide has an inhomogeneous material in it, and has an impedance wall, no formula for calculating mode conversion is yet available. Using the above mentioned mode generation formulae in the hybrid-mode waveguide, the mode conversions can be calculated in terms of relations among the normal hybrid-modes, if the constancy of the wall impedance is assumed for every mode.

Mode coupling factors among the waveguide modes have been obtained already for bends in plain waveguides.(6)(7)(8) The constancy of the wall impedance is assumed for every mode, in the same way as the problem of the wall deformations. Then, the coupling formulae can be described as relations among the normal hybrid-modes.

When the cross section of circular waveguide is deformed to an ellipse, the attenuation constant increases. The TE_{01} mode becomes a hybrid-mode in an elliptic waveguide. Oguchi calculated the increase of attenuation of elliptic waveguides compared with that of the circular waveguide for waveguides having a metal wall.(9) Exact calculation is carried out using the hybrid-mode representation shown above.

2. Mode Excitation in a Waveguide Containing an Inhomogeneous Dielectric

Suppose the distributed electric current $\boldsymbol{J}$ and magnetic current $\boldsymbol{M}$ induced or impressed in the waveguide. The permittivity ε and the permeability μ may be complex numbers and functions of position. The condition at the wall will be designated later. The cross section and the inner material of the waveguide are uniform along the axis of the guide, and the axis is straight. The irregularities along the guide axis, for example, and the irregularity of the thickness of the dielectric layer on the wall are mathematically equivalent to electric current distribution. In the same manner, equivalent magnetic current distributions are substituted for windows in the waveguide.

For the moment, regarding (u, v, z) of general cylindrical coordinates, inhomogeneous equations for a field with time dependence $e^{i\omega t}$ may be written in the form:

$$\left.\begin{aligned} -\nabla\times\boldsymbol{E}&=i\omega\mu\boldsymbol{H}+\boldsymbol{M},\\ \nabla\times\boldsymbol{H}&=i\omega\varepsilon\boldsymbol{E}+\boldsymbol{J},\end{aligned}\right\} \qquad (2.1)$$

where $\boldsymbol{J}$ is the electric current and $\boldsymbol{M}$ is the magnetic current. Let each unit vector along the coordinate axes be $\boldsymbol{i}_u$, $\boldsymbol{i}_v$ and $\boldsymbol{i}_z$, respectively, and multiply (2.1) by $\boldsymbol{i}_z$ vectorilly, then:

$$\left.\begin{aligned} \boldsymbol{i}_z\times(\nabla\times\boldsymbol{E})&=\nabla_t E_z-\frac{\partial}{\partial z}\boldsymbol{E}_t\\ &=i\omega\mu\boldsymbol{H}_t\times\boldsymbol{i}_z+\boldsymbol{M}\times\boldsymbol{i}_z,\\ \boldsymbol{i}_z\times(\nabla\times\boldsymbol{H})&=\nabla_t H_z-\frac{\partial}{\partial z}\boldsymbol{H}_t\\ &=i\omega\varepsilon\boldsymbol{i}_z\times\boldsymbol{E}_t+\boldsymbol{i}_z\times\boldsymbol{J},\end{aligned}\right\} \qquad (2.2)$$

where

$$\nabla_t=\boldsymbol{i}_u\frac{\partial}{e_1\partial u}+\boldsymbol{i}_v\frac{\partial}{e_2\partial v}, \qquad (2.3)$$

and where e_1, e_2 and e_3 are metrical coefficients. $\boldsymbol{E}_t$ and $\boldsymbol{H}_t$ are the transverse electric and magnetic vectors, and E_z and H_z are the z components of the electric and magnetic fields. Next, multiply (2.1) by $\boldsymbol{i}_z$ scalarly, then

$$\left.\begin{aligned} -\boldsymbol{i}_z\cdot(\nabla\times\boldsymbol{E})&=\nabla_t\cdot(\boldsymbol{i}_z\times\boldsymbol{E}_t)=i\omega\mu H_z+M_z,\\ \boldsymbol{i}_z\cdot(\nabla\times\boldsymbol{H})&=\nabla_t\cdot(\boldsymbol{H}_t\times\boldsymbol{i}_z)=i\omega\varepsilon E_z+J_z,\end{aligned}\right\} \qquad (2.4)$$

where M_z and J_z are the z components of the magnetic and electric currents respectively.

The relation between the transverse and axial field components of the mode which propagate in $+z$ or $-z$ direction with the propagation constant γ are as follows: $\boldsymbol{J}$ and $\boldsymbol{M}$ are set equal to zero in equation (2.2), then

$$\left.\begin{aligned} &\nabla_t E_z \pm \gamma\, \boldsymbol{E}_t = i\omega\mu\, \boldsymbol{H}_t \times \boldsymbol{i}_z \\ &\nabla_t H_z \pm \gamma\, \boldsymbol{H}_t = i\omega\varepsilon\, \boldsymbol{i}_z \times \boldsymbol{E}_t \end{aligned}\right\} \qquad (2.5)$$

where the upper part of the double sign concerns the wave propagating in the $+z$ direction and lower part the wave propagating in the $-z$ direction. If in (2.4), $\boldsymbol{J}=\boldsymbol{M}=0$, then

$$\left.\begin{aligned} &H_z = \frac{\nabla_t \cdot \boldsymbol{i}_z \times \boldsymbol{E}_t}{i\omega\mu}, \\ &E_z = \frac{\nabla_t \cdot \boldsymbol{H}_t \times \boldsymbol{i}_z}{i\omega\varepsilon}. \end{aligned}\right\} \qquad (2.6)$$

Each equation of (2.5) is multiplied by $\boldsymbol{i}_z$ vectorilly to separate $\boldsymbol{E}_t$ and $\boldsymbol{H}_t$ from each other, then

$$\left.\begin{aligned} &\boldsymbol{H}_t = \frac{i\omega\varepsilon}{\chi^2} \nabla_t E_z \times \boldsymbol{i}_z \mp \frac{\gamma}{\chi^2} \nabla_t H_z, \\ &\boldsymbol{E}_t = \mp \frac{\gamma}{\chi^2} \nabla_t E_z - \frac{i\omega\mu}{\chi^2} \nabla_t H_z \times \boldsymbol{i}_z, \end{aligned}\right\} \qquad (2.7)$$

where

$$\left.\begin{aligned} &k^2 = \omega^2 \varepsilon\mu, \\ &k^2 + \gamma^2 = \chi^2, \end{aligned}\right\} \qquad (2.8)$$

and χ is a constant value in case of the plain waveguide, but is a function of the position in the cross section here. The eigenvalue of the mode is the propagation constant.

The transverse components of the electric and magnetic fields in the waveguide are expressed in the forms of the series expansion as follows:

$$\left.\begin{aligned} &\boldsymbol{E}_t(u, v, z) = \sum_i V_i(z) \boldsymbol{e}_{ti}(u, v), \\ &\boldsymbol{H}_t(u, v, z) = \sum_i I_i(z) \boldsymbol{h}_{ti}(u, v). \end{aligned}\right\} \qquad (2.9)$$

The single subscripts i is used, for simplicity, instead of the double subscripts mn for designating the various modes. The z-components of the fields are expressed in the following form:

$$\left.\begin{aligned} &E_z(u, v, z) = \sum_i I_i(z) e_{zi}(u, v), \\ &H_z(u, v, z) = \sum_i V_i(z) h_{zi}(u, v), \end{aligned}\right\} \qquad (2.10)$$

where the components $\boldsymbol{e}_{ti}$, $\boldsymbol{h}_{ti}$, e_z and h_z are written in terms of the two scalar functions T_i, and T_i':

$$\left.\begin{aligned} \boldsymbol{e}_{ti}(u, v) &= \nabla_t T_i(u, v) \\ &\quad + \frac{\mu(u, v)}{\mu_0} \nabla_t T_i'(u, v) \times \boldsymbol{i}_z, \\ \boldsymbol{h}_{ti}(u, v) &= -\frac{\varepsilon(u, v)}{\varepsilon_0} \nabla_t T_i(u, v) \times \boldsymbol{i}_z \\ &\quad + \frac{h_i^2}{k_0^2} \nabla_t T_i'(u, v), \\ e_{zi}(u, v) &= \frac{\nabla_t \cdot \boldsymbol{h}_{ti} \times \boldsymbol{i}_z}{i\omega\varepsilon} = \frac{\nabla_t \cdot \left(\frac{\varepsilon}{\varepsilon_0} \nabla_t T_i \right)}{i\omega\varepsilon}, \\ h_{zi}(u, v) &= \frac{\nabla_t \cdot \boldsymbol{i}_z \times \boldsymbol{e}_{ti}}{i\omega\mu} = \frac{\nabla_t \cdot \left(\frac{\mu}{\mu_0} \nabla_t T_i' \right)}{i\omega\mu}, \end{aligned}\right\}$$

$$(2.11)$$

where h_i is defined:

$$h_i = \frac{\gamma_i}{i} = \beta_i - i\alpha_i. \qquad (2.12)$$

The relation $\boldsymbol{h}_t \propto \boldsymbol{i}_z \times \boldsymbol{e}_t$ in the plain waveguide is not valid in general in the hybrid-mode waveguide. The impedance of each mode is given by

$$\frac{V_i}{I_i} = \frac{h_i}{\omega\varepsilon_0} = Z_i = \frac{1}{Y_i}. \qquad (2.13)$$

This is used as the characteristic impedance for the TM mode in the plain waveguide. The expression for the TE mode in the plain waveguide can also be adopted by changing the coefficients of the eigenvectors (2.11) properly. It is only a matter of convenience which is adopted.

If ε and μ can be differentiated, from (2.5), (2.11) and (2.13), the following equations may be derived:

$$\left.\begin{aligned} \nabla_t \frac{\nabla_t \cdot \boldsymbol{h}_{ti} \times \boldsymbol{i}_z}{\varepsilon} &= -\frac{\chi_i^2}{\varepsilon_0} \nabla_t T_i, \\ \nabla_t \frac{\nabla_t \cdot \boldsymbol{i}_z \times \boldsymbol{e}_{ti}}{\mu} &= -\frac{\chi_i^2}{\mu_0} \nabla_t T_i'. \end{aligned}\right\} \tag{2.14}$$

Helmholtz's equation $\nabla_t^2 T + \chi^2 T = 0$, satisfied in the plain waveguide, is not generally valid in the hybrid-mode waveguide. The differential equation to decide T_i and T_i' is obtained by substituting (2.11) into (2.14). If ε and μ can be differentiated, under suitable boundary conditions:

$$\left.\begin{aligned} \nabla_t \left\{ \frac{\varepsilon_0}{\varepsilon} \nabla_t \cdot \left(\frac{\varepsilon}{\varepsilon_0} \nabla_t T_i \right) \right\} &= -\chi_i^2 \nabla_t T_i, \\ \nabla_t \left\{ \frac{\mu_0}{\mu} \nabla_t \cdot \left(\frac{\mu}{\mu_0} \nabla_t T_i' \right) \right\} &= -\chi_i^2 \nabla_t T_i'. \end{aligned}\right\} \tag{2.15}$$

The orthogonality relations of T_i and T_i', $\iint T_i T_j dS = \delta_{ij}$ satisfied in the plain waveguide is not generally valid in the hybrid-mode waveguide. In general, the orthogonal relation is as follows:

$$\iint_S (\boldsymbol{e}_{ti} \times \boldsymbol{h}_{tj}) \cdot \boldsymbol{i}_z dS = \delta_{ij}, \tag{2.16}$$

$$\delta_{ij} = \begin{matrix} 1 & (\text{in case of } i=j), \\ 0 & (\text{in case of } i \neq j), \end{matrix}$$

where S is the cross sectional area of the guide.⁽¹⁰⁾⁽¹¹⁾ From the above relation, the voltage and the current of each mode are obtained:

$$\left.\begin{aligned} V_i &= \iint_S (\boldsymbol{E}_t \times \boldsymbol{h}_{ti}) \cdot \boldsymbol{i}_z dS \\ &= \iint_S \boldsymbol{E}_t \cdot \left(\frac{\varepsilon}{\varepsilon_0} \nabla_t T_i + \frac{h_i^2}{k_0^2} \nabla_t T_i' \times \boldsymbol{i}_z \right) dS, \\ I_i &= \iint_S \boldsymbol{H}_t \cdot (\boldsymbol{i}_z \times \boldsymbol{e}_{ti}) dS \\ &= \iint_S \boldsymbol{H}_t \cdot \left(-\nabla_t T_i \times \boldsymbol{i}_z + \frac{\mu}{\mu_0} \nabla_t T_i' \right) dS. \end{aligned}\right\} \tag{2.17}$$

Now, we rewrite (2.2) as follows:

$$\left.\begin{aligned} -\frac{\partial}{\partial z} \boldsymbol{E}_t &= -\nabla_t E_z + i\omega\mu \boldsymbol{H}_t \times \boldsymbol{i}_z + \boldsymbol{M} \times \boldsymbol{i}_z, \\ -\frac{\partial}{\partial z} \boldsymbol{H}_t &= -\nabla_t H_z + i\omega\varepsilon \boldsymbol{i}_z \times \boldsymbol{E}_t + \boldsymbol{i}_z \times \boldsymbol{J}. \end{aligned}\right\} \tag{2.18}$$

We also rewrite (2.4) as follows:

$$\left.\begin{aligned} H_z &= \frac{\nabla_t \cdot \boldsymbol{i}_z \times \boldsymbol{E}_t - M_z}{i\omega\mu}, \\ E_z &= \frac{\nabla_t \cdot \boldsymbol{H}_t \times \boldsymbol{i}_z - J_z}{i\omega\varepsilon}. \end{aligned}\right\} \tag{2.19}$$

Substituting (2.19) into (2.18), and if J_z/ε and M_z/μ can be differentiated with respect to u and v, then

$$\left.\begin{aligned} -\frac{\partial}{\partial z} \boldsymbol{E}_t &= i\omega\mu \boldsymbol{H}_t \times \boldsymbol{i}_z - \frac{1}{i\omega} \nabla_t \frac{\nabla_t \cdot \boldsymbol{H}_t \times \boldsymbol{i}_z}{\varepsilon} \\ &\quad + \frac{1}{i\omega} \nabla_t \frac{J_z}{\varepsilon} + \boldsymbol{M} \times \boldsymbol{i}_z, \\ -\frac{\partial}{\partial z} \boldsymbol{H}_t &= i\omega\varepsilon \boldsymbol{i}_z \times \boldsymbol{E}_t - \frac{1}{i\omega} \nabla_t \frac{\nabla_t \cdot \boldsymbol{i}_z \times \boldsymbol{E}_t}{\mu} \\ &\quad + \frac{1}{i\omega} \nabla_t \frac{M_z}{\mu} + \boldsymbol{i}_z \times \boldsymbol{J}. \end{aligned}\right\} \tag{2.20}$$

These are fundamental equations relating to the source distribution and the actual fields. The electric and the magnetic currents are functions of u, v, and z; and ε and μ are functions of u and v. In many cases, these functions contain discontinuities. But, assuming δ-function distribution of the electric and magnetic currents, and also assuming a thin transition layer so that ε and μ vary rapidly but continuously, we can expect an exact solution. The upper equation of (2.20) is multiplied by $\boldsymbol{h}_{ti} \times \boldsymbol{i}_z$ scalarly, and the result is integrated over the cross section. Then we obtain:

$$-\frac{dV_i}{dz}=i\omega\iint\mu\boldsymbol{H}_t\times\boldsymbol{i}_z\cdot\boldsymbol{h}_{ti}\times\boldsymbol{i}_z dS$$

$$-\frac{1}{i\omega}\iint\nabla_t\frac{\nabla_t\cdot\boldsymbol{H}_t\times\boldsymbol{i}_z}{\varepsilon}\cdot\boldsymbol{h}_{ti}\times\boldsymbol{i}_z\, dS$$

$$+v_i(z), \qquad (2.21)$$

where

$$v_i(z)=\frac{1}{i\omega}\iint\nabla_t\frac{J_z}{\varepsilon}\cdot\boldsymbol{h}_{ti}\times\boldsymbol{i}_z dS.$$

$$+\iint\boldsymbol{M}\times\boldsymbol{i}_z\cdot\boldsymbol{h}_{ti}\times\boldsymbol{i}_z dS. \qquad (2.22)$$

The wall of the waveguide is assumed to be a perfect conductor. The impedance wall will be discussed later.

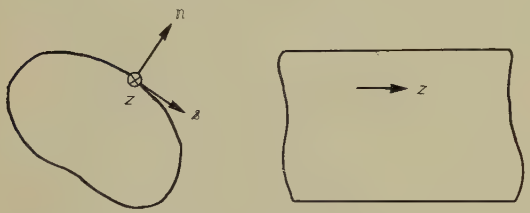

Fig. 1—Transverse and longitudinal cross sections of the waveguide.

Now let us mention of the vector formula, which is useful for the vector calculation. If a scalar function ϕ, a vector function $\boldsymbol{A}$ and their first derivatives are continuous on the surface S including the boundary curve, and the boundary curve is piecewise smooth, then

$$\iint\phi\nabla_t\cdot\boldsymbol{A}dS=-\iint\nabla_t\phi\boldsymbol{A}dS+\int\phi\boldsymbol{A}\cdot\boldsymbol{n}ds, \qquad (2.23)$$

where $\boldsymbol{n}$ is the outward unit vector and $\boldsymbol{s}$ is the tangential unit vector on the boundary curve as shown in Fig. 1; and $\boldsymbol{n}, \boldsymbol{s}$, and $\boldsymbol{i}_z$ make right hand system in this order. Taking advantage of (2.23), the second term of (2.21) becomes:

$$\iint\nabla_t\frac{\nabla_t\cdot\boldsymbol{H}_t\times\boldsymbol{i}_z}{\varepsilon}\cdot\boldsymbol{h}_{ti}\boldsymbol{i}_z dS$$

$$=-\iint\frac{\nabla_t\cdot\boldsymbol{H}_t\times\boldsymbol{i}_z}{\varepsilon}\nabla_t\cdot\boldsymbol{h}_{ti}\times\boldsymbol{i}_z dS$$

$$+\int\frac{\nabla_t\cdot\boldsymbol{H}_t\times\boldsymbol{i}_z}{\varepsilon}\boldsymbol{h}_{ti}\times\boldsymbol{i}_z\cdot\boldsymbol{n}ds$$

$$=-\iint\frac{\nabla_t\cdot\boldsymbol{h}_{ti}\times\boldsymbol{i}}{\varepsilon}\nabla_t\cdot\boldsymbol{H}_t\times\boldsymbol{i}\, dS$$

$$=\iint\nabla_t\frac{\nabla_t\cdot\boldsymbol{h}_{ti}\times\boldsymbol{i}}{\varepsilon}\cdot\boldsymbol{H}_t\times\boldsymbol{i}\, dS$$

$$-\int\frac{\nabla_t\cdot\boldsymbol{h}_{ti}\times\boldsymbol{i}}{\varepsilon}\boldsymbol{H}_t\times\boldsymbol{i}\cdot\boldsymbol{n}ds$$

$$=-\iint\frac{\chi_i^2}{\varepsilon_0}\nabla_t T_i\cdot\boldsymbol{H}_t\times\boldsymbol{i}\, dS. \qquad (2.24)$$

In this calculation, a perfect conducting wall is assumed. Using (2.11), (2.17), and (2.24); (2.21) becomes:

$$-\frac{dV_i(z)}{dz}=i\omega\iint\mu(\boldsymbol{H}_t\times\boldsymbol{i})\cdot\Big(\frac{\varepsilon}{\varepsilon_0}\nabla_t T_i$$

$$+\frac{h_i^2}{k_0^2}\nabla_t T_i'\times\boldsymbol{i}$$

$$-\frac{\chi_i^2}{\omega^2\varepsilon_0\mu}\nabla_t T_i\Big)dS+v_i(z)$$

$$=i\frac{h_i^2}{\omega\varepsilon_0}\iint\boldsymbol{H}\cdot\Big(-\nabla T\times\boldsymbol{i}$$

$$+\frac{\mu}{\mu_0}\nabla T\Big)dS+v(z)$$

$$=i\frac{h^2}{\omega\varepsilon_0}I_i(z)+v_i(z). \qquad (2.25)$$

The lower equation of (2.20) is multiplied by $\boldsymbol{i}_z\times\boldsymbol{e}_{ti}$ scalarly, and integrated over the cross section:

$$-\frac{dI_i}{dz}=i\omega\iint\varepsilon(\boldsymbol{i}\times\boldsymbol{E}_i)\cdot(\boldsymbol{i}\times\boldsymbol{e}_{ti})dS$$

$$-\frac{1}{i\omega}\iint\nabla_t\frac{\nabla_t\cdot\boldsymbol{i}\times\boldsymbol{E}_t}{\mu}\cdot\boldsymbol{i}\times\boldsymbol{e}_{ti}dS+i_i(z)$$

$$(2.26)$$

where,

$$i_i(z)=\frac{1}{i\omega}\iint\nabla_t\frac{M}{\mu}\cdot\boldsymbol{i}_z\times\boldsymbol{e}_{ti}dS+\iint\boldsymbol{i}_z\times\boldsymbol{J}\cdot\boldsymbol{i}_z\times\boldsymbol{e}_{ti}dS. \qquad (2.27)$$

Taking advantage of (2.23), the second term of (2.26) is transformed as follows:

$$\begin{aligned}\iint\nabla_t\frac{\nabla_t\cdot\boldsymbol{i}_z\times\boldsymbol{E}_t}{\mu}\cdot\boldsymbol{i}_z\times\boldsymbol{e}_{ti}dS &=-\iint\frac{\nabla_t\cdot\boldsymbol{i}_z\times\boldsymbol{E}_t}{\mu}\nabla_t\cdot\boldsymbol{i}_z\times\boldsymbol{e}_{ti}dS\\&\quad+\int\frac{\nabla_t\cdot\boldsymbol{i}_z\times\boldsymbol{E}_t}{\mu}\boldsymbol{i}_z\times\boldsymbol{e}_{ti}\cdot\boldsymbol{n}ds\\&=-\iint\frac{\nabla_t\cdot\boldsymbol{i}_z\times\boldsymbol{e}_{ti}}{\mu}\nabla_t\cdot\boldsymbol{i}_z\times\boldsymbol{E}_tdS\\&=\iint\nabla_t\frac{\nabla_t\cdot\boldsymbol{i}_z\times\boldsymbol{e}_{ti}}{\mu}\cdot\boldsymbol{i}_z\times\boldsymbol{E}_tdS\\&\quad-\int\frac{\nabla_t\cdot\boldsymbol{i}_z\times\boldsymbol{e}_{ti}}{\mu}\boldsymbol{i}\times\boldsymbol{E}_t\cdot\boldsymbol{n}ds\\&=-\iint\frac{\chi_i^2}{\mu_0}\nabla_tT_i'\cdot\boldsymbol{i}_z\times\boldsymbol{E}_tdS. \qquad (2.28)\end{aligned}$$

In this calculation, a perfect conducting wall is assumed. Using (2.11), (2.17), and (2.28); (2.26) becomes:

$$\begin{aligned}-\frac{dI_i}{dz}&=i\omega\iint\varepsilon(\boldsymbol{i}_z\times\boldsymbol{E}_t)\cdot\Big(-\nabla_tT_i\times\boldsymbol{i}_z\\&\quad+\frac{\mu}{\mu_0}\nabla_tT_i'-\frac{\chi_i^2}{\omega^2\varepsilon\mu_0}\nabla_tT_i'\Big)dS+i_i(z)\\&=i\omega\varepsilon_0\iint\boldsymbol{i}_z\times\boldsymbol{E}_t\cdot\boldsymbol{h}_{ti}dS+i_i(z)\\&=i\omega\varepsilon_0V_i(z)+i_i(z). \qquad (2.29)\end{aligned}$$

(2.25) and (2.29) are simply rewritten:

$$\left.\begin{aligned}-\frac{dV_i(z)}{dz}&=ih_iZ_iI_i(z)+v_i(z),\\-\frac{dI_i(z)}{dz}&=ih_iY_iV_i(z)+i_i(z).\end{aligned}\right\} \qquad (2.30)$$

Using the vector formula (2.23) the first terms of (2.22) and (2.27) are rewritten:

$$\left.\begin{aligned}\iint\nabla_t\frac{J_z}{\varepsilon}\cdot\boldsymbol{h}_{ti}\times\boldsymbol{i}_zdS&=-\iint\frac{J_z}{\varepsilon}\nabla_t\cdot\boldsymbol{h}_{ti}\times\boldsymbol{i}_zdS\\&\quad+\int\frac{J_z}{\varepsilon}(\boldsymbol{h}_{ti}\times\boldsymbol{i}_z\cdot\boldsymbol{n})ds,\\\iint\nabla_t\frac{M_z}{\mu}\cdot\boldsymbol{i}_z\times\boldsymbol{e}_{ti}dS&=-\iint\frac{M_z}{\mu}\nabla_t\cdot\boldsymbol{i}_z\times\boldsymbol{e}_{ti}dS\\&\quad+\int\frac{M_z}{\mu}(\boldsymbol{i}_z\times\boldsymbol{e}_{ti}\cdot\boldsymbol{n})ds.\end{aligned}\right\} \qquad (2.31)$$

The line integral of the lower equation of (2.31) vanishes because of the perfect conductor assumption. (2.22) and (2.27) are rewritten:

$$\left.\begin{aligned}v_i(z)&=-\iint J_z(u,v,z)e_{zi}(u,v)dS\\&\quad+\iint\boldsymbol{M}(n,v,z)\cdot\boldsymbol{h}_{ti}(u,v)dS\\&\quad+\frac{1}{i\omega}\int\frac{J_z}{\varepsilon}(\boldsymbol{h}_{ti}\times\boldsymbol{i}_z\cdot\boldsymbol{n})ds,\\i_i(z)&=-\iint M_z(u,v,z)h_{zi}(u,v)dS\\&\quad+\iint\boldsymbol{J}(u,v,z)\cdot\boldsymbol{e}_{ti}(u,v)dS.\end{aligned}\right\} \qquad (2.32)$$

These are extensions of the formulae for uniform material constants, given by N. Marcuvitz and J. Schwinger for the case of a non-uniform material.

It is preferable to discuss the relations between the modes in terms of the mode amplitudes, A_i^+ and A_i^-, rather than in terms of the mode voltage V_i and the mode current I_i.

$$\left.\begin{aligned} A_i^+(z) &= \frac{V_i(z)}{\sqrt{Z_i}} + \frac{I_i(z)}{\sqrt{Y_i}}, \\ A_i^-(z) &= \frac{V_i(z)}{\sqrt{Z_i}} - \frac{I_i(z)}{\sqrt{Y_i}}. \end{aligned}\right\} \tag{2.33}$$

$A_i^+(z)$ and $A_i^-(z)$ are the amplitudes of the waves propagating to $+z$ and $-z$ directions respectively. By these definitions, differential equations (2.30) become:

$$\left.\begin{aligned} -\frac{dA_i^+(z)}{dz} &= ih_iA_i^+(z) + a_i^+(z), \\ -\frac{dA_i^-(z)}{dz} &= -ih_iA_i^-(z) + a_i^-(z), \end{aligned}\right\} \tag{2.34}$$

where $a_i^+(z)$ and $a_i^-(z)$ are defined as:

$$\left.\begin{aligned} a_i^+(z) &= \frac{v_i(z)}{\sqrt{Z_i}} + \frac{i_i(z)}{\sqrt{Y_i}}, \\ a_i^-(z) &= \frac{v_i(z)}{\sqrt{Z_i}} - \frac{i_i(z)}{\sqrt{Y_i}}, \end{aligned}\right\} \tag{2.35}$$

where $v_i(z)$ and $i_i(z)$ are the source functions given in (2.32). (2.34) and (2.35) are the fundamental equations to obtain the mode generations in hybrid-mode waveguides by distributed sources. (2.34) can easily be solved. The waves propagating in the $+z$ and $-z$ directions are written as:

$$A_i^{\pm}(z) = -\int_{z1}^{z2} a_i^{\pm}(z')e^{\mp h_i(z-z')}dz'. \tag{2.36}$$

The integration is carried out over the range from $z=z_1$, to $z=z_2$, where the sources are distributed.

3. Electric and Magnetic Field in the Dielectric-Coated Waveguide

We shall discuss several properties of the dielectric-coated waveguide whose geometrical dimension is perfect and whose dissipation loss can be neglected. Some of these properties will be used for the calculation of the mode conversion and the bend, later. The circular cylindrical coordinates (r, φ, z) are used. The interior of the waveguide is composed of two parts as shown in Fig. 2, but the permeability μ is uniform in the waveguide and is μ_0. Two quantities ρ, and δ are defined as:

$$\frac{b}{a} = \rho = 1-\delta, \tag{3.1}$$

and

$$\delta = \frac{a-b}{a}. \tag{3.2}$$

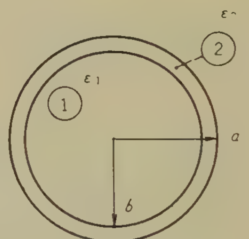

Fig. 2—Cross section of the dielectric-coated waveguide.

Two scalar functions $T_i(r, \varphi)$ and $T_i'(r, \varphi)$ are defined as:

$$T_i = \begin{cases} p_iJ_n(\chi_{1i}r)\begin{matrix}\sin\\ \cos\end{matrix}n\varphi \cdots\cdots\cdots\cdots 0<r<b \\ p_i\dfrac{\chi_{1i}^2}{\chi_{2i}^2}J_n(\chi_{1i}b)\;\dfrac{N_n(\chi_{2i}a)J_n(\chi_{2i}r)-J_n(\chi_{2i}a)N_n(\chi_{2i}r)}{N_n(\chi_{2i}a)J_n(\chi_{2i}b)-J_n(\chi_{2i}a)N_n(\chi_{2i}b)}\begin{matrix}\sin\\ \cos\end{matrix}n\varphi \cdots\cdots b<r<a, \end{cases} \tag{3.3}$$

$$T_i' = \begin{cases} q\,J_n(\chi_{i1}r)\begin{matrix}\cos\\ -\sin\end{matrix}n\varphi \cdots\cdots\cdots\cdots 0<r<b \\ q_1\dfrac{\chi_{1i}^2}{\chi_{2i}^2}J_n(\chi_{1i}b)\;\dfrac{N_n'(\chi_{2i}a)J_n(\chi_{2i}r)-J_n'(\chi_{2i}a)N_n(\chi_{2i}r)}{N_n'(\chi_{2i}a)J_n(\chi_{2i}b)-J_n'(\chi_{2i}a)N_n(\chi_{2i}b)}\begin{matrix}\cos\\ -\sin\end{matrix}n\varphi \cdots\cdots b<r<a. \end{cases} \tag{3.4}$$

These scalar functions satisfy

$$\left.\begin{aligned}\nabla_t^2 T_i + \chi_{\lambda i}^2 T_i &= 0,\\ \nabla_t^2 T_i' + \chi_{\lambda i}^2 T_i' &= 0,\end{aligned}\right\} \tag{3.5}$$

in region ① and ② respectively. The subscript λ represents the region and is 1 or 2. It has been shown in the preceding section that (3.5) is invalid in the general case, but it is valid in the part where both ε and μ are constant. This may be understood easily from the relation of (2.15). The exial components of the field are

$$\begin{aligned} e_{zi} &= -\frac{\chi_{\lambda i}^2}{i\omega\varepsilon_0} T_i,\\ h_{zi} &= -\frac{\chi_{\lambda i}^2}{i\omega\mu_0} T_i' \end{aligned} \tag{3.6}$$

(3.3) and (3.4) satisfy

$$\begin{aligned} &e_{zi} = e_{\varphi i} = 0 && \text{at } r=a,\\ &e_{zi}① = e_{zi}② && \text{at } r=b,\\ &h_{zi}① = h_{zi}② && \text{at } r=b. \end{aligned} \tag{3.7}$$

p_i, q_i, χ_{1i}, χ_{2i} and the propagation constant h_i are obtained from the continuities of $e_{\varphi i}$ and $h_{\varphi i}$ at $r=b$, the normalized orthogonality of the mode vectors and the dielectric constants of both regions. The continuity of $e_{\varphi i}$ at $r=b$ is:

$$\frac{np_i}{b} J_n(\chi_{1i}b) - q_i\chi_{1i} J_n'(\chi_{1i}b) = \frac{np_i}{b}\,\frac{\chi_{1i}^2}{\chi_{2i}^2} J_n(\chi_{1i}b)$$
$$-\frac{q_i\chi_{1i}^2}{\chi_{2i}} J_n(\chi_{1i}b)\,\frac{N_n'(\chi_{2i}a)J_n'(\chi_{2i}b) - J_n'(\chi_{2i}a)N_n'(\chi_{2i}b)}{N_n'(\chi_{2i}a)J_n(\chi_{2i}b) - J_n'(\chi_{2i}a)N_n(\chi_{2i}b)}. \tag{3.8}$$

The continuity of $h_{\varphi i}$ at $r=b$ is:

$$\frac{\varepsilon_1}{\varepsilon_0}\left\{p_i\chi_{1i}J_n'(\chi_{1i}b) - nq_i\frac{h_i^2}{k_1^2 b}J_n(\chi_{1i}b)\right\}$$
$$= \frac{\varepsilon_2}{\varepsilon_0}\left\{\frac{p_i\chi_{1i}^2}{\chi_{2i}}J_n(\chi_{1i}b)\,\frac{N_n(\chi_{2i}a)J_n'(\chi_{2i}b) - J_n(\chi_{2i}a)N_n'(\chi_{2i}b)}{N_n(\chi_{2i}a)J_n(\chi_{2i}b) - J_n(\chi_{2i}a)N_n(\chi_{2i}b)} - nq_i\frac{h_i^2}{k_2^2 b}\,\frac{\chi_{1i}^2}{\chi_{2i}^2}J_n(\chi_{1i}b)\right\} \tag{3.9}$$

If the thickness of the dielectric layer is very thin, namely $1-\rho \ll 1$, and if $\chi^2 a\delta$ is very small compared with unity, T_i and T_i' in the region ② and the cylindrical functions at $\chi_{2i}r$ and $\chi_{2i}b$ in (3.8) and (3.9) can be expanded in power series of δ as follow:

$$\left.\begin{aligned}
&N_n(z)J_n(\rho z) - J_n(z)N_n(\rho z)\\
&\quad = \frac{2\delta}{\pi} + \frac{\delta^2}{\pi} + \frac{z^2}{3\pi}\left(1 - \frac{n^2+2}{z^2}\right)\delta^3 + \cdots\cdots\cdots,\\
&N_n'(z)J_n(\rho z) - J_n'(z)N_n(\rho z)\\
&\quad = \frac{2}{\pi z} - \frac{2}{\pi}\left(1 - \frac{n^2}{z^2}\right)\delta^2 + \cdots\cdots\cdots\cdots\cdots,\\
&N_n'(z)J_n'(\rho z) - J_n'(z)N_n'(\rho z)\\
&\quad = \frac{2}{\pi}\left(1 - \frac{n^2}{z^2}\right)\delta + \frac{1}{\pi}\left(1 - \frac{3n^2}{z^2}\right)\delta^2\\
&\quad\quad - \frac{z^2}{3\pi}\left(1 - \frac{2n^2+2}{z^2} + \frac{n^4+11n^2}{z^4}\right)\delta^3 + \cdots,\\
&N_n(z)J_n'(\rho z) - J_n(z)N_n'(\rho z)\\
&\quad = -\frac{2}{\pi z} - \frac{2\delta}{\pi^2} - \frac{2}{\pi}\left(1 - \frac{n^2+2}{z^2}\right)\delta^2 + \cdots.
\end{aligned}\right\} \tag{3.10}$$

Taking advantage of (3.10), the two continuity equations (3.8) and (3.9) are simplified as:

$$\left.\begin{aligned}
&p\frac{n}{b}\left(\frac{1}{\chi_1^2}-\frac{1}{\chi_2^2}\right)-q\left[\frac{1}{\chi_1}\frac{J_n'(\chi_1 b)}{J_n(\chi_1 b)}\right.\\
&\qquad\left.-\left\{\left(1-\frac{n^2}{\chi_2^2a^2}\right)+\frac{1}{2}\left(1-\frac{3n^2}{\chi_2^2a^2}\right)\delta\right\}a\delta\right]=0,\\
&p\left\{\frac{\varepsilon_1}{\varepsilon_0}\frac{1}{\chi_1}\frac{J_n'(\chi_1 b)}{J_n(\chi_1 b)}+\frac{\varepsilon_2}{\varepsilon_0}\frac{1}{\chi_2^2a\delta}\left(1+\frac{\delta}{2}\right)\right\}\\
&\qquad-qn\frac{h_i^2}{k_0^2b}\left(\frac{1}{\chi_1^2}-\frac{1}{\chi_2^2}\right)=0.
\end{aligned}\right\}\tag{3.11}$$

There are two sets of solutions for these characteristic equations. One of them reduces to that of the TM modes of the plain waveguide when δ is reduced to zero, the other is reduced to that of the TE modes. The modes concerning the former are simply called TM modes, and the latter are called TE modes. We shall distinguish them by enclosing the subscripts in parentheses for TM modes and in brackets for TE modes. χ_1 is a function of the thickness of the layer, and varies greatly from that of the plain waveguide even if δ is very small. Although the approximation is not good, it is useful to expand $J_n(\chi_1 b)$ and $J_n'(\chi_1 b)$ into power series of $\chi_1 a\delta$.

In case of the TM modes, if we set

$$\chi_{1(i)}=\chi_{(i)}+\Delta\chi_{(i)},\quad\text{where } J_n(\chi_{(i)}a)=0,\tag{3.12}$$

then

$$\begin{aligned}
&J_n(\chi_{1(i)}b)\doteqdot(\Delta\chi_{(i)}-\chi_{(i)}\delta)aJ_n'(\chi_{(i)}a),\\
&J_n'(\chi_{1(i)}b)\doteqdot J_n'(\chi_{1(i)}a),
\end{aligned}\tag{3.13}$$

and we obtain from (3.11)

$$\Delta\chi_{(i)}=\chi_{(i)}\left\{1-\frac{\varepsilon_1}{\varepsilon_2}\left(1+\frac{\varepsilon_2-\varepsilon_1}{\varepsilon_0}\frac{k_0^2}{\chi_{(i)}^2}\right)\right\}\delta,\tag{3.14}$$

and

$$q_{(i)}=-p_{(i)}n\frac{\varepsilon_1}{\varepsilon_2}\frac{\varepsilon_2-\varepsilon_1}{\varepsilon_0}\frac{k_0^2}{\chi_{(i)}^2}\delta.\tag{3.15}$$

In case of the TE modes, if we set

$$\chi_{1[i]}=\chi_{[i]}+\Delta\chi_{[i]},\quad\text{where } J_n'(\chi_{[i]}a)=0,\tag{3.16}$$

then

$$\left.\begin{aligned}
&J_n'(\chi_{1[i]}b\doteqdot-(\Delta\chi_{[i]}-\chi_{[i]}\delta)\\
&\qquad\times\left(1-\frac{n^2}{\chi_{[i]}^2a^2}\right)aJ_n(\chi_{[i]}a),\\
&J_n(\chi_{1[i]}b)\doteqdot J_n(\chi_{[i]}a),
\end{aligned}\right\}\tag{3.17}$$

and we obtain from (3.11)

$$\Delta\chi=-\frac{\varepsilon_2-\varepsilon_1}{\varepsilon_2}\frac{n^2k_0^2}{(\chi_{[i]}^2a^2-n^2)\chi_{[i]}}\delta,\tag{3.18}$$

and

$$p_{[i]}=q_{[i]}n\frac{\varepsilon_2-\varepsilon_1}{\varepsilon_2}\frac{h_{[i]}^2}{\chi_{[i]}^2}\delta.\tag{3.19}$$

The φ components of the electric fields at the boundary between the dielectric and the air must be known to calculate the mode generations from the irregularities of the thickness of the dielectric layer. As the thickness of the layer is very thin, we take only the first order of Δr, where,

$$r=a-\Delta r.\tag{3.20}$$

For the TE_{01} mode,

$$E_\varphi=-V_{[01]}q_{[01]}\chi_{[01]}^2\Delta rJ_0(\chi_{[01]}a)\tag{3.21}$$

This is the same expression as the electric field component when $\varepsilon_2=\varepsilon_1$. At the boundary between the dielectric and the air

$$E_\varphi(r=b)=-V_{[01]}q_{[01]}\chi_{[01]}^2a\delta J_0(\chi_{[01]}a)\tag{3.22}$$

For the TM modes,

$$\left.\begin{aligned}
&E_{\varphi\textcircled{1}}=V_{(i)}p_{(i)}n\chi_{(i)}\left\{\frac{\varepsilon_2-\varepsilon_1}{\varepsilon_2}\delta-\frac{\Delta r}{a}\right\}\\
&\qquad\times J_n'(\chi_{(i)}a)\begin{smallmatrix}\cos\\-\sin\end{smallmatrix}n\varphi,\\
&E_{\varphi\textcircled{2}}=-V_{(i)}p_{(i)}\frac{n\chi_{(i)}}{a}\frac{\varepsilon_1}{\varepsilon_2}\\
&\qquad\times J_n'(\chi_{(i)}a)\Delta r\begin{smallmatrix}\cos\\-\sin\end{smallmatrix}n\varphi.
\end{aligned}\right\}\tag{3.23}$$

And for the TE mode

$$\left.\begin{aligned} E_{\varphi①} &= -V_{[i]}q_{[i]}\frac{1}{a}J_n(\chi_{[i]}a)\left\{(\chi_{[i]}^2a^2-n^2)\right. \\ &\quad \times \left.\frac{\Delta r}{a}+\frac{\varepsilon_2-\varepsilon_1}{\varepsilon_2}n^2\delta\right\}\substack{\cos\\ -\sin}n\varphi, \\ E_{\varphi②} &= -V_{[i]}q_{[i]}J_n(\chi_{[i]}a) \\ &\quad \times \frac{\Delta r}{a^2}\left(\chi_{[i]}^2a^2-\frac{\varepsilon_1}{\varepsilon_2}n^2\right)\substack{\cos\\ -\sin}n\varphi. \end{aligned}\right\} \tag{3.24}$$

Substituting $\Delta r = a\delta$ into (3.23) and (3.24), the fields at the boundary can be obtained. In (3.21) to (3.24), $\chi_{[i]}$ and $\chi_{(i)}$ are the roots of $J_n'(\chi_{[i]}a)=0$ and $J_n(\chi_{(i)}a)=0$ respectively.

The coefficients p_i and q_i are calculated from the normalized orthogonality relation which is written, using (2.11) and (2.16), as:

$$\begin{aligned} &\iint_S (\boldsymbol{e}_{ti}\times\boldsymbol{h}_{ti})\cdot\boldsymbol{i}_z\,dS \\ &=\iint_S(\nabla_tT_i+\nabla_tT_i'\times\boldsymbol{i}_z)\cdot\left(\frac{\varepsilon}{\varepsilon_0}\nabla_tT_i\right. \\ &\quad+\left.\frac{h_i^2}{k_0^2}\nabla_tT_i'\times\boldsymbol{i}_z\right)dS \\ &=\iint_S\left\{\frac{\varepsilon}{\varepsilon_0}(\nabla_tT_i)^2+\frac{h_i^2}{k_0^2}(\nabla_tT_i')^2\right. \\ &\quad+\left.\frac{h_i^2+k^2}{k_0^2}\nabla_tT_i\cdot\nabla_tT_i'\times\boldsymbol{i}_z\right\}dS=1. \end{aligned} \tag{3.25}$$

As T_i and T_i' of (3.25) satisfy (3.5) in each region respectively, we can utilize the vector formulae(6):

$$\left.\begin{aligned} &\iint_S(\nabla_tT_i)^2dS=\iint_S\chi^2{}_iT_i^2dS \\ &\qquad\qquad+\int_s T_i\frac{\partial T_i}{e_1\partial u}ds, \\ &\iint_S\nabla_tT_i\cdot\nabla_tT_i'\times\boldsymbol{i}_z\,dS \\ &=\int T_i\cdot\frac{\partial T_i'}{\partial s}ds=-\int T_i'\frac{\partial T_i}{\partial s}ds. \end{aligned}\right\} \tag{3.26}$$

Taking advantage of (3.10) and (3.26), the orthogonality relation (3.25) becomes:

$$\begin{aligned} &\int_0^{2\pi}\int_0^b\frac{\varepsilon_1}{\varepsilon_0}\chi_{1i}^2p_i^2J_n^2(\chi_{1i}r)\substack{\sin^2\\ \cos^2}n\varphi\,rdrd\varphi \\ &+\frac{\varepsilon_1}{\varepsilon_0}\int_0^{2\pi}p_i^2\chi_{1i}J_n(\chi_{1i}b)J_n'(\chi_{1i}b)\substack{\sin^2\\ \cos^2}n\varphi\,bd\varphi \\ &+\int_0^{2\pi}\int_a^b\frac{\varepsilon_2}{\varepsilon_0}\chi_{2i}^2p_i^2\frac{\chi_{1i}^4}{\chi_{2i}^4} \\ &\quad\times J_n^2(\chi_{1i}b)\left(\frac{a-r}{a\delta}\right)^2\substack{\sin^2\\ \cos^2}u\varphi\,rdrd\varphi \\ &+\frac{\varepsilon_2}{\varepsilon_0}\int_0^{2\pi}\left\{p_i\frac{\chi_{1i}^2}{\chi_{2i}^2}J_n(\chi_{1i}b)\substack{\sin\\ \cos}n\varphi\right\} \\ &\quad\times\left\{p_i\frac{\chi_{1i}^2}{\chi_{2i}^2}J_n(\chi_{1i}b)\frac{1}{a\delta}\substack{\sin\\ \cos}n\varphi\right\}bd\varphi \\ &+\frac{h_i^2}{k_0^2}\left[\int_0^{2\pi}\int_0^b\chi_{1i}^2q_i^2J_n^2(\chi_{1i}r)\substack{\cos^2\\ \sin^2}n\varphi\,rdr\,d\varphi\right. \\ &+\int_0^{2\pi}q_i^2\chi_{1i}J_n(\chi_{1i}b)J_n'(\chi_{1i}b)\substack{\cos^2\\ \sin^2}n\varphi\,b\,d\varphi \\ &+\left.\int_0^{2\pi}\int_b^a\chi_{2i}^2q_i^2\frac{\chi_{1i}^4}{\chi_{2i}^4}J_n^2(\chi_{1i}b)\substack{\cos^2\\ \sin^2}n\varphi\,rdr\,d\varphi\right] \\ &+\left[\frac{h_i^2+k_1^2}{k_0^2}\int_0^{2\pi}\left\{p_iJ_n(\chi_{1i}b)\substack{\sin\\ \cos}n\varphi\right\}\right. \\ &\quad\times\left\{q_i\frac{1}{b}J_n(\chi_{1i}b)n\substack{-\sin\\ -(1-\delta_{n0})\cos}n\varphi\right\}b\,d\varphi \\ &-\frac{h_i^2+k_2^2}{k_0^2}\int_0^{2\pi}\left\{p_i\frac{\chi_{1i}^2}{\chi_{2i}^2}J_n(\chi_{1i}b)\substack{\sin\\ \cos}n\varphi\right\} \\ &\quad\times\left\{q_i\frac{1}{b}\frac{\chi_{1i}^2}{\chi_{2i}^2}J_n(\chi_{1i}b)n\substack{-\sin\\ -(1-\delta_{n0})\cos}n\varphi\right\} \\ &\left.b\,d\varphi\right]=1, \end{aligned} \tag{3.27}$$

where δ_{n0} is defined in (2.16). The normalizing factors p, and q are obtained from (3.27). Only the zeroth and first order terms of δ are calculated. For the TM modes,

$$p_{(i)}=p_{(nm)}=\sqrt{\frac{\varepsilon_0}{\varepsilon_1}}\sqrt{\frac{\varepsilon_n}{\pi}}\frac{1}{\chi_{(i)}aJ_{n-1}(\chi_{(i)}a)}$$

$$\times\left(1+\frac{\varepsilon_1}{\varepsilon_2}\frac{\varepsilon_2-\varepsilon_1}{\varepsilon_0}\frac{k_0^2}{\chi_{(i)}^2}\delta\right) \qquad (3.28)$$

where

$$\varepsilon_n=\begin{matrix}1 & \text{if} \quad n=0,\\ 2 & \text{if} \quad n\neq 0.\end{matrix} \qquad (3.29)$$

And for the TE modes,

$$q_{[i]}=q_{[nm]}=\sqrt{\frac{\varepsilon_n}{\pi}}\frac{1}{\sqrt{\chi^2_{[i]}a^2-n^2}\,J_n(\chi_{[i]}a)}$$

$$\times\frac{k_0}{h_{[i]}}(1+F\delta), \qquad (3.30)$$

where

$$F=\frac{n^2}{(\chi_{[i]}^2a^2-n^2)}\left\{1+\frac{\varepsilon_2-\varepsilon_1}{\varepsilon_2}\frac{n^2k_0^2}{(\chi^2_{[i]}a^2-n^2)\chi_{[i]}^2}\right.$$

$$-\frac{1}{\left(1+\frac{\varepsilon_2-\varepsilon_1}{\varepsilon_2}\frac{k_0^2}{\chi_{[i]}^2}\right)^2}+\frac{\varepsilon_n}{2}\frac{\varepsilon_2-\varepsilon_1}{\varepsilon_2}\frac{h_{[i]}+k_1^2}{\chi_{[i]}^2}$$

$$-\frac{\varepsilon_n}{2}\frac{\varepsilon_2-\varepsilon_1}{\varepsilon_2}\frac{k_0^2}{\chi_{[i]}^2}\frac{1}{\left(1+\frac{\varepsilon_2-\varepsilon_1}{\varepsilon_2}\frac{k_0^2}{\chi_{[i]}^2}\right)^2}$$

$$\left.\times\left(\frac{h_{[i]}^2+k_2^2}{k_0^2}+\frac{\varepsilon_2-\varepsilon_1}{\varepsilon_1}\frac{h_{[i]}^2}{\chi_{[i]}^2}\right)\right\}. \qquad (3.31)$$

4. The Mode Conversion by the Irregularity of the Thickness of the Dielectric Layer in the Dielectric-Coated Waveguide

If the thickness of the dielectric layer is not uniform in dielectric-coated waveguides, mode conversion occurs from these non-uniformities. It is known that this kind of waveguide has very excellent characteristics for circular electric wave transmission around bends if it has perfect dimensions.⁽¹⁾ Therefore, it is necessary to know the mode conversion loss by the non-uniformity, of the thickness of the dielectric layer to determine the tolerance of the thickness, and to infer the cause of the attenuation increase if any. But it is very difficult to know precisely the thickness in an actual waveguide. And in the following calculation of the mode conversion, for simplicity several assumptions are made. Therefore, only a rough estimation of the mode conversion can be obtained, but it may be very useful in practice.

We shall use some assumptions in the calculation of the mode conversion. The dimensions of the metal waveguide are perfect, the conductivity of the wall is infinite, and the waveguide is straight. Let the normal thickness of the dielectric layer be t, and its length be l, t is not necessarily the mean thickness. The thickness of the layer is expressed as a function of position as:

$$t+t_1(\varphi, z). \qquad (4.1)$$

t_1 is positive at places thicker than the normal thickness, and is negative at thinner places. Fig. 3 shows an elementary irregularity. We now assume:

$$t\ll a, \qquad (4.2)$$

and

$$t_1\ll t. \qquad (4.3)$$

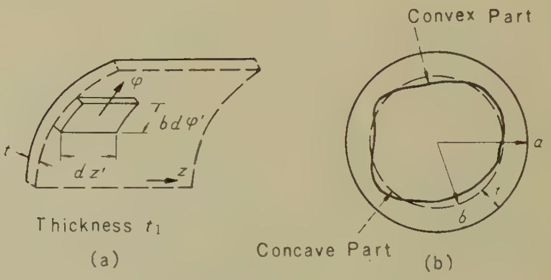

(a) Elementary irreguiarity.
(b) Cross Section.

Fig. 3—Irregularity of the dielectric layer thickness.

At the thickness irregularity, it is considered that there exists the distribution of the dielectric, at $r=b$, which dielectric constant is ε_2 and the thickness is $t_1(\varphi, z)$ in the uniform waveguide for the z direction, and it can be replaced by equivalent current distribution which is equal to partial derivative, with respect to the time, of the polarization vector induced at the dielectric. The mode conversion by the irregularities of the thickness of the layer can be derived from the problem of the mode generation from the distributed current in the waveguide. Strictly speaking, the polarization vector by the exact electric field in which the perturbation of the incident TE$_{01}$ wave by the irregularities is taken into consideration, must be used as the source of the mode generation. But the perturbation is neglected here because of (4.2) and (4.3).

The elementary irregularity whose thickness is t_1 at the point (b, φ', z') is shown in Fig. 3 (a). Then, the equivalent current $\boldsymbol{J}$ is the time derivative of the polarization vector which is the product of $(\varepsilon_2-\varepsilon_1)$ and the eletric field at the part, namely $V_{[01]}(z)\,\boldsymbol{e}_{[01]}(b, \varphi')$. The time variation is assumed as $e^{i\omega t}$, then $i(z)$ of small length part of z direction is:

$$\left.\begin{aligned}
\delta i_i(z') &= b\,d\varphi' \int_{b-t_1}^{b} i\omega(\varepsilon_2-\varepsilon_1)\, V_{[01]}(z')\,\boldsymbol{e}_{t[01]}(b, \varphi')\cdot\boldsymbol{e}_{ti}(b, \varphi')\,dr \qquad \text{in convex part,}\\
\delta i_i(z') &= -b\,d\varphi' \int_{b}^{b-t_1} (\text{the integrand in above equation})\ dr' \qquad \text{in concave part.}
\end{aligned}\right\} \tag{4.4}$$

They are integrated with φ', then in both regions,

$$i_t(z') = i\omega(\varepsilon_2-\varepsilon_1)\, V_{[01]}(z') \int_{-\pi}^{\pi} t_1(\varphi, z')\,\boldsymbol{e}_{t[01]}(b, \varphi')\cdot\boldsymbol{e}_{ti}(b, \varphi')\,b\,d\varphi' \tag{4.5}$$

And $a_i^{\pm}$ of (2.35) is

$$a_i^{\pm}(z') = \pm\sqrt{\frac{h_i}{\omega\varepsilon_0}}\, i_i(z'), \tag{4.6}$$

then, from (2.36) the amplitudes of the mode i generated by the elementary irregularity become:

$$A_i^{\pm}(z) = \mp\sqrt{\frac{h_i}{\omega\varepsilon_0}}\, e^{\mp i h_i z} \int_{z_1}^{z_2} i_i(z')\, e^{\pm i h_{iz'}}\, dz'. \tag{4.7}$$

Here, we define the following quantities:

$$\left.\begin{aligned}
V_{[01]}(z) &= \overline{V}_{[01]} e^{-ih_{[01]}z}\\
A_i^{\pm}(z) &= \overline{A}_i^{\mp} e^{\mp i h_i z},\\
\boldsymbol{e}_{ti}(r, \varphi) &= e_{ri}(r, \varphi)\,\boldsymbol{i}_r + e_{\varphi i}(r, \varphi)\,\boldsymbol{i}_{\varphi},
\end{aligned}\right\} \tag{4.8}$$

then

$$\begin{aligned}
\overline{A}_i^{\pm} = \mp\sqrt{\frac{h_i}{\omega\varepsilon_0}}\, i\omega(\varepsilon_2-\varepsilon_1)\,\overline{V}_{[01]}\\
\times\{-q_{[01]}\chi_{[01]}{}^2 a\delta J_0(\chi_{[01]}a)\}a\\
\times\int_{-\frac{l}{2}}^{\frac{l}{2}}\int_{-\pi}^{\pi} t_1(\varphi', z')\, e_{\varphi i}(b, \varphi')\\
\times\exp(-ih_{[01]}z' \pm ih_i z')\,d\varphi'\,dz'.
\end{aligned} \tag{4.9}$$

where, in cases of the TM and TE modes, respectively, $e_{\varphi i}(b,\varphi')$ becomes as follows from (3.23) and (3.24):

$$\left.\begin{aligned}
e_{\varphi(nm)}(b, \varphi) &= -p_{(nm)} n \chi_{(nm)}\\
&\quad\times \frac{\varepsilon_1}{\varepsilon_2}\,\delta J_n'(\chi_{(nm)}a) \begin{matrix}\cos\\ -\sin\end{matrix} n\varphi\\
e_{\varphi[nm]}(b, \varphi) &= -q_{[nm]}\frac{\delta}{a}\Big(\chi^2{}_{[nm]}a^2\\
&\quad -\frac{\varepsilon_1}{\varepsilon_2}n^2\Big) J_n(\chi_{[nm]}a) \begin{matrix}\cos\\ -\sin\end{matrix} n\varphi
\end{aligned}\right\} \tag{4.10}$$

The mode conversion coefficient is the ratio of the amplitude of the converted mode i to the amplitude of the incident TE$_{01}$ mode. The generated mode is resolved into two parts, one given by the upper part of the double trigonometric functions in (4.10), the other given by the lower part. The former coefficient is written as C_i, the latter as S_i. The double sign $^{\pm}$ shows the direction of propagation of the waves. The four kinds of conversion coefficients are written as:

$$\begin{matrix} C_i^{\pm} \\ S_i^{\pm} \end{matrix} = \frac{\overline{A}^{\pm}}{\dfrac{2\overline{V}_{[01]}}{\sqrt{Z_{[01]}}}} = \sqrt{\frac{h_{[01]}}{\omega\varepsilon_0}}\,\frac{\overline{A}_i^{\pm}}{2\overline{V}_{[01]}}. \qquad (4.11)$$

Substituting (4.9) and (4.10) into (4.11), we get

$$\begin{matrix} C_{(i)}^{\pm} \\ S_{(i)}^{\pm} \end{matrix} = \mp\frac{\phi_{(i)}}{\lambda}\int_{-\frac{l}{2}}^{\frac{l}{2}}\int_{-\pi}^{\pi}\frac{t_1(\varphi', z')}{a}\begin{matrix} \cos \\ -\sin \end{matrix} n\varphi'$$

$$\times\exp(-ih_{[01]}z' \pm ih_{(i)}z')\,d\varphi' dz', \qquad (4.12)$$

where

$$\phi_{(i)} = i\sqrt{2}\,nk_{[01]}\frac{\varepsilon_2-\varepsilon_1}{\varepsilon_2}\sqrt{\frac{h_{(i)}}{h_{[01]}}}\,\delta^2, \qquad (4.13)$$

and

$$\begin{matrix} C_{[i]}^{\pm} \\ S_{[i]}^{\pm} \end{matrix} = \pm\frac{\phi_{(i)}}{\lambda}\int_{-\frac{l}{2}}^{\frac{l}{2}}\int_{-\pi}^{\pi}\frac{t_1(\varphi', z')}{a}\begin{matrix} \cos \\ -\sin \end{matrix} n\varphi'$$

$$\times\exp(-ih_{[01]}z' \pm ih_{[i]}z')\,d\varphi'\, dz', \qquad (4.14)$$

where

$$\phi_{[i]} = i\sqrt{\varepsilon_n}\,\frac{\varepsilon_2-\varepsilon_1}{\varepsilon_1}\,\frac{k_0}{\sqrt{h_{[01]}h_{[i]}}}$$

$$\times\frac{k_{[01]}\{k_{[i]}^2-(\varepsilon_1/\varepsilon_2)n^2\}}{\sqrt{k_{[i]}^2-n^2}}\delta^2. \qquad (4.15)$$

In these equations $k_{(nm)} = \chi_{(nm)}a$ is the mth root of $J_n(z) = 0$ other than zero, and $k_{[nm]} = \chi_{[0m]}a$ is the mth root of $J_n'(z) = 0$ other than zero. Obviously from (4.13), the mode conversion to the TM_{om} modes does not occur.

5. Examples of the Mode Conversion by the Thickness Irregularities of the Dielectric Layer

In the first place, we will calculate the mode conversion from the parts of the dielectric layer thicker than the normal part as shown in Fig. 4. No variation for the φ direction is assumed. In case of thinner parts, only the sign is reversed. The irregularity of the thickness is expressed as:

$$t_1 = t_m\cos\frac{\pi z}{l}. \qquad (5.1)$$

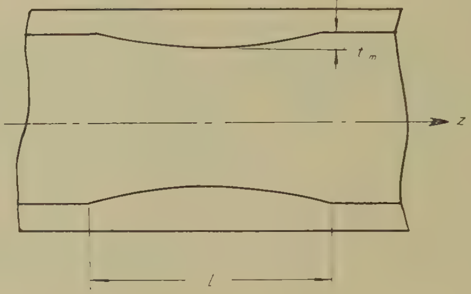

Fig. 4—Bulge of the dielectric layer shickness.

In the thinner case, t_m has a negative value. Obviously from (4.12) and (4.14), only TE_{0m} modes generate.

$$C_{[0m]}^{\pm} = \mp\frac{\phi_{[0m]}}{\lambda}2\pi\frac{t_m}{a}\int_{-\frac{l}{2}}^{\frac{l}{2}}\cos\frac{\pi z'}{l}\exp(-ih_{[01]}\mp ih_{[0m]})z'dz'$$

$$= \mp4\pi^2\phi_{[0m]}\frac{t_m}{a}\,\frac{l}{\lambda}\,\frac{\cos(h_{[01]}\mp h_{[0m]})\dfrac{l}{2}}{\pi^2-(h_{[01]}\mp h_{[0m]})^2l^2}. \qquad (5.2)$$

A numerical calculation will be made with the assumptions:

$$\varepsilon_2 = 2.3,$$

$$\delta = 0.01,$$

$$\frac{t_m}{a} = 1.96\times10^{-3}$$

Table 1

$\phi_{[0m]}$ UNDER THE CONDITION (5.3)

m	1	2	3	4	5	6	7	8
$(1/i)\phi_{[0m]}$	——	3.58×10^{-3}	5.29×10^{-3}	7.17×10^{-3}	9.29×10^{-3}	1.20×10^{-2}	1.46×10^{-2}	2.61×10^{-2}

(when $2a=51$ mm, $t_m=50$ microns). (5.3)

Table 1 shows $-i\phi_{[0m]}$. Fig. 5 shows the mode conversion coefficients as functions of l when the frequency is 50 Gc/s. The insertion loss due to the mode conversions is

$$L=4.343\sum_{m=2}^{\infty}\sum_{\pm}|C_{[0m]}^{\pm}|^2 \text{ dB}, \qquad (5.4)$$

where, $|C_{[0m]}^{\pm}|\ll1$ is assumed. The insertion loss L is shown in Fig. 6 as a function of the length l, and it has a very small value.

The mode conversion loss is proportional to the square of t_m. A large percentage of the converted power is carried by the TE_{02} mode. When $l=20$ cm, TE_{02} contributes about 97.90 % of the total conversion loss, TE_{03} does 1.70 %, TE_{04} does 0.34 %, TE_{05} does 0.04 %, and the sum total of TE_{06}, TE_{07} and TE_{08} and all the modes propagating in the negative direction contribute the remainder. However, when l is very short, the conversions to high order modes are not so small. For example, when $l=4$ cm, TE_{02} contributes 26.37 %, TE_{03} does 42.10 %, TE_{04} does 29.37 %, TE_{05} does 1.33 %, TE_{06} does 0.67 %, TE_{07} does 0.00 %, TE_{08} does 0.17 % and all the modes propagating in the negative direction contribute the remainder.

The second example of the irregularity of the thickness of the layer is the onesided dielectric as shown in Fig. 7. In this case, t_1 is written as:

$$t_1=t_m\cos\varphi\cos\frac{\pi z}{l}. \qquad (5.5)$$

This type of deformation couples TM_{1m} and TE_{1m} modes to the TE_{01} wave.

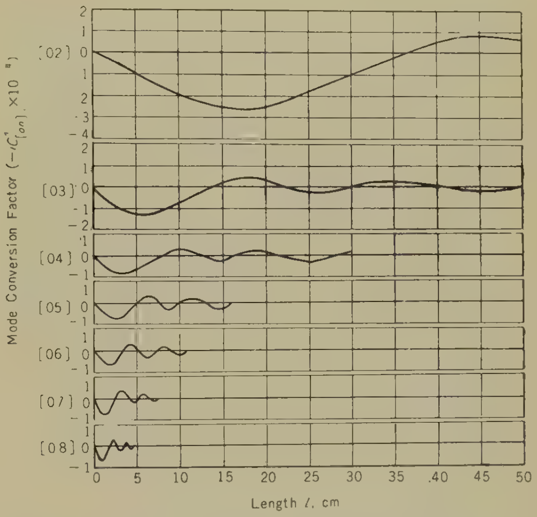

Fig. 5—Mode conversion factor by the bulge of the dielectric layer.

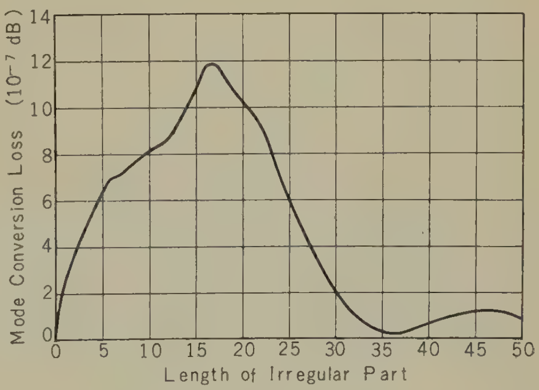

Fig. 6—Mode conversion loss due to the bulge of the dielectric layer.

Table 2

$\phi_{(1m)}$ AND $\phi_{[1m]}$ UNDER THE CONDITION (5.3)

m	1	2	3	4	5	6	7	8
$(1/i)\phi_{[1m]}$	3.07×10^{-4}	3.03×10^{-4}	2.96×10^{-4}	2.87×10^{-4}	2.74×10^{-4}	2.54×10^{-4}	2.40×10^{-4}	1.53×10^{-4}
$(1/i)\phi_{[1m]}$	1.35×10^{-3}	3.82×10^{-3}	6.21×10^{-3}	8.75×10^{-3}	1.15×10^{-2}	1.48×10^{-2}	1.91×10^{-2}	2.66×10^{-2}

Table 3

MODE CONVERSION LOSS BY ONE-SIDES THICKNESS OF THE DIELECTRIC LAYER, AND PERCENTAGE CONTENT RATE OF EACH MODE IN IT

	Mode Conversion Loss (dB)	Content Rate (%)				
		TE_{11}	TE_{12}	TE_{13}	TE_{14}	TM_{11}
$l=45$ cm	1.30×10^{-6}	49.8	49.4	0.16	0.12	0.49
$l=70$ cm	4.85×10^{-6}	2.4	91.8	2.7	—	2.7

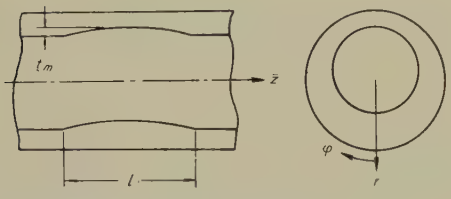

Fig. 7—One-sided thickness part.

$$C_{(1m)}{}^{\pm}=\mp2\pi^2\phi_{(1m)}\frac{t_m}{a}\frac{l}{\lambda}\frac{\cos(h_{[01]}\mp h_{(1m)})\dfrac{l}{2}}{\pi^2-(h_{[01]}\mp h_{(1m)})^2l^2},\tag{5.6}$$

where

$$\phi_{(1m)}=i\sqrt{2}\,k_{[01]}\frac{\varepsilon_2-\varepsilon_1}{\varepsilon_2}\sqrt{\frac{h_{(1m)}}{h_{[01]}}}\delta^2.\tag{5.7}$$

And, for the TE_{1m} modes

$$C_{[1m]}{}^{\pm}=\mp2\pi^2\phi_{(1m)}\frac{t_m}{a}\frac{l}{\lambda}\frac{\cos(h_{[01]}\mp h_{(1m)})\dfrac{l}{2}}{\pi^2-(h_{[01]}\mp h_{[1m]})^2l^2},\tag{5.8}$$

where

$$\phi_{[1m]}=i\sqrt{2}\,k_{[01]}\frac{\varepsilon_2-\varepsilon_1}{\varepsilon_1}\frac{k_0}{\sqrt{h_{[01]}h_{[1m]}}}\frac{k_{[1m]}{}^2-\dfrac{\varepsilon_1}{\varepsilon_2}}{\sqrt{k_{[1m]}{}^2-1}}\delta^2.\tag{5.9}$$

For both modes, we easily find

$$S_{(i)}{}^{\pm}=S_{[i]}{}^{\pm}=0.\tag{5.10}$$

Table 2 shows ϕ_i in case of (5.3). In these calculations, the phase constants of all modes are multiplied by the correction factors obtained by Unger.(1) The mode conversion factors are calculated for the cases where $l=45$ cm and $l=70$ cm at the freqency of 50 Gc/s. The mode conversion loss and the percentage content of each mode of the total converted power is shown in Table 3.

In case of the irregularity of the thickness of the layer expressed as

$$t_1=t_m\cos p\varphi\cos\frac{\pi z}{l},\tag{5.11}$$

the TM_{pm} and TE_{pm} modes generate. Especially, the conversion factor of the mode whose phase constant is near that of the TE_{01} is very large. The phase constant of the TE_{41} mode is the nearest to the TE_{01} among mode in case of dielectric-coated waveguide of (5.3). TE_{31} and TM_{21} are also the near modes. The variation of the thickness in case of $p=4$ in (5.11) is the most important one.

The mode conversion loss due to a single irregular place as shown in Fig. 4 and 7 is negligibly small. But the mode conversion by the iterative irregular places is not so small. It is assumed, for simplicity, that the number of the converted mode is only one. If the attenuation constant for the unwanted mode is very large, then the power generated at every irregular place immediately vanishes, and the mode conversion loss is easily obtained by multiplying the insertion loss (dB) at a single irregular place by the number of irregular places. Actually, the attenuation constants for the unwanted modes are not so high. When the waves generated at the irregular places are in phase with each other, they may cause an extraordinary attenuation even if the conversion factor at each irregular place is very small.(13)(14) The calculation in such case is done for equivalent iterative coupled transmission lines. The coupling coefficient at each coupling place is k (the absolute value is K) and the distances between adjoining coupling points are l_0.(13) The same phase condition of every converted wave is:

$$|h_{[01]}-h_i|\cdot l_0=2p\pi. \tag{5.12}$$

Let the propagation constant and the attenuation constant of the TE$_{01}$ mode be γ_1, and α_1, the attenuation constant of the unwanted mode be α_2; and $\Delta\alpha=\alpha_1-\alpha_2$. Passing n conversion places, an incident TE$_{01}$ mode with an amplitude of unity becomes:

$$A_{1n}=\exp\left\{-\left(\gamma_1+\frac{3K^2}{2l_0}-\frac{K^2}{\Delta\alpha\cdot l_0{}^2}\right)nl_0\right\}$$
$$\times\left[1+\frac{K^2}{\Delta\alpha^2\cdot l_0{}^2}\left\{1-e^{\left(\Delta\alpha-\frac{2K^2}{\Delta\alpha\cdot l_0{}^2}\right)nl_0}\right\}\right], \tag{5.13}$$

when $K\ll|\Delta\alpha|l_0$. Moreover for large n,

$$A_n\doteqdot\exp\left\{-\left(\gamma_1+\frac{3K^2}{2l_0}-\frac{K^2}{\Delta\alpha^2\cdot l_0{}^2}\right)nl_0\right.$$
$$\left.+\log_e\left(1+\frac{K^2}{\Delta\alpha^2\cdot l_0{}^2}\right)\right\}, \tag{5.14}$$

then the attenuation constant of the TE$_{01}$ wave becomes $\alpha_1+\alpha_1$, where

$$\Delta\alpha_1=\frac{3K^2}{2l_0}-\frac{K^2}{\Delta\alpha\cdot l_0{}^2}\,. \tag{5.15}$$

The numerical calculation is carried out for the one-sided case, as shown in Fig. 7, under the condition (5.3). The mode conversion factor to the TE$_{12}$ mode is $K=7.4\times10^{-4}$, when $l=45$ cm. Many irregular points, having the mode conversion factor of $K=7.4\times10^{-4}$ are assumed to be distributed at the intervals of $l_0=4.58$ m, which satisfy the condition (5.12). The attenuation constants of the TE$_{01}$ and TE$_{12}$ modes of the plain waveguide are 1.24×10^{-4} N/m and 4.72×10^{-4} N/m, then $\Delta\alpha l_0=1{,}94\times10^{-3}$ which satisfies the condition $K\ll\Delta\alpha l_0$ which realize (5.13). Then, from (5.15)

$$\Delta\alpha_1=7.5\times10^{-5}\ \text{N/m}, \tag{5.16}$$

which is 60.5 % of the heat loss of the TE$_{01}$ mode in the perfect waveguide. When K becomes much larger so that $K\ll\Delta\alpha l_0$, the attenuation pattern differs from the logarithmic attenuation and it also has a sinusoidal variation.(13)

A theory of the mode conversion by the deformed guide wall of the plain waveguide has been worked out statistically.(4) The theory can be utilized conveniently for the case of the mode conversion by the nonuniformity of the thickness of the dielectric layer in the dielectric-coated waveguide. The thickness of the layer has been written as (4.1) in which the irregular term t_i is expanded in a double Fourier series for the circumferential and the axial directions. Then the waveguide is divided into many parts all of whose lengths are the same. The means of the Fourier coefficients are zero in every part. The mean attenuation due to the mode conversion in the waveguide consists of many parts and is described by the root mean square value of the thickness irregularities.

In a part of the waveguide, t_1 is expressed by the finite Fourier series for $-l/2 \leq z \leq l/2$, $0 < \varphi < 2\pi$,

$$\frac{t_1(\varphi, z)}{a} = \frac{1}{4} \sum_{r=0}^{R} \sum_{s=0}^{S} \varepsilon_r \varepsilon_s \left\{ \left(a_{rs} \cos \frac{2\pi rz}{l} + b_{rs} \sin \frac{2\pi rz}{l} \right) \cos s\varphi + \left(c_{rs} \cos \frac{2\pi rz}{l} + d_{rs} \sin \frac{2\pi rz}{l} \right) \sin s\varphi \right\}, \tag{5.17}$$

where ε_r's are defined in (3.29). The Fourier coefficients a_{rs}, b_{rs}, c_{rs} and d_{rs} are written in matrix form as:

$$\begin{pmatrix} a_{rs} & b_{rs} \\ b_{rs} & d_{rs} \end{pmatrix} = \frac{2}{\pi l} \int_0^{2\pi} \int_{-\frac{l}{2}}^{\frac{l}{2}} \frac{t_1(\varphi, z)}{a} \begin{pmatrix} \cos \frac{2\pi rz}{l} \cos s\varphi & \sin \frac{2\pi rz}{l} \cos s\varphi \\ \cos \frac{2\pi rz}{l} \sin s\varphi & \sin \frac{2\pi rz}{l} \sin s\varphi \end{pmatrix} dz\, d\varphi, \tag{5.18}$$

from which, we can easily find

$$b_{0s} = c_{r0} = d_{0s} = d_{r0} = 0. \tag{5.19}$$

The mean square value of $t_1(\varphi, z)$, namely σ^2 divided by a^2 is

$$\frac{\sigma^2}{a^2} = \frac{1}{2\pi l} \int_0^{2\pi} \int_{-\frac{l}{2}}^{\frac{l}{2}} \frac{t_1^2(\varphi, z)}{a^2} dz\, d\varphi$$

$$= \frac{1}{16} \left[\sum_{r=0}^{R} \sum_{s=0}^{S} \varepsilon_r \varepsilon_s a_{rs}^2 + 2 \sum_{r=0}^{R} \sum_{s=0}^{S} \varepsilon_s b_{rs}^2 + 2 \sum_{r=0}^{R} \sum_{s=0}^{S} \varepsilon_r c_{rs}^2 + 4 \sum_{r=0}^{R} \sum_{s=0}^{S} d_{rs}^2 \right]. \tag{5.20}$$

Now from (4.12) and (4.14), we get

$$\left.\begin{aligned} C_i^{\pm} &= \mp \frac{\phi_i}{\lambda} \frac{\pi}{2} \sum_{r=0}^{R} \varepsilon_r (a_{nr} f_{i,r}^{\pm} - i b_{nr} g_{i,r}^{\pm}), \\ S_i^{\pm} &= \mp \frac{\phi_i}{\lambda} \frac{\pi}{2} \sum_{r=0}^{R} \varepsilon_r (c_{nr} f_{i,r}^{\pm} - i d_{nr} g_{i,r}^{\pm}), \end{aligned}\right\} \tag{5.21}$$

where

$$\left.\begin{aligned} f_{i,r}^{\pm} &= \int_{-\frac{l}{2}}^{\frac{l}{2}} \cos(h_{[01]} \mp h_i) z' \cos \frac{2\pi rz'}{l} dz' \\ &= \frac{(-)^r 2(h_{[01]} \pm h_i) l^2 \sin (h_{[01]} \mp h_i) \frac{l}{2}}{(h_{[01]} \mp h_i)^2 l^2 - 4\pi^2 r^2}, \\ g_{i,r}^{\pm} &= \int_{-\frac{l}{2}}^{\frac{l}{2}} \sin(h_{[01]} \mp h_i) z' \sin \frac{2\pi rz'}{l} dz' \\ &= \frac{(-)^r 4\pi rl \sin(h_{[01]} \mp h_i) \frac{l}{2}}{(h_{[01]} \mp h_i)^2 l^2 - 4\pi^2 r^2}. \end{aligned}\right\} \tag{5.22}$$

Then, from (5.21)

$$\left.\begin{aligned} |C_i^{\pm}|^2 &= \frac{\pi^2 \phi_i^2}{4\lambda^2} \sum_{r=0}^{R} \sum_{r'=0}^{R} \varepsilon_r \varepsilon_{r'} (a_{rn} f_{i,r}^{\pm} - i b_{rn} g_{i,r}^{\pm})(a_{r'n} f_{i,r'}^{\pm} + i b_{r'n} g_{i,r'}), \\ |S_i^{\pm}|^2 &= \frac{\pi^2 |\phi_i|^2}{4\lambda^2} \sum_{r=0}^{R} \sum_{r'=0}^{R} \varepsilon_r \varepsilon_{r'} (c_{rn} f_{i,r}^{\pm} - i d_{rn} g_{i,r}^{\pm})(c_{r'n} f_{i,r'}^{\pm} + i d_{r'n} g_{i,r'}^{\pm}). \end{aligned}\right\} \tag{5.23}$$

The waveguide have been divided into many parts of length l, and the mean of any quantities of every part is expressed with the sign $\langle\rangle$. We assume that

$$\left.\begin{aligned} \langle a \rangle_{rs} &= \langle b \rangle_{rs} = \langle c \rangle_{rs} = \langle d \rangle_{rs} = 0 \\ \langle ab \rangle_{rs} &= \langle ac \rangle_{rs} = \cdots\cdots = \langle cd \rangle_{rs} = 0 \end{aligned}\right\} \tag{5.24}$$

$$\langle a_{rs}^2\rangle=\langle b_{rs}^2\rangle=\langle c_{rs}^2\rangle=\langle d_{rs}^2\rangle=\frac{\sigma_{rs}^2}{a^2},\quad \Big\}$$

where σ_{rs} is the standard deviation. The mean σ^2 about every part of the waveguide is written as:

$$\langle\sigma^2\rangle=\frac{1}{61}\sigma_{00}^2+\frac{1}{4}\sum_{s=1}^{S}\sigma_{0s}^2$$

$$+\frac{1}{4}\sum_{r=1}^{R}\sigma_{r0}^2+\sum_{r=1}^{R}\sum_{s=1}^{S}\sigma_{rs}^2 \qquad (5.25)$$

The mean of the sum of two of (5.23) is obtained from (5.19) and (5.24) as:

$$\langle|C_i^{\pm}|^2+|S_i^{\pm}|^2\rangle$$

$$=\varepsilon_n\frac{\pi^2|\phi_i|^2}{4\lambda^2a^2}\Big[(f_{i,0}^{\pm})^2\sigma_{0n}^2$$

$$+4\sum_{r=1}^{R}\{(f_{i,r}^{\pm})^2+(g_{i,r}^{\pm})^2\}\sigma_{rn}^2\Big]$$

$$=\varepsilon_n\pi^2|\phi_i|^2\frac{l^2}{\lambda^2}\sin^2\Big\{(h_{[01]}\mp h_i)\frac{l}{2}\Big\}$$

$$\sum_{r=0}^{R}\varepsilon_r^2\frac{(h_{[01]}\mp h_i)^2l^2+4\pi^2r^2}{\{(h_{[01]}\mp h_i)^2l^2-4\pi^2r^2\}^2}\frac{\sigma_{rn}^2}{a^2}. \qquad (5.26)$$

The value of (5.26) is calculated for every mode, and the mean mode conversion loss is obtained from

$$\langle L\rangle=\frac{4.343}{l}\sum_{n=0}^{S}\sum_{m}[\langle C_{(nm)}^{+2}+S_{(nm)}^{+2}\rangle$$

$$+\langle C_{(nm)}^{-2}+S_{(nm)}^{-2}\rangle$$

$$+\langle|C_{[nm]}^{+}|^2+|S_{[nm]}^{+}|^2\rangle$$

$$+\langle|C_{[nm]}^{-}|^2+|S_{[nm]}^{-}|^2\rangle]\quad \text{dB/m.} \qquad (5.27)$$

This is the equation for the mean attenuation by the mode conversion by random irregularities of the layer thickness.

Figs. 8 and 9 are two measured thicknesses of the polyethylene layers in the dielectric-coated waveguide constructed in our Laboratory.(2) Fig. 8 shows the thickness variation for the circumferential direction of the polyethylene layer peeled off from the dielectric-coated waveguide constructed by the whirl sinter method. A micrometer was used to measure, and the measurements were made at every 40 divided point of the circumference of about 160 mm. The measuring spacing may not be so narrow that exact tracing of

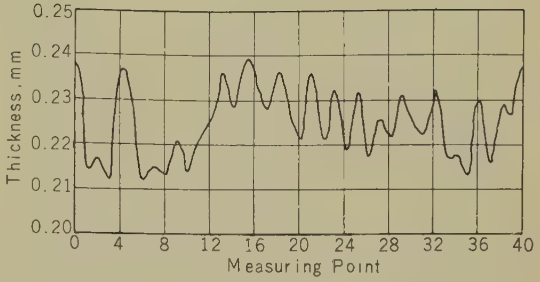

Fig. 8—Circumferential direction variation of dielectric layer thickness in the dielectric-coated waveguide constructed by the whirl sinter method.

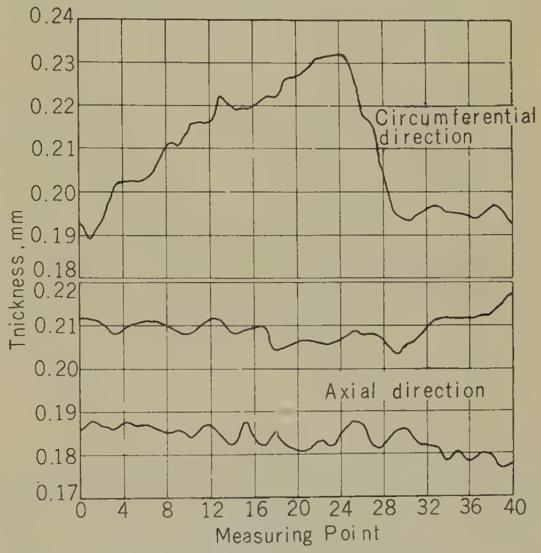

Fig. 9—Circumferential and axial direction variation of dielectric layer thickness in the dielectric-coated waveguide constructed by tube bonding method. Distance between adjoining measuring points are 4 mm.

the thickness is possible. The thickness variation for the axial direction is the same as that for the circumferential direction. Fig. 9 shows the result of the dielectric-coated waveguide constructed by the tube bonding method. The polyethylene tube was made by the inflation method, so the uniformity of the thickness for the circumferential direction is not very good. After the manufacturing process, the tube is folded and rolled up, and it is difficult to keep good uniformity for the circumferential direction. But in the axial direction, the uniformity is excellent. Even if there is nonuniformity in the circumferential direction, if it is uniform in the axial direction mode conversion does not occurs except at the junction between two waveguides whose axes of nonuniformities do not coincide with each other.

First, it is assumed that the irregularity of the thickness variation curve for the axial direction does not differ from that for the circumferential directions, and the unit length l is taken as $2\pi a$. That means there is no variation having a period longer than $2\pi a$. The subscripts r and s of the Fourier series in (5.17) are assumed to be zero unless

$$0 \leqq \frac{r}{s} \leqq 4. \tag{5.28}$$

That means the thickness variation is very slow. Let the subscript for the mode number be nm, then it is sufficient to take only the modes of $n \leqq 4$ into consideration. If the Fourier coefficients of the irregularity which generates the nm mode are such that s is equal to n, then it is sufficient to consider to take only $s \leqq 4$. Next for r, when l is very short as $2\pi a$, it is sufficient to take $r \leqq 4$ also. The large part of the converted power is contained in the modes of $r=0$ and $r=1$ only.

The converted modes are assumed to be only the next seven. For much longer l, many more modes must be taken into consideration.

$$\left.\begin{array}{l} \mathrm{TM}_{11}{}^+,\ \mathrm{TM}_{21}{}^+,\ \mathrm{TE}_{11}{}^+,\ \mathrm{TE}_{12}{}^+, \\ \mathrm{TE}_{21}{}^+,\ \mathrm{TE}_{31}{}^+,\ \text{and}\ \mathrm{TE}_{41}{}^+ \end{array}\right\} \tag{5.29}$$

In the third equation of (5.24), we set

$$\sigma_{rs} = \begin{array}{ll} \sigma_1 & \text{for } 0 \leqq \frac{r}{s} \leqq 4 \\ 0 & \text{otherwise.} \end{array} \tag{5.30}$$

Under above assumption, we get from (5.25)

$$\langle \sigma^2 \rangle = 18.06\, \sigma_1{}^2 \tag{5.31}$$

Again in case of (5.3) (t_m will be designated later) the values ϕ_i's are shown in Table 4.

Table 4

ϕ_i OF THE MODES OF (5.29) UNDER THE CONDITION (5.3)

nm	11	12	21	31	41
$(1/i)\phi(nm)$	3.07×10^{-4}	—	6.11×10^{-4}	—	—
$(1/i)\phi[nm]$	1.35×10^{-3}	3.82×10^{-3}	2.32×10^{-4}	3.33×10^{-3}	4.28×10^{-3}

When the frequency is 50 Gc/s, (5.26) becomes:

$$\begin{aligned} &\langle C_i{}^{+2} + S_i{}^{+2} \rangle \\ &= 39.5 |\phi_i|^2 \frac{\langle \sigma^2 \rangle}{a^2} \sin^2\{(h_{[01]} - h_i) a\pi\} \\ &\times \sum_{r=0}^{4} \varepsilon_r{}^2 \frac{(h_{[01]} - h_i)^2 a^2 + r^2}{(h_{[01]} - h_i)^2 a^2 - r^2}, \end{aligned} \tag{5.32}$$

and after numerical calculation the mean attenuation $\langle L \rangle$ becomes:

$$\langle L \rangle = 0.581 \frac{\langle \sigma^2 \rangle}{a^2} \text{ dB/m.} \tag{5.33}$$

The attenuation constant of the waveguide without the dielectric layer (L_0) is 1.07 dB/km, therefore

$$\frac{\langle L \rangle}{L_0} = 5.43 \times 10^4 \frac{\langle \sigma^2 \rangle}{a^2} \ \%. \tag{5.34}$$

For example, if $a=0.0255$ m, and $\langle\sigma\rangle=2\times 10^{-5}$ m, then the percentage attenuation to the heat loss of (5.34) is 0.033 %.

In the next place, we will consider a much longer l. In such a case fairly large conversion may occur to modes whose phase constants are not very near to that of the TE_{01} and having large r. That means there is a sinusoidal thickness variation having r periods in a fairly long transmission line. This differs from the initial assumption of random irregularity. The iterative reflections or mode conversions along the axis cause not only the logarithmic attenuation, but also trigonometric variation of amplitude.(13)(14)

The numerical example will be shown under the same condition as before except that the length l is changed to 12 m. In this case

$$\langle |C_i^{\pm}|^2+|S_i^{\pm}|^2\rangle$$
$$=3.04\times 10^4|\phi_i|^2\frac{\langle\sigma^2\rangle}{a^2}\sin^2\{6(h_{[01]}-h_i)\}$$
$$\times\sum_{r=0}^{4}\varepsilon_r^2\frac{(h_{[01]}-h_i)^2+0.274\,r^2}{\{(h_{[01]}-h_i)^2-0.274\,r^2\}^2}, \tag{5.35}$$

from which we get

$$\langle L\rangle=10.2\frac{\langle\sigma^2\rangle}{a^2}\quad \text{dB/m.} \tag{5.36}$$

When $a=0.0255$ m, and $\langle\sigma\rangle=2\times 10^{-5}$ m, the percentage attenuation to the heat loss is 0.63 % which is 19 times as large as the result when $l=2\pi a$. If many more modes are added to (5.29), and the limitation (5.28) is extended, the attenuation may increase much more.

Even when the standard deviation of the thickness irregularity is constant, the attenuation varies according to the nature of the irregularity. Therefore, an exact value must be calculated for the practical condition. Though, the mode conversion by the thickness irregularity may not give rise to a serious attenuation; that is, because the thickness irregularity exists close to the metal wall where the electric field intensity is feeble, the conversion factors have the term δ^2. That is one of the excellent features of this kind of waveguide.

6. Mode Conversion through a Junction between Plain and Dielectric-Coated Waveguides

The mode conversion occurs at the junction between the plain and the dielectric-coated waveguide. Unger obtained an approximate conversion factor for such a joint.(1) A standard method by Iiguchi(15) to obtain the conversion factor at such junction enables us to obtain the exact solution. Hereafter, the sign m stands for $[0m]$. Fig. 10 shows the junction in question. The incident TE_{01} wave propagates from the left to the junction in the figure, and the transverse components of the electric and magnetic fields of the incident and converted waves are written as:

$$\left.\begin{array}{l} V_1\boldsymbol{e}_1e^{-j\beta_1z}+RV_1\boldsymbol{e}_1e^{j\beta_1z}+\sum V_m\boldsymbol{e}_me^{j\beta_mz},\\ I_1\boldsymbol{h}_1e^{-j\beta_1z}-RI_1\boldsymbol{h}_1e^{j\beta_1z}-\sum I_m\boldsymbol{h}_me^{j\beta_mz},\\ NTV_1\boldsymbol{e}_1'e^{-j\beta_1'z}+\sum V_m'\boldsymbol{e}_m'e^{-j\beta_m'z},\\ \dfrac{1}{N}TI_1\boldsymbol{h}_1'e^{-j\beta_1z}+\sum I_m'\boldsymbol{h}_m'e^{-j\beta_m'z}, \end{array}\right\} \tag{6.1}$$

where R is the reflection coefficient; β_m is the phase constant of the TE_{0m} mode; N is the transformation ratio, and T is the transmission factor. In section 2 we used the mode voltage V and the mode current I as functions of z, but here they are not functions of z. The primed quantities are those for the dielectric-

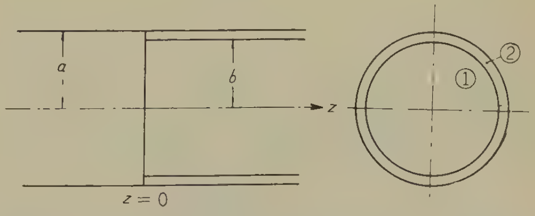

Fig. 10—Junction between the dielectric-coated and plain waveguides.

coated waveguide. The continuity conditions at the junction plane, $z=0$, are

$$\left.\begin{aligned} &(1+R)V_1\boldsymbol{e}_1+\sum V_m\boldsymbol{e}_m=NTV_1\boldsymbol{e}_1'+\sum V_m'\boldsymbol{e}_m', \\ &(1-R)I_1\boldsymbol{h}_1-\sum I_m\boldsymbol{h}_m=\frac{1}{N}TI_1\boldsymbol{h}_1'+\sum I_m'\boldsymbol{h}_m'. \end{aligned}\right\} \tag{6. 2}$$

The mode vectors in (6.2) are written, using the symbols in section 3 as:

$$\left.\begin{aligned} \boldsymbol{e}_m &= q_m\chi_m J_1(\chi_m r)\boldsymbol{i}_\varphi, \\ \boldsymbol{e}_m' &= \begin{cases} q_m'\chi_{1m}J_1(\chi_{1m}r)\boldsymbol{i}_\varphi & \text{in the region ①} \\ -q_m'\chi_{1m}^2 J_0(\chi_{1m}b)\Delta r\boldsymbol{i}_\varphi & \quad〃 \qquad\quad ②, \end{cases} \\ \boldsymbol{h}_m &= -\frac{h_m^2}{k_0^2}\boldsymbol{e}_m\times\boldsymbol{i}_z, \\ \boldsymbol{h}_m' &= -\frac{h_m'^2}{k_0^2}\boldsymbol{e}_m'\times\boldsymbol{i}_z \qquad \text{in the regions ① and ②.} \end{aligned}\right\} \tag{6. 3}$$

The first equation of (6.2) is multiplied by $J_1(\chi_m r)r$ and is integrated with r from 0 to a for an integer m larger than one. Taking into consideration that V_m/V_1 and V_m'/V_1 are $O(\delta)$ at most, that $N=1+O(\delta)$, and that $q_m/q_m'=1+O(\delta)$, the relation between V_i and V_i' with regard to the lowest order terms of δ is obtained as:

$$V_i-V_i'=AV_1, \tag{6. 4}$$

where

$$A=\frac{1}{3\sqrt{2}}\frac{k_{[01]}k_{[0m]}}{k_{[01]}^2-k_{[0m]}^2}\frac{h_{[01]}}{h_{[0m]}} \times(k_{[01]}^2-\chi_{2[01]}a^2)\delta^3. \tag{6. 5}$$

The lower part of (6.2) is multiplied by $J_1(\chi_m r)r$ and is integrated with r from 0 to a; then under the above assumption we get

$$Y_mV_m+Y_m'V_m'=-A\frac{h_{[01]}^2}{h_{[0m]}^2}Y_1V_1. \tag{6. 6}$$

(6.5) and (6.6) are easily solved.

$$\left.\begin{aligned} V_m &= A\frac{Y_m'-\dfrac{h_{[01]}^2}{h_{[0m]}^2}Y_1}{Y_m+Y_m'}V_1 \\ V_m' &= A\frac{-Y_m'+\dfrac{h_{[01]}^2}{h_{[0m]}^2}Y_1}{Y_m+Y_m'}V_1 \end{aligned}\right\} \tag{6. 7}$$

The mode conversion factors $C^\pm$ are

$$\left.\begin{aligned} C_m^+ &= \frac{\dfrac{V_m'}{\sqrt{Z_m'}}+\dfrac{I_m'}{\sqrt{Y_m'}}}{\dfrac{V_1}{\sqrt{Z_1}}+\dfrac{I_1}{\sqrt{Y_1}}}=\sqrt{\frac{Z_1}{Z_m'}}\frac{V_m'}{V_1}, \\ C_m^- &= \frac{\dfrac{V_m}{\sqrt{Z_m}}-\dfrac{-I_m}{\sqrt{Y_m}}}{\dfrac{V_1}{\sqrt{Z_1}}+\dfrac{I_1}{\sqrt{Y_1}}}=\sqrt{\frac{Z_1}{Z_m}}\frac{V_m}{V_1}. \end{aligned}\right\} \tag{6. 8}$$

They are rewritten as:

$$C_m^\pm=\frac{1}{3\sqrt{2}}\frac{\varepsilon_2-\varepsilon_0}{\varepsilon_0}\frac{k_{[01]}k_{[0m]}}{k_{[01]}^2-k_{[0m]}^2} \times K_0^2a^2\sqrt{\frac{h_{[01]}}{h_{[0m]}}}\frac{h_{[01]}(h_{[01]}\mp h_{[0m]})}{2h_{[0m]}^2}\delta^3. \tag{6. 9}$$

A numerical calculation is performed under the condition $\varepsilon_2=2.3\varepsilon_0$, $k_0a=26.7$ (this corresponds to a frequency of 50 Gc/s and to a waveguide diameter of 51 mm) and $\delta=0.01$. The C_m^+ values for m from 2 to 8 are shown in Table 5.

The mode conversion to TE_{08} is the largest of all in Table 5, because this mode is near the cutoff. The conversion factor to such

Table 5

MODE CONVERSION FACTORS TO TE_{0m} AT THE JUNCTION IN CASE OF $\varepsilon_2=2.3\varepsilon_0$, $k_0a=26.70$, AND $\delta=0.01$

m	2	3	4	5	6	7	8
C_m^+ (−dB)	75. 0	79. 2	80. 6	81. 3	80. 5	80. 0	63. 9

mode may be very large, but this value suffers serious influence from the heat loss of the waveguide in general. Therefore, in the practical case such large conversion never occurs.

7. Mode Conversion through Slightly Deformed Wall of Hybrid-Mode Waveguide

When the guide wall is deformed slightly in the circular cylinder and the direction of this deformation varies along the guide axis, mode conversion occurs. In the plain waveguide, general formulae concerning such waveguide deformation have been obtained by Morgan.(4) Using (2.30), that is, the general formulae of the mode generation in the waveguide with nonuniform material in it, the mode conversion by the wall deformation in the dielectric-coated waveguide can be obtained. And also in the waveguide having not only nonuniform material, but also an impedance wall, the general formulae of the mode conversion by such deformation can be obtained. The results coincide with the Morgan's formulae(4) obtained by different method from that in the presenting paper when the material constant reduces to that of air, and the wall impedance reduces to zero.

For the mode conversion by nonuniformity of the dielectric layer thickness; if the mode conversion loss is very small as obtained in the section 5, then the tolerance of the waveguide itself is rather important.

To prevent serious attenuation and the phase distortion due to the mode conversion-reconversion it is necessary to absorb the unwanted modes generated by the imperfect junction or wall deformation, by inserting the helix waveguide. And also, a whole transmission line may consist of the helix waveguide.(8)

The helix waveguide having metallic shield is also one of the promising waveguide for bend of the TE_{01} wave transmission line.(8)(16) The progress of the manufacturing technique has enabled us to obtain the accurate helix waveguide.(17) When still more improvement of the accuracy is attempted, it is necessary to calculate the mode conversion due to the wall deformation. The mode conversion due to the wall deformation in these two kinds of waveguide will be discussed hereafter.

The wall of a waveguide having nonuniform material in it is assumed to be deformed as shown in Fig. 11. The position of the wall is written as a function of φ and z.

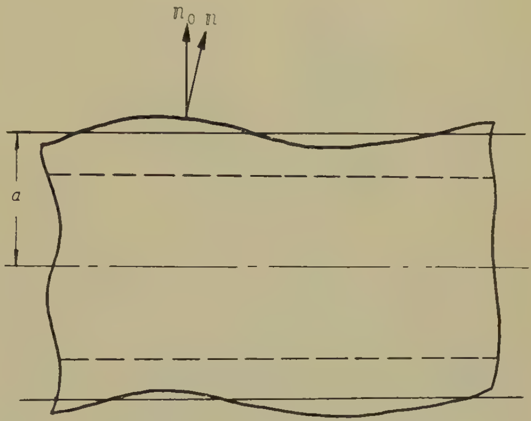

Fig. 11—Slightly deformed wall of dielectric-coated waveguide.

$$r = a + r_1(\varphi, z), \qquad (7.1)$$

where r_1 is much less than a. Equation (7.1) means that every point on the perfect circular cylinder wall is moved toward r direction by the amount r_1. At that time the normal direction on the wall might vary at each point. It is also assumed the angle variation is very small. The outward unit normal vector on the deformed wall is

$$\boldsymbol{n} = \boldsymbol{n}_0 + \boldsymbol{n}_1, \qquad (7.2)$$

where $\boldsymbol{n}_0$ is the outward unit vector on the perfect waveguide, but $\boldsymbol{n}_1$ is not the unit vector. The electric and magnetic fields of the incident wave are written as:

$$\left.\begin{aligned} \boldsymbol{E} &= \boldsymbol{E}_0 + \boldsymbol{E}_1, \\ \boldsymbol{H} &= \boldsymbol{H}_0 + \boldsymbol{H}_1, \end{aligned}\right\} \qquad (7.3)$$

where $\boldsymbol{E}_0$ and $\boldsymbol{H}_0$ are the electric and magnetic fields in the distortionless waveguide. The electric field in the deformed guide is expanded as:

$$\{\boldsymbol{E}_0\}_{a+r_1}=\{\boldsymbol{E}_0\}_a+r_1\left\{\frac{\partial \boldsymbol{E}_0}{\partial r}\right\}_a. \qquad (7.4)$$

The tangential component of the electric field at the wall is

$$\boldsymbol{n}\times\{\boldsymbol{E}\}_{a+r_1}. \qquad (7.5)$$

Neglecting the higher order of infinitesimal quantities (7.5) becomes:

$$(\boldsymbol{n}_0+\boldsymbol{n}_1)\times[\{\boldsymbol{E}_0\}_{a+r_1}+\{\boldsymbol{E}_1\}_{a+r_1}]$$
$$=\boldsymbol{n}_0\times\{\boldsymbol{E}_0\}_{a+r_1}+\boldsymbol{n}_0\times\{\boldsymbol{E}_1\}_a+\boldsymbol{n}_1\times\{\boldsymbol{E}_0\}_a. \qquad (7.6)$$

If the incident wave is TE_{01} mode, then $\{\boldsymbol{E}_0\}_a=0$ (The partial derivative of it with respect to r has a finite value) at the wall, the tangential component of the electric field in the cross section of the waveguide is zero, and the electric field tangential to the wall and perpendicular to the circumferencial line of the cross section is related to the tangential magnetic component by the following equation:

$$\boldsymbol{n}\times\{\boldsymbol{E}\}_{a+r_1}=r_1\boldsymbol{n}_0\times\left\{\frac{\partial \boldsymbol{E}_0}{\partial r}\right\}_a+\boldsymbol{n}_0\times\{\boldsymbol{E}_1\}_a$$
$$=-Z_z\{\boldsymbol{H}\}_{a+r_1}$$
$$\cdot\frac{\boldsymbol{n}\times\boldsymbol{i}_z}{\{1-(\boldsymbol{n}\cdot\boldsymbol{i}_z)^2\}}\boldsymbol{n}\times\boldsymbol{i}_z. \qquad (7.7)$$

Since the incident wave is the TE_{01} mode

$$\left.\begin{aligned}&\boldsymbol{E}_0=E_0\boldsymbol{i}_\varphi,\\&\boldsymbol{H}_0=H_0\boldsymbol{i}_z,\\&\left\{\frac{\partial H_0}{\partial r}\right\}_a=0.\end{aligned}\right\} \qquad (7.8)$$

Using these equations, equation (7.7) is resolved into two components as:

$$\left.\begin{aligned}&E_{1\varphi}(a,\varphi,z)=-r_1(\varphi,z)\left\{\frac{\partial E_0(r,\varphi,z)}{\partial r}\right\}_a,\\&E_{1z}(a,\varphi,z)=-Z_zH_{1\varphi}(a,\varphi,z).\end{aligned}\right\} \qquad (7.9)$$

The second equation of (7.9) means that the existence of fields $(E_{1z}, H_{1\varphi})$ other than those of the incident TE_{01} wave satisfying the relation are permitted, but they are not related with the incident TE_{01} wave at all. That is, the wall deformation never generates such fields. From the upper equation of (7.9), we obtain the magnetic current to be set at the guide wall surface as:

$$\boldsymbol{M}(a,\varphi,z)=-\boldsymbol{n}_0\times\boldsymbol{E}_1$$
$$=r_1(\varphi,z)\left\{\frac{\partial E_0(r,\varphi,z)}{\partial r}\right\}_a\boldsymbol{i}_z. \qquad (7.10)$$

The mode conversion by the deformation of the dielectric-coated waveguide wall can be obtained from (2.36) and (7.10). In the dielectric layer, the T-function of the dielectric-coated waveguide of the TE_{01} mode is

$$T_{[01]}'=q_{[01]}\frac{\chi_{1[01]}^2}{\chi_{2[01]}^2}J_0(\chi_{1[01]}b)\left(1-\frac{\chi_{2[01]}^2\,\Delta r^2}{2}\right). \qquad (7.11)$$

Consequently,

$$E_0(r,\varphi)=-V_{[01]}\frac{\partial T'_{[01]}}{\partial r}$$
$$=-V_{[01]}\,q_{[01]}\chi_{1[01]}^2J_0(\chi_{1[01]}b)\,\Delta r. \qquad (7.12)$$

Accordingly,

$$\left\{\frac{\partial E_0}{\partial r}\right\}_a=V_{[01]}\,q_{[01]}\frac{k_{[01]}^2}{a^2}J_0(k_{[01]}). \qquad (7.13)$$

Of the generated mode i in the dielectric layer,

$$\left.\begin{aligned}&h_{zi}(r,\varphi)=-\frac{\chi_{2i}^2}{i\omega\mu}T_i',\\&T_i'=q_i\frac{\chi_{1i}^2}{\chi_{2i}^2}J_n(\chi_{1i}b)-\sin n\varphi.\end{aligned}\right\} \qquad (7.14)$$

Substituting from (7.12) to (7.14) into (2.36), the amplitude of the generated mode i is

$$A_i^{\pm}(z)=\pm\sqrt{\frac{h_i}{\omega\varepsilon_0}}\,q_{[01]}\frac{k_{[01]}^2}{a^2}J_0(k_{[01]})\left\{-\frac{k_i^2}{i\omega\mu_0 a^2}q_i\right\}J_n(\chi_{1i}b)$$

$$\times\int_0^z\int_0^{2\pi}r_1(\varphi,z')\,V_{[01]}(z')\begin{matrix}\cos\\-\sin\end{matrix}n\varphi\,a\,d\varphi\,e^{\mp ih_i(z-z')}dz'. \tag{7.15}$$

Different from the plain waveguide, not only the TE modes but the TM modes other than $n=0$ are generated. However, in the case of one of the TM modes, the amplitude has two $O(\delta)$ terms; q_1 and $J_n(\chi_{1i}b)$, and it is a very small quantity. Thus usually, only the TE modes are taken into consideration. The conversion factor from the incident TE_{01} mode to the $\mathrm{TE}_{[i]}$ mode is

$$\begin{matrix}C_i^{\pm}\\S_i^{\pm}\end{matrix}=\pm i\frac{\sqrt{\varepsilon_n}}{2\pi\sqrt{h_{[01]}h_{[i]}}}\frac{k_{[01]}}{a}\frac{k_{[i]}^2}{a^2\sqrt{k_{[i]}^2-n^2}}$$

$$\times\int_0^z\int_0^{2\pi}r_1(\varphi,z')e^{-i(h_{[01]}\mp h_{[i]})z'}\begin{matrix}\cos\\-\sin\end{matrix}n\varphi\,d\varphi\,dz', \tag{7.16}$$

The form of this equation is the same as that for the plain waveguide which has been obtained by Morgan.(4) The mode conversion due to the wall deformation in the dielectric-coated waveguide is roughly the same as that of the plain waveguide.

We will now proceed to the mode conversion due to the wall deformation in the helix waveguide. First, it will be shown that (2.36) is roughly satisfied even when the guide wall has an impedance. (2.24), (2.28) and (2.32) have been derived under the assumption of perfect conductive wall. This assumption will be abandoned hereafter. The boundary condition on the wall surface is written as:

$$e_{zi}=-Z_z\boldsymbol{n}\cdot\boldsymbol{h}_{ti}\times\boldsymbol{i}_z=-Z_z h_{si}, \tag{7.17}$$

$$h_{zi}=-Y_s\boldsymbol{n}\cdot\boldsymbol{i}_z\times\boldsymbol{e}_{ti}=Y_s e_{si}. \tag{7.18}$$

Where Z_z and Y_s are constants not depending on mode. A part of (2.21) is transformed as:

$$\iint\nabla_t\frac{\nabla_t\cdot\boldsymbol{H}_t\times\boldsymbol{i}_z}{\varepsilon}\cdot\boldsymbol{h}_{ti}\times\boldsymbol{i}_z dS$$

$$=-\iint\frac{\nabla_t\cdot\boldsymbol{H}_t\times\boldsymbol{i}_z}{\varepsilon}\nabla_t\cdot\boldsymbol{h}_{ti}\times\boldsymbol{i}_z dS$$

$$+\int\frac{\nabla_t\cdot\boldsymbol{H}_t\times\boldsymbol{i}_z}{\varepsilon}(\boldsymbol{h}_{ti}\times\boldsymbol{i}_z\cdot\boldsymbol{n})ds$$

$$=-\iint\frac{\nabla_t\cdot\boldsymbol{h}_{ti}\times\boldsymbol{i}_z}{\varepsilon}\nabla_t\cdot\boldsymbol{H}_t\times\boldsymbol{i}_z dS$$

$$-i\omega Z_z\int H_s(\boldsymbol{h}_{ti}\times\boldsymbol{i}_z\cdot\boldsymbol{n})ds$$

$$=\iint\nabla_t\frac{\nabla_t\cdot\boldsymbol{h}_{ti}\times\boldsymbol{i}_z}{\varepsilon}\cdot\boldsymbol{H}_t\times\boldsymbol{i}_z dS$$

$$+i\omega Z_z\left\{\int h_{sj}(\boldsymbol{H}_t\times\boldsymbol{i}_z\cdot\boldsymbol{n})ds\right.$$

$$\left.-\int H_s(\boldsymbol{h}_{ti}\times\boldsymbol{i}_z\cdot\boldsymbol{n})ds\right\}. \tag{7.19}$$

The second term in the last equation becomes zero if the impedances are the same for all modes, and (2.24) is satisfied also for the case of the helix waveguide.

By a procedure similar to (7.19), a part of (2.26) is transformed as:

$$\iint\nabla_t\frac{\nabla_t\cdot\boldsymbol{i}_z\times\boldsymbol{E}_t}{\mu}\cdot\boldsymbol{i}_z\times\boldsymbol{e}_{ti}dS$$

$$=-\iint\frac{\nabla_t\cdot\boldsymbol{i}_z\times\boldsymbol{E}_t}{\mu}\nabla_t\cdot\boldsymbol{i}_z\times\boldsymbol{e}_{ti}dS$$

$$+\int\frac{\nabla_t\cdot\boldsymbol{i}_z\times\boldsymbol{E}_t}{\mu}(\boldsymbol{i}_z\times\boldsymbol{e}_{ti}\cdot\boldsymbol{n})ds$$

$$=-\iint\frac{\nabla_t\cdot\boldsymbol{i}_z\times\boldsymbol{e}_{ti}}{\mu}\nabla_t\cdot\boldsymbol{i}_z\times\boldsymbol{E}_t dS$$

$$+j\omega Y_s\int E_s(\boldsymbol{i}_z\times\boldsymbol{e}_{ti}\cdot\boldsymbol{n})ds$$

$$
\begin{aligned}
&=\iint \nabla_t \frac{\nabla_t\cdot \boldsymbol{i}_z\times \boldsymbol{e}_{ti}}{\mu}\cdot \boldsymbol{i}_z\times \boldsymbol{E}_t dS\\
&\quad -i\omega Y_s\left\{\iint e_{si}(\boldsymbol{i}_z\times \boldsymbol{E}_t\cdot \boldsymbol{n}ds\right.\\
&\quad \left.-\int E_s(\boldsymbol{i}_z\times \boldsymbol{e}_{ti}\cdot \boldsymbol{n})ds\right\}. \qquad (7.20)
\end{aligned}
$$

The second term of the last equation becomes zero if the admittances are the same for all modes, and (2.28) is also satisfied.

The inhomogeneous term of (2.32) is transformed as:

$$
\left.
\begin{aligned}
v_i(z)=&-\iint J_z(u,v,z)e_{zi}(u,v)dS\\
&+\iint \boldsymbol{M}(u,v,z)\cdot \boldsymbol{h}_{ti}(u,v)dS\\
&+\iint \frac{1}{j\omega\varepsilon}J_z(u,v,z)h_{si}(u,v)ds,\\
i_i(z)=&-\iint M_z(u,v,z)h_{zi}(u,v)dS\\
&+\iint \boldsymbol{J}(u,v,z)\cdot \boldsymbol{e}_{ti}(u,v)dS\\
&+\iint \frac{1}{i\omega\mu}M_z(u,v,z)e_{si}(u,v)ds.
\end{aligned}
\right\}
\qquad (7.21)
$$

The mode generation due to the wall deformation of the helix waveguide is calculated by replacing the deformation with its equivalent magnetic current distribution. For simplicity, the impedance to the electric field in the circumferential direction is assumed to be zero. Then, Y_s in (7.18) is infinite. In this case the magnetic current due to the incident TE_{01} wave is the same as that in a perfect conductive waveguide. Substituting M_z of (7.10) into (7.21), the amplitude of the converted mode i from the TE_{01} due to the wall distortion is

$$
\begin{aligned}
A_i^{\pm}(z)=&\pm\sqrt{\frac{h_i}{\omega\varepsilon_0}}\,q_{[01]}\chi_{[01]}{}^2J_0(\chi_{[01]}a)\bar{V}_{[01]}e^{\pm ih_iz}\\
&\times\int_0^z\int_0^{2\pi} r(\varphi,z')h_{zi}ad\varphi e^{-i(h_{[01]}\mp h_i)z'}dz'.
\end{aligned}
\qquad (7.22)
$$

Now, the fields in the helix waveguide are obtained from the following two scalar functions, (2.11), the wall impedance Z_z and the boundary condition (7.17):

$$
\left.
\begin{aligned}
T_i&=p_{1i}J_n(\chi_{1i}r)\begin{matrix}\sin\\ \cos\end{matrix}n\varphi,\\
T_i'&=q_{1i}J_n(\chi_{1i}r)\begin{matrix}\cos\\ -\sin\end{matrix}n\varphi.
\end{aligned}
\right\}
\qquad (7.23)
$$

Different from the plain waveguide, the transverse electric modes are only the TE_{0m} modes, which do not need p_{1i}. Transverse magnetic modes are only the TM_{0m} modes, which do not need q_{1i}. The modes other than these kinds of modes are designate HY_{nm} $(n\neq 0)$.(18)

If the wall impedance is a constant value for every mode, the characteristics and structure of the outside of the wall need not be known to discuss the transmission of the mode in most cases. In such cases, the integration region of the orthogonality relation (2.16) may be limited within the impedance wall. If $(\boldsymbol{E}_1, \boldsymbol{H}_1)$ and $(\boldsymbol{E}_2, \boldsymbol{H}_2)$ are the electric and magnetic fields of two modes, then from Maxwell's equation

$$
\nabla\cdot(\boldsymbol{E}_1\times \boldsymbol{H}_2-\boldsymbol{E}_2\times \boldsymbol{H}_1)=0 \qquad (7.24)
$$

which can be rewritten as:

$$
\begin{aligned}
&\nabla\cdot(\boldsymbol{E}_1\times \boldsymbol{H}_2-\boldsymbol{E}_2\times \boldsymbol{H}_1)_t\\
&\quad+\frac{\partial}{\partial z}(\boldsymbol{E}_1\times \boldsymbol{H}_2-\boldsymbol{E}_2\times \boldsymbol{H}_1)_z=0. \qquad (7.25)
\end{aligned}
$$

Here, the waveguide is assumed to be laid in the straight state. If γ_1 and γ_2 are the propagation constants of two modes respectively, (7.25) is integrated as:

$$
\iint(\boldsymbol{E}_1\times \boldsymbol{H}_2-\boldsymbol{E}_2\times \boldsymbol{H}_1)_z dS
$$

$$=\frac{1}{\gamma_1+\gamma_2}\int(\boldsymbol{E}_1\times\boldsymbol{H}_2-\boldsymbol{E}_2\times\boldsymbol{H}_1)\cdot\boldsymbol{n}ds. \quad (7.26)$$

The boundary conditions at the wall are $E_z=-Z_zH_s$, and $E_s=Z_sH_z$, then the line integral in the right hand of (7.26) becomes:

$$\int\{(Z_{s1}-Z_{s2})H_{z1}H_{z2}+(Z_{z1}-Z_{z2})H_{s1}H_{s2}\}\,ds. \quad (7.27)$$

$\int H_{z1}H_{z2}ds$ and $\int H_{s1}H_{s2}ds$ are not generally zero. But in the case when only the impedance has a constant value for every mode, (7.27) always becomes zero. Accordingly, the left hand of (7.26) always becomes zero in such a case. When the waveguide is symmetric, namely, if it does not contain any non-reversible element, the equation made by equating the left hand of (7.26) to zero, easily becomes (2.16).

The wall impedances differ for every mode in general. If ε_2, μ_2 are the material constants of the outside of the helix, and we define $k_2^2=\omega^2\varepsilon_2\mu_2$ and χ_{2i} by the relation

$$\chi_{2i}^2=k_2^2-h_i^2. \quad (7.28)$$

Corresponding to (7.23), in the outside of the waveguide,

$$\left.\begin{aligned} T_i&=p_{2i}H_n^{(2)}(\chi_{2i}r)\begin{matrix}\sin\\ \cos\end{matrix}n\varphi,\\ T_i'&=q_{2i}H_n^{(2)}(\chi_{2i}r)\begin{matrix}\cos\\ -\sin\end{matrix}u\varphi.\end{aligned}\right\} \quad (7.29)$$

From (2.11) and (7.23), we get in the outside

$$\left.\begin{aligned} e_{zi}&=-\frac{\chi_{2i}^2}{i\omega\varepsilon_0}p_{2i}H_n^{(2)}(\chi_{2i}r)\begin{matrix}\sin\\ \cos\end{matrix}n\varphi,\\ h_{\varphi i}&=\frac{\varepsilon_2}{\varepsilon_0}\chi_{2i}p_{2i}H_n^{(2)\prime}(\chi_{2i}r)\begin{matrix}\sin\\ \cos\end{matrix}n\varphi,\\ &\quad-\frac{h_i^2}{k_0^2}q_{2i}\frac{n}{r}H_n^{(2)}(\chi_{2i}r)\begin{matrix}\sin\\ \cos\end{matrix}n\varphi.\end{aligned}\right\} \quad (7.30)$$

Using the asymptotic expansion of the Hankel function, in case of $|x|\gg(4n^2-1)/8$, $|x|\gg|n|$

$$\frac{H_n^{(2)\prime}(x)}{H_n^{(2)}(x)}=-i. \quad (7.31)$$

Then the impedance for the the mode i is

$$Z_{zi}\doteqdot\frac{\chi_{2i}}{\omega\varepsilon_2}. \quad (7.32)$$

If we put $\mu_2=\mu_0$, and $\varepsilon_2=(\varepsilon'-i\varepsilon'')\varepsilon_0$ and the diameter of the waveguide is much larger than the wavelength, and $|\varepsilon'-1-i\varepsilon''|\gg(\chi_{1i}/k_0)^2$, then

$$Z_{zi}=\sqrt{\frac{\mu_0}{\varepsilon_0}}\frac{\sqrt{\varepsilon'-1-i\varepsilon''}}{\varepsilon'-i\varepsilon''}\left\{1+\frac{1}{2}\frac{\chi_{1i}^2}{k_0^2}\frac{1}{\varepsilon'-1-i\varepsilon''}\right\}, \quad (7.33)$$

which enables us to believe that the impedance is approximately a constant value for the modes except the very high order ones when the outside part of the helix is formed of usual dielectrics.

Hereafter, we assume that Z_z has a constant value for every mode, Z_s is zero, and the inner part of the guide is filled with air. Then, $\varepsilon=\varepsilon_0$ and $\mu=\mu_0$ at the interior part of the z waveguide. χ_{1i} is simply written as χ_i, and

$$\left.\begin{aligned} \nabla_t^2T_i&=-\chi_i^2T_i,\\ \nabla_t^2T_i'&=-\chi_i^2T_i',\end{aligned}\right\} \quad (7.34)$$

where χ_i is a constant not depending on the position in the cross section of the waveguide. The components of the fields are:

$$\left.\begin{aligned} e_{zi}&=-\frac{\chi_i^2}{i\omega\varepsilon_0}T_i,\\ h_{zi}&=-\frac{\chi_i^2}{i\omega\mu_0}T_i'.\end{aligned}\right\} \quad (7.35)$$

If p_{1i} and q_{1i} are written simply as p_i and q_i, then the mode conversion factors from the TE$_{01}$ mode to the mode i by the deformation of the wall are represented as:

$$\begin{matrix}C_i^{\pm}\\ S_i^{\pm}\end{matrix}=\pm i\frac{1}{2\sqrt{\pi}}k_{[01]}\chi_i^2\frac{1}{k_0a}\sqrt{\frac{h_i}{h_{[01]}}}q_iJ_n(\chi_ia)$$

$$\times\int_0^z\int_0^{2\pi} r_1(\varphi, z')e^{-i(h_{[01]}\mp h_i)z'} \begin{matrix}\cos\\ -\sin\end{matrix} n\varphi d\varphi dz', \tag{7.36}$$

where $k_{[01]}$ is the first root of $J_1(x)=0$ other than zero, namely 3.832.

The characteristic equation to decide χ_i is obtained from the boundary condition. From $e_{zi}=-Z_z h_{\varphi i}$,

$$\frac{\chi_i^2}{i\omega\varepsilon_0} p_i J_n(k_i)$$

$$=Z_z\left\{p_i\chi_i J_n'(k_i) - q_i\frac{h_i^2}{k_0^2}\frac{n}{a}J_n(k_i)\right\}. \tag{7.37}$$

And from $e_{\varphi i}=0$,

$$p_i=\frac{k_i}{n}\frac{J_n'(k_i)}{J_n(k_i)}q_i, \tag{7.38}$$

where $k_i=\chi_i a$. From these two equations, the characteristic equation

$$\frac{k_0 a}{k_i}\frac{J_n'(k_i)}{J_n(k_i)}-\frac{n^2h_i^2a}{k_i^3k_0}\frac{J_n(k_i)}{J_n'(k_i)}=-i\frac{Z_0}{Z_z}, \tag{7.39}$$

is obtained, but $Z_0=\sqrt{\mu_0/\varepsilon_0}$. One more equation is needed to determine p_i and q_i. The normalizing orthogonality relation satisfies this requirement. From

$$\iint_S(\boldsymbol{e}_{ti}\times\boldsymbol{h}_{ti})\cdot\boldsymbol{i}_z dS=1, \tag{7.40}$$

we can get provided $n\neq 0$

$$\pi\left[\frac{k_i^2}{2}\left(p_i^2+\frac{h_i^2}{k_0^2}q_i^2\right)\left\{\left(1-\frac{n^2}{k_i^2}\right)J_n^2(k_i)\right.\right.$$

$$\left.+J_n'^2(k_i)\right\}-np_iq_i\left(1+\frac{h_i^2}{k_0^2}\right)J_n^2(k_i)$$

$$\left.+k_i\left(p_i^2+\frac{h_i^2}{k_0^2}q_i^2\right)J_n(k_i)J_n'(k_i)\right]=1, \tag{7.41}$$

where h_i can be obtained from $h_i^2=k_0^2-\chi_i^2$.

Since it is difficult to get the mode convertion factor as a functional form of an arbitrary impedance, we will show a numerical example. The helix waveguide is divided into two. In the case of bends, the outside of the helix is made of low loss dielectric and is shielded with a metal tube over it. Then, the impedance has only a reactance component. In case of the mode filter, the outer part is made of lossy material. In the former case, it is said that the thickness of the dielectric layer of about a quarter wavelength in this material is adequate.(8) In such case, Z_z is infinite, and the numerical calculation will be made for such a condition.

First, k_i is determined from the characteristic equation (7.39) in which Z_z is equated to be infinite. Important modes in regard to the mode conversion due to the wall deformation are such that the phase constants are close to that of the TE_{01}. The HY_{nm} modes, where n is a number from one to four, and where m is a small number are taken into consideration. In case of infinite Z_z, the TM_{0m} modes degenerate to the TE_{0m}, but the conversion to these modes does not occur.

We assume $k_0a=26.70$ which is the value for the case when the diameter is 51 mm and the frequency is 50 Gc/s. In case of infinite Z_z, k_i is a real number. Table 6 shows several k_i values.

Table 6

k_i IN CASE OF $Z_z=\infty$ AND $k_0a=26.70$

n \ m	1	2	3
1	2.403	5.05	5.52
2	3.826	6.38	
3	5.13		
4	6.36		

We can find from Table 6 that the HY_{21} mode has the closest phase constant to that of the TE_{01} mode. This kind of the waveguide is manufactured straight and is later bent to the desired bending radius. In general, when the circular tube is bent, the shape of the cross section is apt to be deformed to the elliptic shape, especially at the center part of the bend. Elliptic deformation generates the HY_{2m} modes in which the HY_{21} is the most important one. It is very complicated to consider the problems of the bend and the deformation at the same time, when the guide axis is assumed to be in the straight state, and the cross section is perfect circular at both ends and elliptic at the center, and the ellipticity varies continuously from one end to the other. The dimension of such waveguide is written as;

$$r_1(\varphi, z) \doteqdot \frac{1}{2} r_0 \cos 2\varphi \left(1+\cos \frac{\pi z}{l}\right). \qquad (7.42)$$

At the center part,

$$MAXIMUM\ DIAMETER - MINIMUM\ DIAMETER = 4r_0. \qquad (7.43)$$

The ellipticity e is obtained from

$$e^2 \doteqdot \frac{4r_0}{a}. \qquad (7.44)$$

Fig. 12 shows the elliptic deformation in question. (7.36) and (7.42) enable us to understand that the generating modes are only the HY_{2m}, moreover $S_i^{\pm}$ is zero, and $c_i^{\pm}$ is

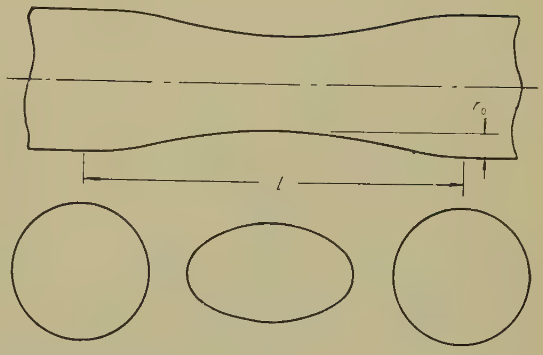

Fig. 12—Elliptical deformed part at the center of the waveguide.

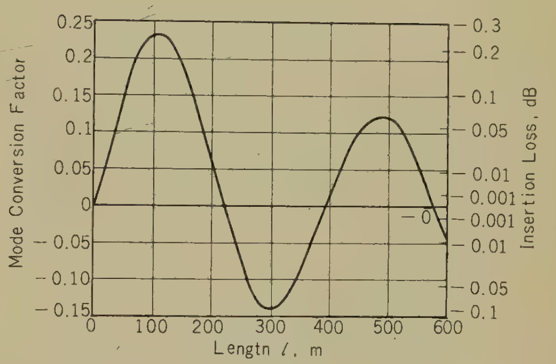

Fig. 13—Mode conversion factor to the HY_{21} mode in the helix waveledge deformed by 40 μ diameter difference at the center part.

$$C_{2m}^{\pm} = \pm i \frac{\sqrt{\pi}}{4} k_{[01]} \chi_{2m}^2 \frac{1}{k_0 a} \sqrt{\frac{h_{2m}}{h_{[01]}}} q_{2m} J_2(\chi_{2m} a) r_0 \int_{-l/2}^{l/2} \left(1+\cos \frac{\pi z}{l}\right) e^{-i(h_{[01]} \mp h_{2m})z} dz. \qquad (7.45)$$

From (7.39), (7.42) and k_{21} in Table 6, in case of $k_0 a = 26.70$, we get

$$\left.\begin{aligned} q_{21} &= 0.37 \\ p_{21} &= -0.36. \end{aligned}\right\} \qquad (7.46)$$

Then, C_{21}^{+} is calculated from the next equation when the diameter is 51 mm long.

$$C_{21}^{+} = i \frac{\sqrt{\pi}}{4} k_{[01]} k_{21}^2 \frac{1}{k_0 a} \sqrt{\frac{k_{21}}{h_{[01]}}} q_{21} J_2(k_{21}) \frac{r_0}{a} \left[\frac{\sin(h_{[01]}-h_{21})(l/2)}{(h_{[01]}-h_{21})(l/2)} - \frac{\pi}{2} \frac{\cos(h_{[01]}-h_{21})(l/2)}{(h_{[01]}-h_{21})^2 (l/2)^2 - (\pi/2)^2} \right] \frac{l}{a} = i\, 0.137 \frac{r_0}{a} \left\{ \frac{\sin 0.0165 l}{0.0165 l} - \frac{\pi}{2} \frac{\cos 0.0165 l}{(0.0165 l)^2 - (\pi/2)^2} \right\} \frac{l}{a}. \qquad (7.47)$$

Fig. 13 shows the mode conversion factor versus the length of the deformed waveguide for the case of $r_0 = 10\ \mu$, namely, a diameter difference of 0.04 mm. The amplitude of the conversion factor except i of the complex number and conversion loss in dB are read from the left and right ordinates respectively. The conversion maximum occurs for a l of about 100 m, and the conversion loss, which is proportional to the square of the diameter difference, is a little less than 0.3 dB.

Different from the helix waveguide with lossless jacket, in case of the helix waveguide with lossy jacket, h_i in (7.36) is a complex quantity. But the converted power can be obtained by a procedure similar to that for the lossless case. Substituting k_i obtained from (7.39), q_i obtained from (7.38) and (7.41) and the designated deformation $r_1(\varphi, z)$, into (7.36), we can get the converted output. However, the converted output is not all the power that the incident TE_{01} has lost. To obtain the conversion entire loss, heat loss of the mode i due to the attenuation from the converting point to the output point must be added. Let α be the attenuation constant for the mode i, namely $-\mathfrak{I}_m(h_i)$. Taking into consideration that C^+ etc. are the amplitude of the converted power divided by $e^{\mp ih_i z}$, the heat loss lost after the conversion is obtained provided the incident unit TE_{01} power,

$$\int_0^L 2\alpha\{|C^+(z)|^2e^{-2\alpha z}+|C^-(z)|^2e^{2\alpha z}$$

$$+|S^+(z)|^2e^{-2\alpha z}+|S^-(z)|^2e^{2\alpha z}\}\,dz, \qquad (7.48)$$

where $C^+(z)$ etc. are C^+ etc. in (7.36) in which the integration limit z is regarded as the variable. Finally, the mode conversion loss of the TE_{01} is calculated from the converted output and the heat loss of (7.48).

8. Couplings between the Modes in Hybrid-Mode Waveguide Bends

The TE_{01} mode in the circular waveguide suffers serious loss due to mode conversion to the TM_{11} mode in bends. In general, each mode in the multi-mode waveguide is coupled with other modes in the bend. Several papars already have given the solutions to this problem,(6)(7)(8) using the generalized telegraphist's equations derived by Schelkunoff.(19) Two of these papers discuss the problem in case the waveguide contains an inhomogeneous dielectric.(7)(8) The Morgan analysis(7) is suitable to solve the proble when the dielectric constant is not much larger than ε_0 anywhere in the guide. If $(\varepsilon-\varepsilon_0)/\varepsilon_0$ becomes so large that it cannot be ignored compared with unity, the accuracy of the calculation is not maintained even when

$$\frac{1}{S}\int_S \frac{\varepsilon-\varepsilon_0}{\varepsilon_0}\,dS \ll 1, \qquad (8.1)$$

where S means the cross section of the waveguide. The Unger analysis(8) is carried out for the two layer waveguide such as the helix waveguide, therefore it may apply to the case of the dielectric-coated waveguide. The calculation, which will be made hereafter, is very general, because the material constants are arbitrary; and is very convenient, because the integral region is limited within the innrr part of the waveguide. The electric and magnetic fields are expanded with the normal modes of the straight hybrid-mode waveguide, not with the plain waveguide, and the couplings among these normal modes are obtained.

At first, the mode couplings in the bent waveguide containing an inhomogeneous dielectric will be calculated generally, then the result will be applied to the dielectric-coated waveguide. The mathematical treatment in section 2 will be utilized.

For the bent waveguide, as shown in Fig. 14, the center of the bending radius lies in the plane $\varphi=\pi$, and,

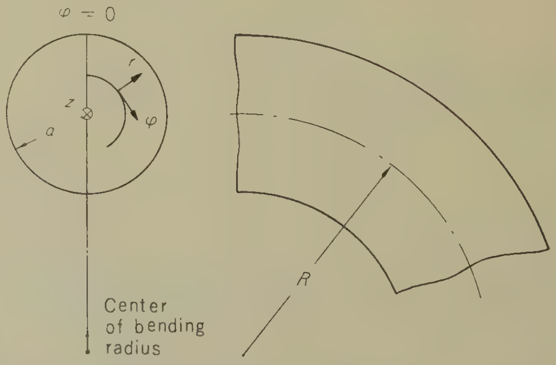

Fig. 14—Bent waveguide containing an inhomogeneous dielectric.

$$\left.\begin{aligned} &e_3=1+\xi,\\ &\xi=\frac{r\cos\varphi}{R},\\ &\frac{\partial e_1}{\partial z}=\frac{\partial e_2}{\partial z}=0, \end{aligned}\right\} \qquad (8.2)$$

where

$$\frac{a}{R}\ll 1, \qquad (8.3)$$

is assumed. For the moment, general orthogonal curvilinear coordinates (u, v, z) are used. In case of the bent waveguide (2.18) becomes:

$$\left.\begin{aligned} &-\frac{1}{e_3}\left\{\frac{\partial}{\partial z}(\boldsymbol{i}_z\times\boldsymbol{E}_t)\right\}\times\boldsymbol{i}_z\\ &=i\omega\mu\boldsymbol{H}_t\times\boldsymbol{i}_z-\frac{1}{e_3}\nabla_t(e_3E_z),\\ &-\frac{1}{e_3}\boldsymbol{i}_z\times\left\{\frac{\partial}{\partial z}(\boldsymbol{H}_t\times\boldsymbol{i}_z)\right\}\\ &=i\omega\varepsilon\boldsymbol{i}_z\times\boldsymbol{E}_t-\frac{1}{e_3}\nabla_t(e_3H_z). \end{aligned}\right\} \qquad (8.4)$$

Of course, inhomogeneous terms in (2.18) are not needed. Equation (2.19) are valid except for the inhomogeneous terms. Namely,

$$\left.\begin{aligned} &H_z=\frac{\nabla_t\boldsymbol{\cdot}(\boldsymbol{i}_z\times\boldsymbol{E}_t)}{i\omega\mu},\\ &E_z=\frac{\nabla_t\boldsymbol{\cdot}(\boldsymbol{H}_t\times\boldsymbol{i}_z)}{i\omega\varepsilon}. \end{aligned}\right\} \qquad (8.5)$$

The electric and magnetic fields are expanded with the normal modes of the straight guide as (2.9) and (2.10). The transverse electric and magnetic field vectors $\boldsymbol{e}_{ti}$ and $\boldsymbol{h}_{ti}$ are the functions of u and v, and are written as (2.11). The characteristic impedance is given by (2.13). Equations (2.14), (2.16) and (2.17) are also valid. Substituting (8.5) into (8.4), then,

$$\left.\begin{aligned} &-\left\{\frac{\partial}{\partial z}(\boldsymbol{i}_z\times\boldsymbol{E}_t)\right\}\times\boldsymbol{i}_z=i\omega\mu e_3\boldsymbol{H}_t\times\boldsymbol{i}_z\\ &\qquad-\frac{1}{i\omega}\nabla_t\frac{e_3\nabla_t\boldsymbol{\cdot}\boldsymbol{H}_t\times\boldsymbol{i}_z}{\varepsilon}\\ &-\boldsymbol{i}_z\times\left\{\frac{\partial}{\partial z}(\boldsymbol{H}_t\times\boldsymbol{i}_z)\right\}=i\omega\varepsilon e_3\boldsymbol{i}_z\times\boldsymbol{E}_t\\ &\qquad-\frac{1}{i\omega}\nabla_t\frac{e_3\nabla_t\boldsymbol{\cdot}\boldsymbol{i}_z\times\boldsymbol{E}_t}{\mu}. \end{aligned}\right\} \qquad (8.6)$$

The upper part of (8.6) is multiplied by $\boldsymbol{h}_{ti}\times\boldsymbol{i}_z$ scalarly and integrated over the cross section of the waveguide. The lower part is multiplied by $\boldsymbol{i}_z\times\boldsymbol{e}_{ti}$ scalarly and integrated over the same area as before. Then we get

$$\left.\begin{aligned} &-\frac{dV_i}{dz}=i\omega\iint e_3\mu\boldsymbol{H}_t\times\boldsymbol{i}_z\boldsymbol{\cdot}\boldsymbol{h}_{ti}\times\boldsymbol{i}_z dS\\ &\qquad-\frac{1}{i\omega}\iint\nabla_t\frac{e_3\nabla_t\boldsymbol{\cdot}\boldsymbol{H}_t\times\boldsymbol{i}_z}{\varepsilon}\boldsymbol{\cdot}\boldsymbol{h}_{ti}\times\boldsymbol{i}_z dS,\\ &-\frac{dI_i}{dz}=i\omega\iint e_3\varepsilon\boldsymbol{i}_z\times\boldsymbol{E}_t\boldsymbol{\cdot}\boldsymbol{i}_z\times\boldsymbol{e}_{ti}dS\\ &\qquad-\frac{1}{i\omega}\iint\nabla_t\frac{e_3\nabla_t\boldsymbol{\cdot}\boldsymbol{i}_z\times\boldsymbol{E}_t}{\mu}\boldsymbol{\cdot}\boldsymbol{i}_z\times\boldsymbol{e}_{ti}dS. \end{aligned}\right\} \qquad (8.7)$$

Now, from (2.11) we can easily get

$$\left.\begin{aligned} &\boldsymbol{h}_{ti}\times\boldsymbol{i}_z=\frac{\varepsilon}{\varepsilon_0}\nabla_tT_i+\frac{h_i^2}{k_0^2}\nabla_tT_i'\times\boldsymbol{i}_z,\\ &\boldsymbol{i}_z\times\boldsymbol{e}_{ti}=-\nabla_tT_i\times\boldsymbol{i}_z+\frac{\mu}{\mu_0}\nabla_tT_i', \end{aligned}\right\} \qquad (8.8)$$

where, of course ε and μ are functions of u and v. The second terms of (8.7) are transformed, using the vector formula (2.23), as follows:

$$\begin{aligned} &\iint\nabla_t\frac{e_3\nabla_t\boldsymbol{\cdot}\boldsymbol{H}_t\times i_z}{\varepsilon}\boldsymbol{\cdot}\boldsymbol{h}_{ti}\times\boldsymbol{i}_z dS\\ &\qquad=-\frac{1}{\varepsilon_0}\iint\chi_i^2\nabla_tT_i\boldsymbol{\cdot}\boldsymbol{H}_t\times\boldsymbol{i}_z+i\omega D_1, \qquad (8.9) \end{aligned}$$

where

$$D_1=\frac{1}{i\omega}\iint\nabla_t\frac{\xi\nabla_t\boldsymbol{\cdot}\boldsymbol{h}_{ti}\times\boldsymbol{i}_z}{\varepsilon}\boldsymbol{\cdot}\boldsymbol{H}_t\times\boldsymbol{i}_z dS. \qquad (8.10)$$

And,

$$\iint \nabla_t \frac{e_3 \nabla_t \cdot \boldsymbol{i}_z \times \boldsymbol{E}_t}{\mu} \cdot \boldsymbol{i}_z \times \boldsymbol{e}_{ti} dS$$

$$= -\frac{1}{\mu_0} \iint \chi_i^2 \nabla_t T_i' \cdot \boldsymbol{i}_z \times \boldsymbol{E}_t dS + i\omega E_1, \quad (8.11)$$

where

$$E_1 = \frac{1}{i\omega} \iint \nabla_t \frac{\xi \nabla_t \cdot \boldsymbol{i}_z \times \boldsymbol{e}_{ti}}{\mu} \cdot \boldsymbol{i}_z \times \boldsymbol{E}_t dS. \quad (8.12)$$

At the time of derivation of the above equations, a perfect conductive wall was assumed, but these equations are also valid even when the wall has an impedance only if the impedance is a contant value for every mode. The varification of that fact may be done similarly to (7.19) and (7.20). Using (8.9) through (8.12), (8.7) are rewritten as:

$$\left.\begin{aligned} \frac{dV_i(z)}{dz} + ih_i Z_i I_i(z) &= D_1 + D_2, \\ \frac{dI_i(z)}{dz} + ih_i Y_i V_i(z) &= E_1 + E, \end{aligned}\right\} \quad (8.13)$$

where

$$\left.\begin{aligned} D_2 &= -i\omega \iint \xi \mu \boldsymbol{H}_t \times \boldsymbol{i}_z \cdot \boldsymbol{h}_{ti} \times \boldsymbol{i}_z dS, \\ E_2 &= -i\omega \iint \xi \varepsilon \boldsymbol{i}_z \times \boldsymbol{E}_t \cdot \boldsymbol{i}_z \times \boldsymbol{e}_{ti} dS. \end{aligned}\right\} \quad (8.14)$$

Now, the mode amplitudes are defined as (2.33):

$$A_i^{\pm}(z) = \frac{V_i(z)}{\sqrt{Z_i}} \pm \frac{I_i(z)}{\sqrt{Y_i}}. \quad (8.15)$$

Then, (8.13) are rewritten as:

$$\frac{dA_i^{\pm}(z)}{dz} \pm ih_i A_i^{\pm}(z) = a_i^{\pm}(z), \quad (8.16)$$

where the double sign is taken in the same order. $a_i^{\pm}(z)$ are defined as:

$$a_i^{\pm}(z) = \frac{D_1 + D_2}{\sqrt{Z_i}} \pm \frac{E_1 + E_2}{\sqrt{Y_i}}. \quad (8.17)$$

From (8.10), (8.12) and (8.14), we get

$$\left.\begin{aligned} D_1 + D_2 &= -i\omega \sum_j I_j \iint \boldsymbol{h}_{tj} \times \boldsymbol{i}_z \\ &\quad \times \left(\xi \mu \boldsymbol{h}_{ti} \times \boldsymbol{i}_z + \nabla_t \frac{\xi \nabla_t \cdot \boldsymbol{h}_{ti} \times \boldsymbol{i}_z}{\omega^2 \varepsilon} \right) dS, \\ E_1 + E_2 &= -i\omega \sum V_j \iint \boldsymbol{i}_z \times \boldsymbol{e}_{tj} \\ &\quad \times \left(\xi \varepsilon \boldsymbol{i}_z \times \boldsymbol{e}_{ti} + \nabla^t \frac{\xi \nabla_t \cdot \boldsymbol{i}_z \times \boldsymbol{e}_{ti}}{\omega^2 \mu} \right) dS. \end{aligned}\right\} \quad (8.18)$$

Substituting the relation derived from (8.15) into the mode voltages and currents in (8.18), and substituting the results into (8.17), then

$$a_i^{\pm} = -\frac{i\omega}{\sqrt{Z_i}} \sum_j \frac{A_j^+ - A_j^-}{2\sqrt{Z_j}} \iint \boldsymbol{h}_{tj} \times \boldsymbol{i}_z \cdot \left(\xi \mu \boldsymbol{h}_{ti} \times \boldsymbol{i}_z \right.$$

$$\left. + \nabla_t \frac{\xi \nabla_t \cdot \boldsymbol{h}_{ti} \times \boldsymbol{i}_z}{\omega^2 \varepsilon} \right) dS \mp \frac{i\omega}{\sqrt{Y_i}} \sum_j \frac{A_j^+ + A_j^-}{2\sqrt{Y_j}}$$

$$\times \iint \boldsymbol{i}_z \times \boldsymbol{e}_{ti} \cdot \left(\xi \varepsilon \boldsymbol{i}_z \times \boldsymbol{e}_{ti} + \nabla_t \frac{\xi \nabla_t \cdot \boldsymbol{i}_z \times \boldsymbol{e}_{ti}}{\omega^2 \mu} \right) dS.$$

$$(8.19)$$

In the mode coupling equation

$$\left.\begin{aligned} a_i^{+}(z) &= i \sum_j (c_{ij}^+ A_j^+ + c_{ij}^- A_j^-), \\ a_i^{-}(z) &= -i \sum_j (c_{ij}^- A_j^+ + c_{ij}^- A_j^-), \end{aligned}\right\} \quad (8.20)$$

the coupling coefficient between modes *i* and *j* $c_{ij}^{\pm}$ is obtained from the following calculation:

$$c_{ij}^{\pm} = \pm \frac{\omega}{2\sqrt{Z_i Z_j}} \iint \boldsymbol{h}_{tj} \times \boldsymbol{i}_z \cdot \left(\xi \mu \boldsymbol{h}_{ti} \times \boldsymbol{i}_z \right.$$

$$\left. + \nabla_t \frac{\xi \nabla_t \cdot \boldsymbol{h}_{ti} \times \boldsymbol{i}_z}{\omega^2 \varepsilon} \right) dS + \frac{\omega}{2\sqrt{Y_i Y_j}}$$

$$\times \iint \boldsymbol{i}_z \times \boldsymbol{e}_{tj} \cdot \left(\xi \varepsilon \boldsymbol{i}_z \times \boldsymbol{e}_{ti} + \nabla_t \frac{\xi \nabla_t \cdot \boldsymbol{i}_z \times \boldsymbol{e}_{ti}}{\omega^2 \mu} \right) dS.$$

$$(8.21)$$

This is the general formula for the mode couplings in a bent waveguide having an inhomogeneous dielectric in it. The coupling between the TE$_{01}$ and one of the other modes is especially important for the practical application. When the mode i is the TE$_{01}$ mode,

$$c_{[01]j}^{\pm}=\pm\frac{\omega}{2\sqrt{Z_{[01]}Z_j}}\iint\left\{\frac{\varepsilon}{\varepsilon_0}\nabla_t T_j+\frac{h_j^2}{k_0^2}\nabla_t T_j'\times\boldsymbol{i}_z\right\}\cdot\left\{\xi\mu_0\frac{h_{[01]}^2}{k_0^2}\nabla_t T'_{[01]}\times\boldsymbol{i}_z\right\}dS+\frac{\omega}{2\sqrt{Y_{[01]}Y_j}}\iint\{-\nabla_t T_j\times\boldsymbol{i}_z+\nabla_t T_j'\}\cdot\left\{\xi\varepsilon\nabla_t T'_{[01]}+\nabla_t\frac{\xi\nabla_t^2 T'_{[01]}}{\omega^2\mu_0}\right\}dS. \tag{8.22}$$

The coupling coefficients between the TE$_{01}$ and one of the other modes in the bent dielectric-coated waveguide can be derived from (8.22). The TE$_{1m}$ and TM$_{1m}$ modes have coupling with the TE$_{01}$ mode. In the plain waveguide the TM$_{1m}$ modes do not have the coupling with the TE$_{01}$ mode, and even in the case of the dielectric-coated waveguide the coupling coefficients between one of the TM$_{1m}$ and TE$_{01}$ modes are in the order of δ^2 at most.

The most important mode in regard to the coupling with the TE$_{01}$ is the TM$_{11}$ mode, which is calculated for the zeroth and first order terms of δ. The coupling coefficients between one of the TM$_{1m}$ and TE$_{01}$ modes are

$$c_{[01](1m)}^{\pm}=\pm\frac{\sqrt{h_{[10]}}^3}{2\sqrt{h_{(1m)}}}\left\{\frac{\varepsilon_1}{\varepsilon_2}I_1+\frac{\varepsilon_2}{\varepsilon_0}I_2+\frac{h_{(1m)}^2}{k_0^2}(I_3+I_4)\right\}+\frac{\sqrt{h_{[01]}h_{(1m)}}}{2}\left\{\frac{\varepsilon_1}{\varepsilon_0}I_1+\frac{\varepsilon_2}{\varepsilon_0}I_2+\frac{\varepsilon_1}{\varepsilon_0}I_3+\frac{\varepsilon_2}{\varepsilon_0}I_4+\frac{1}{k_0^2}(\chi_{1[01]}^2I_5+\chi_{2[01]}^2I_6-\chi_{1[01]}^2I_7-\chi_{2[01]}^2I_8)\right\}, \tag{8.23}$$

where

$$\left.\begin{aligned}I_1&=\iint_{①}\xi\nabla_t T_{(1m)}\cdot\nabla_t T'_{[01]}\times\boldsymbol{i}_z dS,\\ I_3&=\iint_{①}\xi\nabla_t T'_{(1m)}\cdot\nabla_t T'_{[01]}dS,\\ I_5&=\iint_{①}\nabla_t T_{(1m)}\times\boldsymbol{i}_z\cdot\nabla_t(\xi T'_{[01]})dS,\\ I_7&=\iint_{①}\nabla_t T'_{(1m)}\cdot\nabla_t(\xi T'_{[01]})dS,\end{aligned}\right\} \tag{8.24}$$

and I_2, I_4, I_6 and I_8 are the same as I_1, I_3 I_5 and I_7 except that the integration regions are changed from regin 1 to region 2. (refer to Fig. 2) These integrals can be calculated using the formula in Shimizu's paper.$^{(6)}$ When $m=1$, $I_2=0(\delta^3)$; $I_4=0(\delta^2)$ and $I_8=(\delta^2)$, the terms of $0(\delta^0)$ is I_1 and the terms of $0(\delta)$ are I_1, I_3, I_5, I_6 and I_7. After a long calculation, we get

$$c_{[01](11)}^{\pm}=\frac{k_0 a}{2\sqrt{2}\,k_{[01]}R}\left(1-\frac{1}{2}\frac{\varepsilon_2-\varepsilon_1}{\varepsilon_2}\delta\right)(1\pm1). \tag{8.25}$$

If we set $\delta=0$, the above equation coincides with that of the plain waveguide. The mode coupling coefficient between the TE$_{01}$ and TM$_{T1}$ modes is the little smaller than that of the plain waveguide. The coupling to the backward TM$_{11}$ is zero so far as $0(\delta)$.

We will now proceed to the problem of coupling between the TE$_{01}$ and the other modes in the helix waveguide. We have two sorts of helix waveguides, one of which is composed of closely would insulated were, covered with a glass fiber rainforced low loss region and inserted into a metal pipe; the other is composed of the same wire covered with lossy dielectric. The former is used for bends, and the latter is used for mode filters. It is assumed that the inner material is air, the cross sectional shape is a circle, and the impedance is constant for all the modes. From (7.23), T functions of the helix waveguide are

$$\left.\begin{aligned} T_i &= p_i J_n(\chi_i r) \begin{matrix}\sin\\ \cos\end{matrix} n\varphi, \\ T_i' &= q_i J_n(\chi_i r) \begin{matrix}\cos\\ -\sin\end{matrix} n\varphi. \end{aligned}\right\} \tag{8.26}$$

The characteristic equation (7.39) and the normalized orthogonality condition (7.41) are also valid.

If the bending radius center lies in the plane $\varphi=\pi$ in the helix waveguide bend, the modes which have coupling with the TE$_{01}$ mode are only the HY$_{1m}$ which correspond upper parts in the double trigonometric sign of (8.26). Substitution, j to 1m, in (8.22) enables us to obtain the coupling factors between the TE$_{01}$ and one of the HY$_{1m}$ modes as:

$$c_{[01]j}^{\pm} = \pm \frac{\sqrt{h_{[01]}^3}}{2\sqrt{h_j}}\left(I_1' + \frac{h_j^2}{k_0^2} I_2'\right) + \frac{\sqrt{h_{[01]}h_j}}{2}\left\{I_1' + I_2' + \frac{\chi_{[01]}^2}{k_0^2}(I_3' - I_4')\right\}, \tag{8.27}$$

where

$$\left.\begin{aligned} I_1' &= \iint \xi \nabla_t T_j \cdot \nabla_t T'_{[01]} \times \boldsymbol{i}_z dS, \\ I_2' &= \iint \xi \nabla_t T_j' \cdot \nabla_t T'_{[01]} dS, \\ I_3' &= \iint \nabla_t T_j \times \boldsymbol{i}_z \cdot \nabla_t (\xi T'_{[01]}) dS, \\ I_4' &= \iint \nabla_t T_j' \cdot \nabla_t (\xi T'_{[01]}) dS. \end{aligned}\right\} \tag{8.28}$$

After the calculation we obtain

$$c_{[01]j}^{\pm} = q_j \frac{\sqrt{\pi}\, k_{[01]} k_j^2}{2k_0 a (k_j^2 - k_{[01]}^2)\sqrt{h_{[01]}h_j}\, R} \times\left[\pm h_{[01]}\left\{k_j J_1'(k_j) + \frac{2h_j^2}{h_{[01]}^2 - h_j^2} J_1(k_j)\right\} + h_j\left\{k_j J_1'(k_j) + \frac{h_{[01]}^2 + h_j^2}{h_{[01]}^2 - h_j^2} J_1(k_j)\right\}\right], \tag{8.29}$$

where the subscript j means 1m.

Let the wall impedance be zero at first. The characteristic equation (7.39) has two kinds of solutions in case $Z_z=0$. One of them, the solutions of $J_1'(k_j)=0$, is to determines the TE$_{1m}$ modes, at that time (8.29) becomes:

$$c_{[01][1m]}^{\pm} = \frac{k_{[01]} k_{[1m]}^2 a}{\sqrt{2}\sqrt{k_{[1m]}^2 - 1}\,(k_{[1m]}^2 - k_{[01]}^2)^2 \sqrt{h_{[01]}h_{[1m]}}\, R}(h_{[1m]} \pm h_{[01]})^2. \tag{8.30}$$

q_j in (8.29) is obtained from (7.41), but it has been already obtained in (3.30) if δ is set to zero. The other kind of solution, that of $J_1(k_j)=0$, is to determine the TM$_{1m}$ modes (the coupling exists only when $m=1$), but at that time the following substitution is made, since q_j is zero:

$$q_j \to \frac{p_j}{k_j} \frac{J_1(k_j)}{J_1'(k_j)}, \tag{8, 31}$$

In case of the TM$_{11}$, $k_{[01]}=k_j$, then (8.29) becomes infinite. But if k_j is assumed to differ from $k_{[01]}$ by a small amount, and the difference is brought to zero, then we obtain:

$$\left.\begin{aligned} c_{[01](11)}^{+} &= \frac{k_0 a}{\sqrt{2}\, k_{[01]} R}, \\ c_{[01][11]}^{-} &= 0. \end{aligned}\right\} \tag{8.32}$$

Equation (8.30) is the coupling factor between the TE$_{01}$ and the TE$_{1m}$, and (8.32) are factors between the TE$_{01}$ and TM$_{11}$ modes which have been already obtained.(6)(7) After all, (8.29) is the general formula of the mode coupling in the bent waveguide having arbitrary wall impedance.

Table 7 shows q_{1m} values of the HY$_{1m}$ modes, calculated from (7.37), (7.38), and the p_{1m} values, for the cases where m is 1, 2, and 3. k_j values have already been shown in Table 6, in case that Z_z is infinite and $k_0 a=26.70$.

The coupling coefficients for these three modes will be shown in the following equations, with the coupling coefficient for the TM$_{11}$ mode in the plain bent waveguide:

$$\left.\begin{aligned} c_{[01]11}^{+} &= 4.50\frac{1}{R}, \\ c_{[01]12}^{+} &= -5.69\frac{1}{R}, \\ c_{[01]13}^{+} &= -4.32\frac{1}{R}, \\ c_{[01](11)}^{+} &= 4.94\frac{1}{R}. \end{aligned}\right\} \qquad (8.33)$$

Table 7

p_{1m} AND q_{1m} OF THE HELIX WAVEGUIDE IN CASE OF $Z_z=\infty$ AND $k_0a=26.70$

m	p_{1m}	q_{1m}
1	−0.45	0.45
2	0.38	0.26
3	−0.30	0.30

These values have been calculated for the case where $k_0a=26.70$. The dimensions of these values are m^{-1}. These three modes play the leading part in the bent helix waveguide instead of the TM$_{11}$, TE$_{11}$ and TE$_{12}$ modes in the bent plain waveguide.

9. Attenuation Increase for the TE$_{01}$ Mode due to Elliptical Distortion of the Helix Waveguide

The helix waveguide is a necessary line element in the TE$_{01}$ mode transmission line of circular waveguide to absorb the unwanted modes converted at waveguide defects such as tilt or offset at a junction. It is also possible to construct all the lines with helix waveguides. If a geometrically perfect helix waveguide is deformed, the attenuation increases. If the cross section of the circular metal drawn waveguide is deformed to an ellipse, the attenuation increases, and the characteristic of the circular electric wave that the attenuation decreases monotonously with the frequency increase is lost, and an optimal frequency at which the attenuation becomes minimum exists.(9) In case of the helix waveguide, an axial component of the wall current arises owing to the elliptical deformation, and to the axial current, and the impedance is much higher than that of the metal waveguide. Therefore, elliptical deformation seriously affecs the attenuation in the case of the helix waveguide.

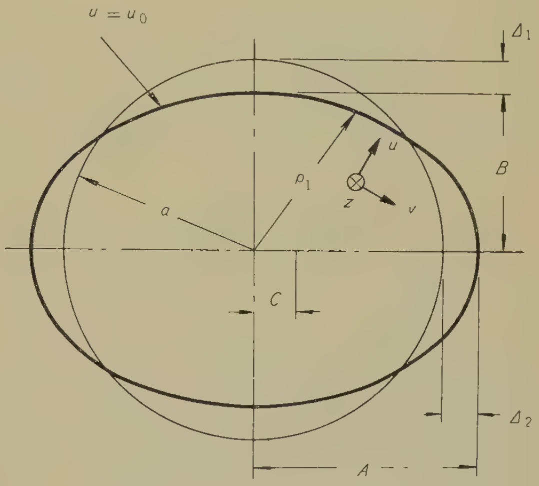

Fig. 15—Cross section of elliptic waveguide.

The attenuation increase due to the elliptical deformation of the helix waveguide is expanded in a power series of the ellipticity, and the lowest term only is calculated. T functions in elliptic waveguide are expanded in terms of those of the circular waveguide,(9) and the coefficient is obtained up to fourth power of the ellipticity. The boundary condition is prescribed by the wall impedance. Exactly speaking, the impedance for the mode in question must be known previously to be calculated by this method. But practically, the approximate impedance in (7.33) can be satisfactorily used neglecting the second term in the braces. Fig. 15 shows the elliptically deformed cross section from the circle; the major axis is 2A and the minor axis is 2 B. The mode vectors of such an elliptic waveguide can be obtained from the following two scalar functions T and T', using the cylindrical coordinates (r, φ, z):

$$\left.\begin{aligned} T(r,\varphi) &= pJ_0(\chi r) + sJ_2(\chi r)\sin 2\varphi + \cdots\cdots, \\ T'(r,\varphi) &= qJ_0(\chi r) + tJ_2(\chi r)\cos 2\varphi + \cdots\cdots. \end{aligned}\right\} \tag{9, 1}$$

The components of the electric and magnetic fields are written as follows, using the elliptic cylindrical coordinates and (2.11):

$$\left.\begin{aligned} e_u &= V(z)\left(\frac{\partial T}{e_1\partial u} + \frac{\partial T'}{e_2\partial v}\right), \\ e_v &= V(z)\left(\frac{\partial T}{e_2\partial v} - \frac{\partial T'}{e_1\partial u}\right), \\ h_u &= -I(z)\left(\frac{\partial T}{e_2\partial v} - \frac{h^2}{k_0^2}\frac{\partial T'}{e_1\partial u}\right), \\ h_v &= I(z)\left(\frac{\partial T}{e_1\partial u} + \frac{h^2}{k_0^2}\frac{\partial T'}{e_2\partial v}\right), \\ h_z &= -V(z)\frac{\chi^2}{i\omega\mu_0}T', \\ e_z &= -I(z)\frac{\chi^2}{i\omega\varepsilon_0}T. \end{aligned}\right\} \tag{9. 2}$$

Before substituting (9.1), expressed by circular cylindrical coordinates, into (9.2), expressed by the elliptic cylindrical coordinates, the relation between both kinds of coordinates must be obtained. As shown in Fig. 15, let C be the distance between the original and focus points, e be ellipticity: and ρ_1 be the distance between the original point and the wall. Let the wall be at the elliptic coordinate $u=u_0$, then we can get

$$\left.\begin{aligned} u_0 &= \frac{1}{e}, \\ r &= C\sqrt{u^2+v^2-1}, \\ \rho_1 &= C\sqrt{u_0^2+v^2-1}, \\ A &= Cu_0, \\ B &= C\sqrt{u_0^2-1}, \\ \varphi &= \tan^{-1}\frac{\sqrt{(u^2-1)(1-v^2)}}{uv}, \\ e_1 &= C\sqrt{\frac{u^2-v^2}{u^2-1}}, \\ e_2 &= C\sqrt{\frac{u^2-v^2}{1-v^2}}, \\ e_3 &= 1. \end{aligned}\right\} \tag{9. 3}$$

The relations of the differentiation

$$\left.\begin{aligned} \frac{\partial}{\partial u} &= \frac{\partial r}{\partial u}\frac{\partial}{\partial r} + \frac{\partial\varphi}{\partial u}\frac{\partial}{\partial\varphi}, \\ \frac{\partial}{\partial v} &= \frac{\partial r}{\partial v}\frac{\partial}{\partial r} + \frac{\partial\varphi}{\partial v}\frac{\partial}{\partial\varphi}, \end{aligned}\right\} \tag{9. 3}$$

are also obtained. From the assumption that the peripheral lengths of the circle and ellipse in Fig. 15 are the same, ρ_1 can be expanded in the power series of the ellipticity by circular cyrindrical coordinates as:

$$\begin{aligned} \rho_1 = a\Big\{ & 1 + \left(\frac{1}{4}\cos 2\varphi\right)e^2 \\ & + \left(\frac{3}{64}\cos 4\varphi + \frac{1}{8}\cos 2\varphi - \frac{1}{16}\right)e^4 \Big\}. \end{aligned} \tag{9. 5}$$

The impedance for the v direction electric field in the helix waveguide is much less than that for the z direction electric field, and only the attenuation increase by Z_z is calculated. Therefore, the boundary conditions at the wall surface $u=u_0$ are

$$\left.\begin{aligned} e_z &= -Z_z h_v, \\ e_v &= 0. \end{aligned}\right\} \tag{9. 6}$$

Using (9.2), these equations become:

$$\left.\begin{aligned}&\frac{\chi^2}{i\omega\varepsilon_0}T-Z_z\left(\frac{\partial T}{e_1\partial u}+\frac{h^2}{k_0^2}\frac{\partial T'}{e_2\partial v}\right)=0,\\&\frac{\partial T}{e_2\partial v}-\frac{\partial T'}{e_1\partial u}=0.\end{aligned}\right\}\quad(9.7)$$

To expand these equations in the power series of the ellipticity by the circular cylinder coordinates, the following quantities must be calculated:

$$\left.\begin{aligned}&\frac{\partial r}{\partial u}\bigg|_{u=u_0}=ae\left\{1+\left(-\frac{1}{4}\cos 2\varphi+\frac{1}{2}\right)e^2\right.\\&\qquad\left.+\left(-\frac{1}{64}\cos 4\varphi-\frac{1}{4}\cos 2\varphi+\frac{3}{8}\right)e^4\right\},\\&\frac{\partial\varphi}{\partial u}\bigg|_{u=u_0}=e^3\left(\frac{1}{2}+\frac{1}{2}e^2\right)\sin 2\varphi,\\&\frac{\partial r}{\partial v}\bigg|_{u=u_0}=ae^2\left(1+\frac{1}{4}e^2\right)\cos\varphi,\\&\frac{\partial\varphi}{\partial v}\bigg|=\left\{-1+\left(\frac{3}{4}\cos 2\varphi+\frac{1}{4}\right)e^2\right\}\operatorname{cosec}\varphi.\end{aligned}\right\}\quad(9.8)$$

Using (9.4), (9.7) becomes:

$$\left.\begin{aligned}&-\frac{\chi^2}{Z_z i\omega\varepsilon_0}T+\frac{1}{e_1}\left(\frac{\partial T}{\partial r}\frac{\partial r}{\partial u}+\frac{\partial T}{\partial\varphi}\frac{\partial\varphi}{\partial u}\right)\\&\quad+\frac{h^2}{e_2k_0^2}\left(\frac{\partial T'}{\partial r}\frac{\partial r}{\partial v}+\frac{\partial T'}{\partial\varphi}\frac{\partial\varphi}{\partial v}\right)=0,\\&\frac{1}{e_2}\left(\frac{\partial T}{\partial r}\frac{\partial r}{\partial v}+\frac{\partial T}{\partial\varphi}\frac{\partial\varphi}{\partial v}\right)\\&\quad-\frac{1}{e_1}\left(\frac{\partial T'}{\partial r}\frac{\partial r}{\partial u}+\frac{\partial T'}{\partial\varphi}\frac{\partial\varphi}{\partial u}\right)=0.\end{aligned}\right\}\quad(9.9)$$

And, the separation constant χ is expanded in a power series of the ellipticity as:

$$\chi=\chi_0(1+\lambda e^2+\mu e^4).\qquad(9.10)$$

where χ_0 is the first root except zero of

$$J_0'(\chi_0 a)=0.\qquad(9.11)$$

In this section, λ and μ are not the wavelength and the permeability respectively. To obtain the expansion of the Bessel functions required for the calculation of the boundary condition, we set

$$\chi\rho_1=\chi_0 a(1+\delta)\qquad(9.12)$$

where

$$\delta=\left(\lambda+\frac{1}{4}\cos 2\varphi\right)e^2+\left\{\left(\mu-\frac{1}{16}\right)\right.$$
$$\left.+\left(\frac{\lambda}{4}+\frac{1}{8}\right)\cos 2\varphi+\frac{3}{64}\cos 4\varphi\right\}e^4.\qquad(9.13)$$

In (9.9), the partial derivatives of T and T' by r and φ have the Bessel functions, which can be expanded with δ in (9.13). The coefficients p, q, s, and t of T and T' functions in (9.1) are expanded with the ellipticity, except q, as:

$$\left.\begin{aligned}&p=p_1e^2+p_2e^4+\cdots\cdots\cdots,\\&s=s_1e^2+s_2e^4+\cdots\cdots\cdots,\\&t=t_1e^2+t_2e^4+\cdots\cdots\cdots.\end{aligned}\right\}\quad(9.14)$$

The metrical coefficients e_1 and e_2 are expressed as functions of the ellipticity as:

$$\left.\begin{aligned}&\frac{1}{e_1}C\sqrt{u_0^2-v^2}\doteqdot\frac{1}{e}\left(1-\frac{e^2}{2}\right),\\&\frac{1}{e_2}C\sqrt{u_0^2-v^2}\doteqdot\left\{1+\left(\frac{1}{4}+\frac{1}{4}\cos 2\varphi\right)e^2\right\}\sin\varphi,\\&C\sqrt{u_0^2-v^2}\doteqdot a\left(1-\frac{1}{4}\cos 2\varphi\, e^2\right).\end{aligned}\right\}\quad(9.15)$$

The expansion for h is

$$\frac{h^2}{k_0^2}=1-\frac{\chi_0^2}{k_0^2}(1+2\lambda e^2).\qquad(9.16)$$

Using the above equations, the first equation of (9.9) is expanded as:

$$
\begin{aligned}
&-\frac{\chi_0{}^2 a}{Z_z i\omega\varepsilon_0 k_0{}^2}(1+2\lambda e^2)\Bigl(1-\frac{1}{4}\cos 2\varphi\, e^2\Bigr)\{(p_1-s_1\sin 2\varphi)e^2+E_1 e^4\}\\
&+\frac{1}{e}\Bigl(1-\frac{e^2}{2}\Bigr)\Bigl[ae\Bigl(\frac{2s_1}{a}\sin 2\varphi\, e^2+E_2 e^4\Bigr)\Bigl\{1+\Bigl(\frac{1}{2}-\frac{1}{4}\cos 2\varphi\Bigr)e^2\Bigr\}-s_1\cos 2\varphi\sin 2\varphi\, e^5\Bigr]\\
&+\Bigl(1-\frac{\chi_0{}^2}{k_0{}^2}-2\frac{\lambda\chi_0{}^2}{k_0{}^2}e^2\Bigr)\Bigl\{1+\Bigl(\frac{1}{4}+\frac{1}{4}\cos 2\varphi\Bigr)e^2\Bigr\}\sin\varphi\Bigl[\chi_0{}^2\Bigl\{-\chi_0 a\Bigl(\lambda+\frac{1}{4}\cos 2\varphi\Bigr)+\frac{2t_1}{\chi_0 a}\cos 2\varphi\Bigr\}\\
&\times ae^4\cos\varphi+(2t_1\sin 2\varphi\, e^2+E_3 e^4)\Bigl\{-1+\Bigl(\frac{1}{4}+\frac{3}{4}\cos 2\varphi\Bigr)e^2\Bigr\}\operatorname{cosec}\varphi\Bigr]=0 \qquad (9.17)
\end{aligned}
$$

where

$$
\left.
\begin{aligned}
&E_1=p_2+2s_1\Bigl(\lambda+\frac{1}{4}\cos 2\varphi\Bigr)\sin 2\varphi-s_2\sin 2\varphi,\\
&E_2=\chi_0\Bigl\{-p_1\chi_0 a\Bigl(\lambda+\frac{1}{4}\cos 2\varphi\Bigr)\\
&\quad+\frac{2}{\chi_0 a}(s_1\lambda+s_2)\sin 2\varphi\\
&\quad+s_1\chi_0 a\Bigl(1-\frac{6}{\chi_0{}^2a^2}\Bigr)\Bigl(\lambda+\frac{1}{4}\cos 2\varphi\Bigr)\sin 2\varphi\Bigr\},\\
&E_3=-4t_1\Bigl(\lambda+\frac{1}{4}\cos 2\varphi\Bigr)\sin 2\varphi+2t_2\sin 2\varphi.
\end{aligned}
\right\} \qquad (9.18)
$$

In (9.17) the terms of the same order of the ellipticity are picked up, and in these terms the constant terms in regard to φ and $\sin 2\varphi$ terms are set equal to zero, then we get

$$
\left.
\begin{aligned}
&p_1=0,\\
&p_2=0,\\
&\Bigl(2+\frac{\chi_0{}^2 a}{Z_z i\omega\varepsilon_0}\Bigr)s_1-2\Bigl(1-\frac{\chi_0{}^2}{k_0{}^2}\Bigr)t_1=0.
\end{aligned}
\right\} \qquad (9.19)
$$

Next, from the second equation of (9.9), we obtain

$$
\begin{aligned}
&\Bigl\{1+\Bigl(\frac{1}{4}+\frac{1}{4}\cos 2\varphi\Bigr)e^2\Bigr\}\sin\varphi\Bigl[2s_1\sin 2\varphi\cos 2\varphi\, e^4+(-2s_1\cos 2\varphi\, e^2+E_4 e^4)\\
&\quad\times\Bigl\{-1+\Bigl(\frac{1}{4}+\frac{3}{4}\cos 2\varphi\Bigr)e^2\Bigr\}\operatorname{cosec}\varphi\Bigr]-\frac{1}{e}\Bigl(1-\frac{e^2}{2}\Bigr)\Bigl[ae\Bigl\{\Bigl(-\chi_0{}^2 a\lambda-\frac{\chi_0{}^2 a}{4}\cos 2\varphi\\
&\quad+2\frac{t_1}{a}\cos 2\varphi\Bigr)e^2+E_5 e^4\Bigr\}\Bigl\{1+\Bigl(\frac{1}{2}-\frac{1}{4}\cos 2\varphi\Bigr)e^2\Bigr\}+t_1\sin^2 2\varphi\, e^5\Bigr]=0, \qquad (9.20)
\end{aligned}
$$

where

$$
\left.
\begin{aligned}
&E_4=4s_1\Bigl(\lambda+\frac{1}{4}\cos 2\varphi\Bigr)\cos 2\varphi-2s_2\cos 2\varphi\\
&\quad+4t_2\Bigl(1-\frac{24}{\chi_0{}^2a^2}\Bigr)\cos 4\varphi\\
&E_5=\chi_0\Bigl[-\lambda\chi_0 a\Bigl(\lambda+\frac{1}{4}\cos 2\varphi\Bigr)-\chi_0 a\Bigl\{\Bigl(\mu-\frac{1}{16}\Bigr)\\
&\quad+\Bigl(\frac{\lambda}{4}+\frac{1}{8}\Bigr)\cos 2\varphi+\frac{3}{64}\cos 4\varphi\Bigr\}\\
&\quad+\frac{\chi_0 a}{2}\Bigl(\lambda+\frac{1}{4}\cos 2\varphi\Bigr)^2+\frac{2}{\chi_0 a}(t_1\lambda\\
&\quad+t_2)\cos 2\varphi+t_1\chi_0 a\lambda\Bigl(1-\frac{6}{\chi_0{}^2a^2}\Bigr)\cos 2\varphi\\
&\quad+\frac{1}{4}t_1\chi_0 a\Bigl(1-\frac{6}{\chi_0{}^2a^2}\Bigr)\cos^2 2\varphi\Bigr].
\end{aligned}
\right\} \qquad (9.21)
$$

The terms of $0(e^2)$ in (9.20) are picked up, and in these terms the constant terms in regard to φ and $\cos 2\varphi$ terms are set equal to zero respectively, then we obtain

$$\left.\begin{aligned}&\lambda=0,\\&s_1-t_1=-\frac{\chi_0^2a^2}{8}.\end{aligned}\right\}\qquad(9.22)$$

From (9.19) and (9.22), we get

$$\left.\begin{aligned}&s_1=\frac{\chi_0^2a^2-k_0^2a^2}{4\left(\dfrac{i\omega\mu_0 a}{Z_z}-2\right)},\\&t_1=\frac{\dfrac{i\omega\mu\chi_0^2a^3}{Z_z}-2k_0^2a^2}{8\left(\dfrac{i\omega\mu_0 a}{Z_z}-2\right)},\end{aligned}\right\}\qquad(9.23)$$

From the term of $0(e^4)$ in (9.21), we get

$$\mu=\frac{\dfrac{i\omega\mu\chi_0^2a}{Z_z}(\chi_0^2a^2+3)-6\chi_0^2-2k_0^2\chi_0^2a^2}{64\chi_0^2\left(\dfrac{i\omega\mu a}{Z_z}-2\right)}.\qquad(9.24)$$

Let h of the circular waveguide be h_0, then there exist the following relations:

$$\left.\begin{aligned}&h_0^2=k_0^2-\chi_0^2,\\&h^2=h_0^2\left(1-\frac{2\chi_0^2\mu e^4}{h_0^2}\right).\end{aligned}\right\}\qquad(9.25)$$

If the ellipticity is so small that $|2\chi_0^2\mu e^4|\ll|h^2_0|$ then the attenuation constant is

$$\alpha=\frac{\chi_0^2}{h_0}\Im(\mu)e^4.\qquad(9.26)$$

Let the wall impedance be $Z_z=R+iX$, then we obtain

$$\alpha=\frac{R}{\zeta a}\frac{e^4}{32}\chi_0^2a^2\sqrt{1-\nu^2}\times\frac{1}{\left(1-\dfrac{2X}{k_0\zeta a}\right)^2+\dfrac{4R^2}{(k_0\zeta a)^2}},\qquad(9.27)$$

where

$$\left.\begin{aligned}&\zeta=\sqrt{\frac{\mu_0}{\varepsilon_0}},\\&\nu=\frac{f_c}{f},\end{aligned}\right\}\qquad(6.28)$$

and f is the frequency, and f_c is the cutoff frequency of the TE_{01} mode in the waveguide before it suffers deformation.

Let $f=50$ Gc/s and $2a=51$ mm, then $k_0\zeta a=10070$, and the fractional term in (9.27) is almost equal to 1, and if it is assumed to be exactly 1 (9.27) coincides with Oguchi's result.(9) The attenuation increase by the elliptic deformation of the helix waveguide is

$$\alpha=0.048\,Re^4=416\,Re^4\ \text{dB/km}.\qquad(9.29)$$

In the case where $R=150$ ohms and the difference between the maximum and minimum diameters is 33.4 μ, the attenuation increase is 10 %.

10. Conclusion

It is considered that the future TE_{01} wave long distance transmission line will be constructed not only of drawn copper pipes, but also of dielectric-coated and helix waveguides. The latter two are general hybrid-mode waveguides, and the relations between the several modes in the hybrid-mode waveguides, especially, the coupling and the conversion at geometrical imperfections or in the bends have been discussed. The mode vectors and the radiation in the waveguide due to the distributed electric and magnetic currents are obtained in the form of the normal hybrid-modes expression. As applications of this principle, the mode conversion due to the irregularity of the dielectric layer in the dielectric-coated waveguide, and due to the waveguide wall deformations, and the mode couplings in bent waveguides are calculated in terms of the relations between the normal hybrid-modes.

In waveguides having the impedance wall, if the wall impedance is assumed to be a constant value for every mode, the method developed above is appricable to the mode coupling problems. The mode conversion factors between the TE$_{01}$ and one of the HY$_{1m}$ modes are obtained at an arbitrary wall impedance, and these results generalize the usual coupling formulae of the plain waveguide. The attenuation increase due to the elliptical deformation of the helix waveguide is also obtained using the hybrid-mode vector expressions.

Acknowledgment

The author wishes to thank Mr. Miwa, Dr. Oguchi, Mr. Iiguchi, and Mr. Yamaguchi for helpful discussions on the subject.

References

(1) H. G. Unger, "Circular Electric Wave Transmission in a Dielectric-Coated Waveguide," *B.S.T.J.*, **36**, 5, p. 1253, 1957.

(2) K. Noda and K. Yamaguchi, "Dielcetric-Coated Waveguide Construction and Characteristics," *Review of the E.C.L.*, **8**, 7-8, p. 309, 1960.

(3) N. Marcuvitz and J. Schwingar, "On the Representation of the Electric and Magnetic Fields Produced by Currents and Discontinuities in Wave Guides. I," *J. A. Phys.*, **22**, 6, p. 806, 1951.

(4) S. P. Morgan, "Mode Conversion Losses in Transmission of Circular Electric Wave through Slightly Non-Cylindrical Guides," *J. A. Phys.*, **21**, 4, p. 329, 1950.

(5) Van Bladel, J, "Normal Modes Methods for Boundary Excited Wave Guides," *ZAMP*, vol. Ⅸa, Fasc. 2, p. 193, 1958. 07. 25.

(6) Y. Shimizu, "Theory of Transmitting Circular Electric Waves around Bends," presented at the International Conference on Ultra-High-Frequency Circuits and Antennas, Paris, October, 1957.

(7) S. P. Morgan, "Theory of Curved Circular Waveguide Containing an Inhomogeneous Dielectric," *B. S. T. J.*, **36**, 5, p. 1209, 1957.

(8) H. G. Unger, "Helix Waveguide Theory and Application," *B. S. T. J.*, **37.**, 6, p, 1599, 1958.

(9) B. Oguchi and M. Kato, "On Elliptic Waveguides," presented at the International Conference on Ultra-High-Frequency Circuits and Antennas, Paris, 1957.

(10) R. B. Adler, "Waves on Inhomogeneons Cylindrical Structures," *Proc. I. R. E.*, **40**, 3, p. 339, 1952.

(11) A. C. Bresler, G. H. Joshi and N. Marcuvitz, "Orthogonality Properties for Modes in Passive and Active Uniform Wave Guides," *J. A. Phys.*, **29**, 5, p. 794, 1958.

(12) B. Oguchi and M. Kato, "The influence of the TE$_{1m}$ modes in the bent waveguide for the TE$_{01}$ mode transmission," presented at the International Conference on Ultra-High-Frequency Circuits and Antennas, Paris, October, 1957.

(13) K. Noda, A. Konose, T. Fujii and K. Miyauchi, "The Characteristics of the Waveguide for Low Loss Transmission," *Elect. Comm. Lab. Tech. Journ.* N. T. T., **7**, 9, P. 741, 1958.

(14) H. G. Unger, "Circular Electric Wave Transmission through Serpentine Bends," *B.S.T.J.*, **36**, 5, p. 1279, 1957.

(15) S. Iiguchi, "Mode Conversion in the Transmission of TE$_{01}$ Wave Through a Slight Tilt and a Slight Off-set of Waveguide," presented at the International Conference on Ultra-High Frequency Circuits and Antennas, Paris, October, 1957.

(16) Marcuse, "Attenuation of the TE$_{01}$ Wave within the Curved Helix Waveguide," *B.S.T. J.*, **37**, 6, p. 1649, 1958.

(17) C. F. P. Rose, "Research Models of Helix Waveguides," *B. S. T. J.*, **37**, 3, p. 679, 1958.

(18) T. Hosono, S. Kohno, "The Transmission of TE$_{01}$ Wave in Helix Waveguides," *Trans. I. R.E.*, MTT-7, 3, p. 370, 1959.

(19) S. A. Schelkunoff, "Conversion of Maxwell's Equation into Generalized Telegraphist's Equations," *B.S.T.J.*, **34**, 5, P. 995, 1955.

* * * *

REVIEW OF THE ELECTRICAL COMMUNICATION LABORATORY
VOLUME 8, NUMBERS 9-10, SEPTEMBER-OCTOBER, 1960

U.D.C. 621.372.823 : 621.372.85

Mode Exciters in Circular Waveguides*

***Ken-ichi NODA*†**

For the purpose of obtaining various modes in circular waveguides, new type exciters have been developed. If rectangular and circular waveguides are closely placed on both sides of a common wall, and the dimensions of the resonant irises located on the wall and their positions are chosen properly, it is possible to convert the incident wave from the rectangular waveguide into only the designated mode in the circular waveguide. At the same time, if the heat loss is negligible, it is possible to make the junction reflectionless with respect to the terminals of both waveguides, and to realize ideal conversion.

In the low-loss transmission by the TE_{01} *mode, undesired mode conversions into the* TE_{11}, TM_{11}, TE_{12}, TE_{21} *modes, etc. are a serious problem; therefore it is necessary to obtain these pure modes to study the characteristics of the undesired converted modes. In connection with these modes, exciters have been successfully made. They are of simple constrution and reflectionless, having high transformation efficiency and high mode purity. By a thermochemical method, the output electric field distributions have been made visible and good images have been obtained by taking their photographs.*

1. Introduction

There are many methods of exciting a specified mode in a multi-mode circular waveguide. The coupled-wave transducer which was developed by Miller is one of them.(1) Rectangular and circular waveguides are placed adjacent to each other on both sides of a common wall, making both guide axis directions coincide; and many irises are located in this wall. This structure is very broadband and reflectionless, and has a function of a directional coupler. However when large magnitude of coupling is desired, especially when the total electric power in the rectangular waveguide must be transformed to a specified mode in the circular waveguide, the number of coupling irises usally increases, and consequently, the length of the coupler also increases. In order to make the phase constants of both the waveguides equal, the dimensions must be kept within extremely strict tolerances, and special attention is necessary in the process of fabricating, especially to processes such as soldering. It is not easy to minimize the insertion loss.

In addition to the coupled transmission line type, several other mode exciters have been obtained already. The taper from rectangular to circular waveguide for the purpose of rotational resistance attenuator, gyrator etc. is the simplest TE_{11} mode exciter and has extremely wide band characteristics, A TM_{01} mode exciter has already been developed to be used for the antenna feeder of a radar and a design has been given for the 24 Gc/s band.(2) The TE_{01} mode exciter has been also well studied in order to be used for the lowloss transmission by the circular waveguide; in addition to the above coupled transmission line type, taper type,(3) resonant iris type,(4) center-excited type,(5) etc. have been reported.

In the exciters described in this paper, resonant irises are utilized, and they are very light in weight. Moreover, the dimension accuracy is not strict, and the electroforming

---

* MS in Japanese received by the Electrical Communication Laboratory, May 21, 1960. Originally published in the *Kenkyû Zituyôka Hôkoku* (*Electrical Communication Techinical Journal*), N.T.T., Vol. 9, No. 9, pp. 1065–1075, 1960.

† Hyper-frequency Research Section.

method can be applied, then the insertion loss can be made small and the price is low. The only defect is that frequency characteristics can not be extremely wide band, though they are wide enough for most practical purposes.

2. Design and Adjustment Procedures

The characteristics required in good mode exciters are as follows: mode transformation efficiency should be good; mode impurity should be small; reflection should be small; frequency characteristics should be broadband; etc. The design and adjustment must proceed in the following order: as the first step, the dimensions of the circular waveguide are chosen so that modes higher than the required mode can not propagate; secondly in order to prevent other modes from appearing, the directions of the slots are chosen; thirdly, in order to generate the required mode, the relative positions of rectangular and circular waveguides are selected; fourthly, in order to get good impedance matching seen from the rectangular side at the required frequency, the sizes of the slots are adjusted; fifthly, if the impure mode are found to be too much, the sizes of the slots are readjusted to get the impure mode as small as possible. At this moment, impedance matching is checked again whether it is within certain magnitude. In this manner, after repeating many tedious experiments the required mode exciter may be perfected.

There are various measuring instruments and methods to investigate the characteristics of the exciter experimentally. A standing-wave detector may be used for the matching of input impedance or for measuring, S-matrix elements of the exciter by Storer's method.(6) Available mode exciters and coupled transmission line type mode couplers whose characteristics are known, and mode exciters developed by the method explained in this paper, will be useful in various measurements when new mode exciters are to be manufactured. The interior field distribution measuring instrument by a probe or slot is used to measure the contents of the impure modes. Though strictly quantitative measurement is not possible, there is a method of making the electric field distribution visible by use of paper soaked with cobalt chlorite solution.(7)

Circular waveguides for low-loss transmission have diameters of approximately 51 mm when the frequency is in the 50 Gc/s band. But at terminal stations; in cases of channel branching filters, power observation, or mode separation; this diameter is too large because of technical difficulties; thus, smaller diameters are used, and when necessary, connection is made to the part of larger diameter with taper waveguides. The mode exciters discussed in this paper are for the 24 Gc/s band, and in this frequency band the diameter 22.2 mm is standard in our laboratory. In cases when mode exciters have output diameters smaller than this, a taper part is attached to match the output diameter of the exciters.

3. TM_{01} Mode Exciter

As TM_{01} mode exciters are used in radar antenna systems, they have been widely studied, and so those with good characteristics are now available.(2) This exciter can also be used as the field distribution measuring instrument for other mode exciters.

The structure of this exciter is shown in Fig. 1. The output diameter is 22.2 mm but the diameter which has been transformed from the rectangular to the circular TM_{01} is 11.8 mm, and in case of 24 Gc/s, only the TE_{11} and TM_{01} modes can propagate. Approximately at 24.72 GC, the TE_{21} mode, which has the next higher cutoff frequency becomes able to propagate. Consequently, if there is any unwanted mode, it is the TE_{11} mode only. Of the output field of this exciter φ direction distribution of magnetic field, $H\varphi$ has been measured in a plane perpendicular to the axis, and the result is shown in the lower part of Fig. 1. If there is no impurity mode, we will have perfect circle in the figure, but actually some distortion is found. If this is due only to the mixed TE_{11} mode a simpler pattern should have been obtained. Other modes which are produced from taper part, imperfection of the revolving mechanism

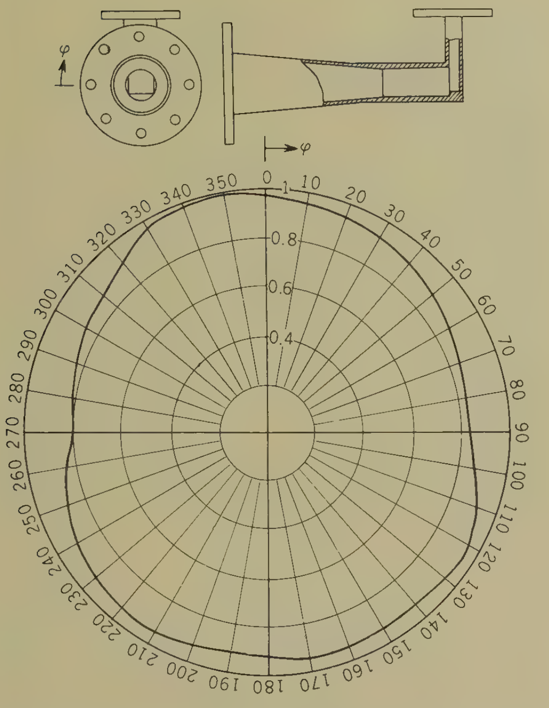

Fig. 1—The structure and measured H_φ of the TM_{01} mode exciter. The amplitude is proportional to the magnetic field strength. The frequency is 24 Gc/s.

of the field distridution measuring instrument, and imperfect contact are the causes of the complex pattern, it is believed.

In order to investigate the composition of the TE_{11} mode, the distribution of the axial components of the magnetic field H_z is measured. If there is pure TM_{01} mode only, nothing can be obtained by measuring H_z. Now, it is supposed that the impure mode is the TE_{11} mode only. H_z of the output is measured with field distribution measuring instrument which is placed in front of the reflectionless termination. If the H_z distribution is measured when the same electric power was injected through the TE_{11} exciter, and compared with that of the TM_{01} mode exciter output, then the H_z of the TE_{11} component included as impure mode can be obtained. The solid line of Fig. 2 is the measured result of the φ direction distribution of H_z of the TE_{11} mode exciter, and it is fairly symmetric. The dotted line of the same figure is the measured H_z of the TM_{01} mode exciter output. The output difference between the tow results is about 20.5 dB, and because the TE_{11} mode component ratio is exceedingly small, and as will be explained later, the insertion loss of the TM_{01} exciter was also very small; then this value is the TE_{11} contents ratio. In receiving with the TE_{11} excitor the TM_{01} exciter output through a fixed buffer attenuator, an output of -22 dB was obtained. This coincides with the result obtained from the field distribution with the error of 1.5 dB. This fixed attenuator consists of a waveguid filled with lossy dielectric, and as the dielectric a wall construction material called *Misasaboard*, was used.

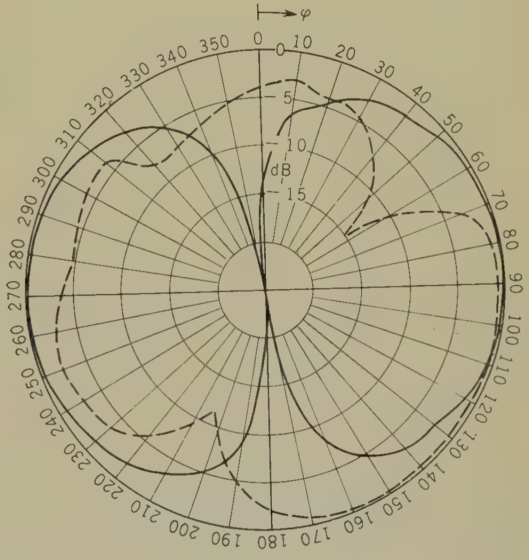

Fig. 2—The measured H_z φ direction distribution of the TM_{01} (dotted line) and TE_{11} (solid line) mode exciters. 0 dB of the dotted line is under 20.5 dB from the 0 dB of the solid line. The frequency is 24 Gc/s.

Now, a method of measuring the field distribution of other exciters using a TM_{01} exciter will be shown. As shown at the upper part of Fig. 3, klystron output in the rectangular waveguide is transformed into the TM_{01} mode in the circular waveguide by means of No. 1 exciter, it is again transformed back to the rectangular waveguide by means of No. 2

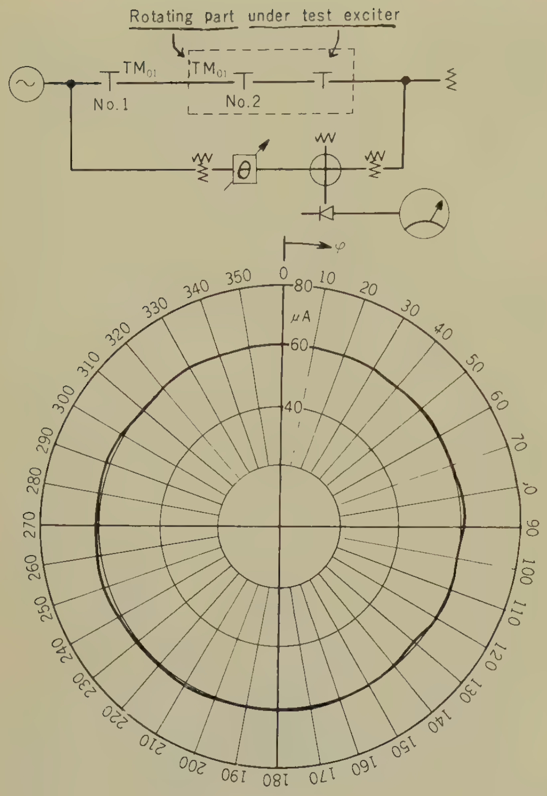

Fig. 3—The field analyser using the TM_{01} mode exciters, and its rotating characteristic. The frequency is 24 Gc/s.

exciter, and then it is fed to the exciter under test. An arrangement is made between No. 1 and No. 2 exciters so that they can rotate around the same central axis, and similar arrangement is made between the exciter under test and its adjacent circular waveguide; so if No. 2 TM_{01} exciter and the exciter under test are rotated at the same time, the field distribution measuring instrument does not have to rotate. Consequently, in order to measure the amplitude and phase of the output, it is very easy to make a balancing network between standard and picked up signals. In order to make such a measuring method possible, it is necessary that the output amplitude and phase of No. 2 are not changed by the rotation of the rotating part. The lower part of Fig. 3 is the measured result of the output amplitude when No. 2 excitor is rotated, and the maximum change was only 0.1 dB. When a mode filter which absorbs the TE_{11} mode is inserted between two TM_{01} exciters, it is believed that this change becomes smaller. A filter that passes all the TM modes and absorbs all the TE modes can easily be made by allocating axial direction slots in the wall of the waveguide.

In regard to the insertion loss of the TM_{01} mode exciter, measurement was done by Storer's method but it was found that the loss was so small that this measurement was not suitable.

The frequency characteristics of the input impedance will be given later in comparison with other mode exciters.

4. TE_{21} Mode Exciter

As shown in the upper part of Fig. 4, the TE_{21} mode exciter consists of rectangular

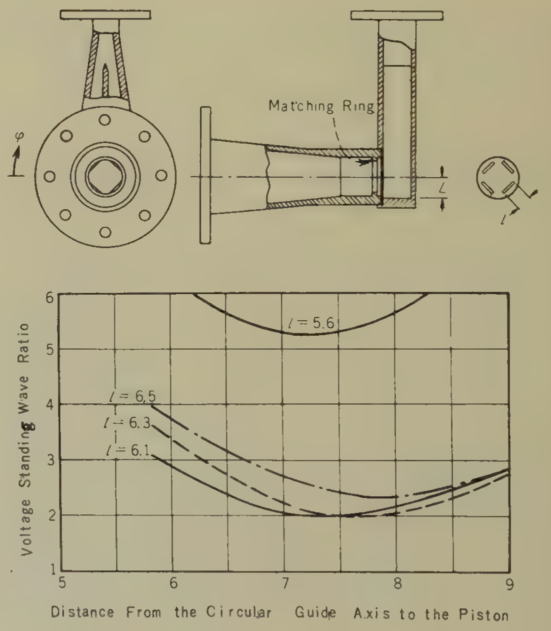

Fig. 4—The structure of the TE_{21} mode exciter and the voltage standing wave ratio against distance from the circular guide axis to the piston. The frequency is 24 Gc/s.

and circular waveguides. The former has a bifurcating plate in the direction perpendicular to the electric field, and the latter is coupled with the former through resonant irises. The resonant irises consist of four holes as shown on the right side of the same figure, and the positions of the centers are located in such a way that the distance between two of them along the rectangular guide axis direction is half of the guide wavelength in the rectangular waveguide. Then, the magnetic field which excites the two slots on the side near the entrance of the rectangular waveguide and the magnetic field which excites the two slots on the side far from the entrance have equal amplitudes in antiphase; therefore they coincide with the magnetic field distribution of the TE_{21} mode, and close coupling may be obtained.

Since the diameter of the circuler waveguide is selected to cut off modes higher than the TE_{21} mode, pure TE_{21} mode can be obtained unless the TE_{11} and TM_{01} modes are generated. An individual iris generates these unwanted modes. But since these modes generated by four irises cancel out one another, only the wanted mode is obtained.

It will be clearly shown that the TM_{01} mode which is generated by a certain coupling iris and the TM_{01} mode generated by the iris at the symmetrical position against the bifurcating plate cancel each other. TE_{11} modes generated by the coupling irises at two positions which are points symmetric with respect to the axis of circular waveguide cancel each other.

But the above covers only the explanation of the principle, and there are many causes for generating unwanted modes. The above explanations are not accurate because of the fact that the two groups of coupling irises at the separation of half guide wavelength on axis of rectangular waveguide excite antiphase and equal amplitudes in the circular waveguide. If the coupling iris can be represented as an epuivalent lumped admittance which is in parallel with the rectangular waveguide line, current with epual amplitude and anti-phase flows always through the two admittances connected at a distance of one half guide wavelength. But in fact, the coupling iris can not be represented by a lumped admittance, because its length in the axial direction can not be neglected in comparison with the guide wavelength. Consequently, comparison between the iris near the input of the rectangular waveguide and that on the far side shows a differrence in excitation strengths and a phase lag of 180°.

The slot excitation caused by the magnetic field component along the length is the strongest, but excitation caused by the magnetic field component along the slot width also exists. Also, if there is an electric field perpendicular to the wall having resonant irises, coupling will occur. As has been said above, by various causes, a small amount of impure modes which in principle should not occur are generated. In order to decrease impure modes in every mode exciter, it is necessary to study concrete means for each case. Though some insertion loss is unavoidable, it is possible to purify the mode by attaching absorbing type mode filters taking advantage of the specific property of the mode.

The next process is choosing the dimensions so as to make the input impedance matching as nearly perfect as possible. The lower part of Fig. 4 shows the voltage standing wave ratio seen from the rectangular guide as a function of L and l when the circular waveguide is terminated with a reflectionless termination. L is the distance between the axis of the circular waveguide and the short circuit plate, and l is the length of the slot. With these dimensions, a suitable combination of L and l by which input impedance was matched could not be found; but by attaching a matching ring in the circular waveguide as shown in Fig. 4, good matching could be obtained. When the ring shape metal is inserted, electric and magnetic fields are of course disturbed, but as the TE_{11} and TM_{01} modes are not newly generated, it is correct to think of it is a mere impedance element. The frequency characteristics of the input impedance will be shown later.

The measurement is shown, in Fig. 5, of φ direction distribution of H_φ and H_z of the output of the TE_{21} exciter matched in the

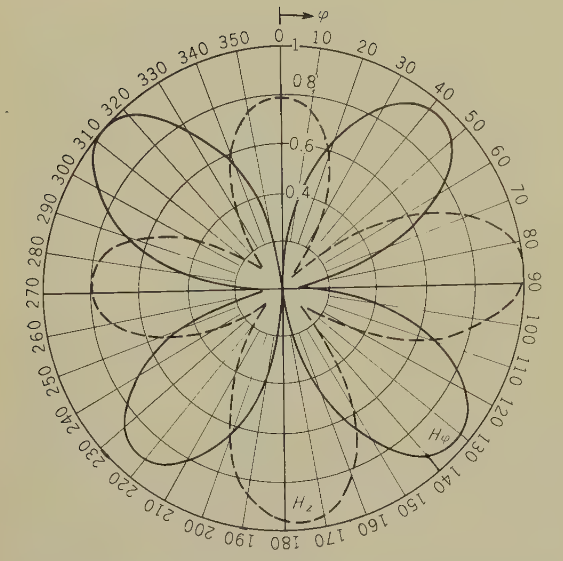

Fig. 5—Measured H_z and H_φ φ direction distribution. The amplitude is proportional to the magnetic field strength. The frequency is 24 Gc/s.

manner described above. The values are relative amplitudes, proportional to magnetic field strength. Though the shape is slightly distorted, H_z is proportional to $\cos 2\varphi$ and H_φ is proportional to $\sin 2\varphi$. The method of measuring the the impure mode contents did not depend on analysis of the measured result of these field distribution, but it was done by means of utilizing the TE_{11} and TM_{01} modes exciters which had been already obtained. However, it must be considered when the contents percentage of the TM_{01} mode is measured with the TM_{01} mode exciter, it receives, even not sensitive, the TE_{11} mode if any, and it creates the cause of error. But as denoted in Fig. 6, the contents percentages of the two modes differ only by few dB, and the sensitivity for impure mode of the TM_{01} exciter is worse than sensitivity for the TM_{01} mode by 20 dB; for these reasons, it may be neglected as the measuring error.

5. TM_{11} Mode Exciter

The structure of the TM_{11} mode exciter is shown in the upper part of Fig. 7, three

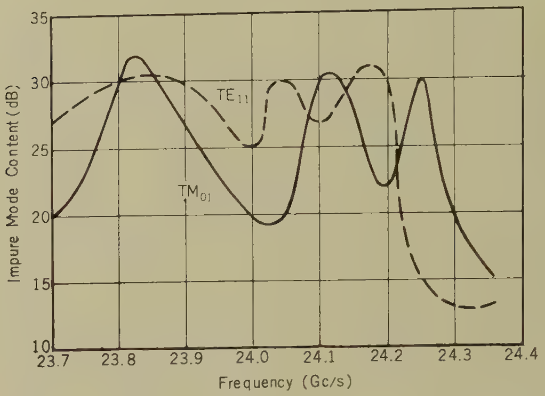

Fig. 6—Measured impure mode contents in the TE_{21} mode exciter output.

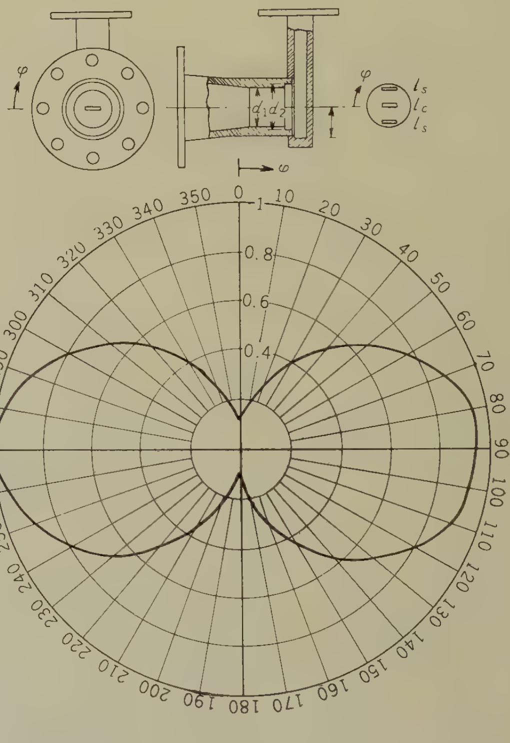

Fig. 7—The structure and measured H_φ φ direction distribntion. The amplitude is relative value proportional to the magnetic field strength. The frequency is 24 Gc/s.

slots are placed on the wall of the longer side of the rectangular waveguide which is connected with the circular waveguide. Since the distance between the two adjacent slots is half the guide wavelength in the rectangular guide, the two (same dimensions) on both ends excite the wave with the same phase and the same amplitude, and the one at the center excites anti-phase. Since such a phase relation agrees with the phase relation of the transverse tangential magnetic field component of the TM_{11} mode at the positions of the three slots, it is convenient to excite the TM_{11} mode. Now, let us investigate whether three such slots generate other modes or not. The diameter $d_1(=16\text{ mm})$ in Fig. 7 is designed to cut off higher order modes than the TM_{11} mode. The central slot does not excite the TM_{01} mode, and the TM_{01} mode excited by the slots on both ends cancel each other because of anti-phase and equal amplitudes. In regard to the TE_{21} mode the mechanism is similar to that of the TM_{01} mode and so the explanation is identical.

Regarding to the TE_{01} mode, the tangential component of magnetic field has only H_r, and it is clear that these slots do not excite H_r, and thus no question arises. At last, the TE_{11} mode only remains. In regard to this mode, the TE_{11} mode excited by the slots of both ends combines with each other in the same phase; the TE_{11} generated by the central slot is anti-phase with respect to those waves, and in order to make the total into zero, we must search for the correct relation between the dimensions of l_s of both end slots and the dimension l_c of the central slot. From the standpoint of impedance, we must obtain a good combination by adjusting the ditance L from the axis of the circular waveguide to the rectangular guide short circuit plate; also l_s and l_c. Moreover, if there are many combinations which fulfil all these requirements, the one with the besf broadband characteristic is of course the best.

When the circular guide is reflectionless, and the piston of the rectangular guide is moved, the impedance locus becomes a circle on a Smith chart. In case the dimension of d_2 (Fig. 7) is the same as d_1 (16 mm), this circle becomes one rotating about the center of the Smith chart and the voltage standing wave ratio can not be reduced to less than 1.8 for any combinations of l_s and l_c.

When d_2 is 18 mm long and the length of its part is nearly 3 mm, the impedance locus passes through the center of the Smith chart.

In order to make the TE_{11} mode contents extremely small at matching conditions, various combinations of l_s and l_c were sought; but it was found that the TE_{11} mode was largest among the impure modes in all cases.

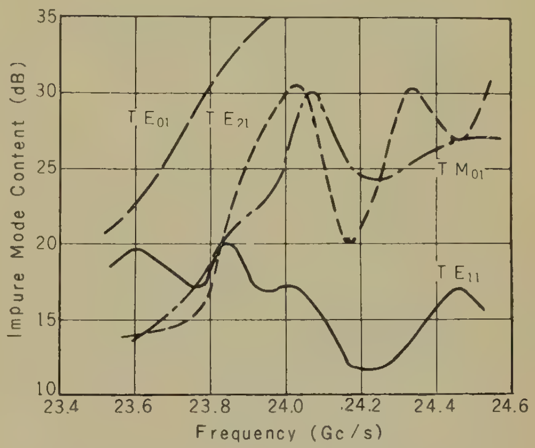

Fig. 8—Measured impure mode contents in the TM_{11} mode exciter output.

The result of measurement at that time of H_φ circumferential direction distribution is shown in the lower part of Fig. 7. Impure mode contents ratio of the TM_{11} mode exciter is shown in Fig. 8. In general, a mode filter which does not give any loss to all the TM modes, and gives high loss to all the TE modes can easily be made by the following method: many long slots are made in the circular guide wall in the axial direction, then suitable absorbing material is placed on the outside of the slots. Consequently, speaking from impurity point of view, it is not hard to get lower TE_{11} mode contents ratio by means of a mode filter.

Impedance frequency characteristics and field distribution will be shown later.

6. TE$_{31}$ Mode Exciter

The structure of this exciter is shown on upper part of Fig. 9, and its operation is similar to that of the TE$_{21}$ mode exciter and therefore details will be omitted. As there may be many impure modes, it is difficult to get the mode of high purity. Among impure modes, the TE$_{11}$ mode content is the highest, and it occupies approximately 9 per cent of all output power. The TM$_{11}$ mode is the next having 2.4 per cent, and other ones are the TM$_{01}$ 0.5 per cent, the TE$_{01}$ 0.2 per cent and the TE$_{21}$. Though many impure modes are implied, field distribution was comparatively fine. On the lower part of Fig. 9, measured circumferential direction distribution of H_z is shown.

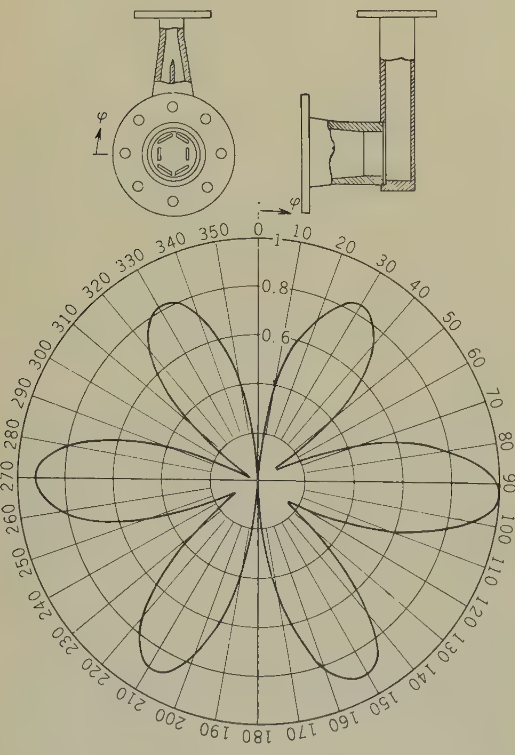

Fig. 9—The structure of the TE$_{31}$ mode exciter and H_z φ direction distribution. The amplitude is the relative value proportional to the magnetic field strength. The frequency is 24 Gc/s.

The purity of this mode can be raised easily by a mode filter. Six radial resistive cards held at equal angles in a polyfoam cylinder can absorb most modes except the TE$_{01}$. A comparison of H_φ circumferential distribution of the exciter output in two cases, one with a filter present, the other without a filter, is shown in Fig. 10. The input voltage standing wave ratio and field distribution aspect will be shown later.

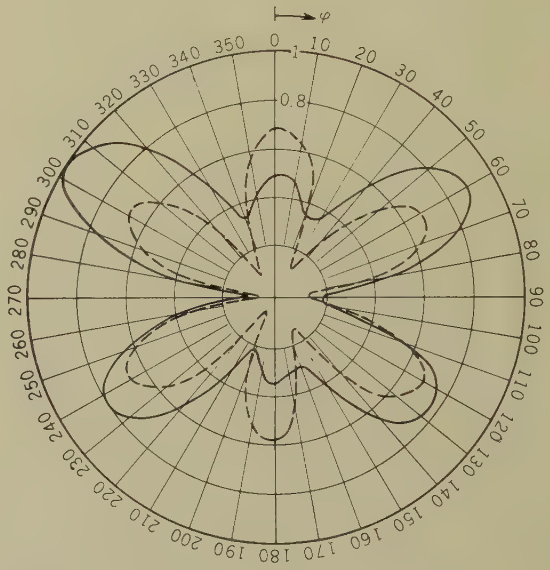

Fig. 10—Measured H_φ φ direction distribution of the TE$_{31}$ mode exciter. The solid curve is measured without the mode filter, and the dotted curve is measured with the mode filter. The amplitude is the relative value proportional to the magnetic field strength. The frequency is 24 Gc/s.

This exciter did not show satisfactory characteristics in respect to impure mode; it is believed that more pure mode can be obtained if the ring shape waveguide is adopted in the design, the same as TE$_{41}$ mode exciter, as shown later.

The insertion loss of this exciter was approximately 2.9 dB when the mode filter was used at 24 Gc/s.

7. TE_{41} Mode Exciter

This exciter is constructed as shown on the upper part of Fig. 11. On the opposite side of the ring type waveguide, two rectangular waveguides are connected. One of them is used for the purpose of matching by making a short circuit at a suitable position, and the other is used as input waveguide. The ring type waveguide is connected to the circular waveguide by eight slots on the side wall. The distances between adjacent slots are one half of the guide wavelength.

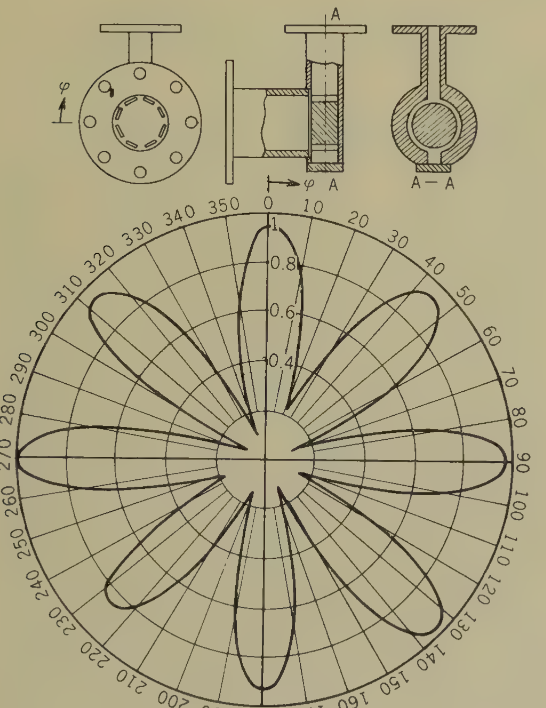

Fig. 11—The structure of the TE_{41} mode exciter and the measured H_z φ direction distribution at 24 Gc/s. The amplitude is the relative value proportional to the magnetic field strength.

When the slots are closed and the outer diameter of the ring type waveguide is 22.2 mm, the input standing wave ratio is 2.17 in case the inner diameter is 16 mm; it is 1.79 in case of 17 mm; it is 1.5 in case of 18 mm, at the frequency of 24 Gc/s. It looks that the bigger the inner diameter the better it is. But if the space between the outer and inner diameters is too narrow, a portion of the slot will be hidden, so the inner diameter of 18 mm has been decided. The measured circumferential direction distribution of H_z is pretty and has a shape of petal, as shown on the lower part of Fig. 11, but H_φ pattern is not so pretty as shown in Fig. 12; the TE_{21} mode seems to be mixed in it.

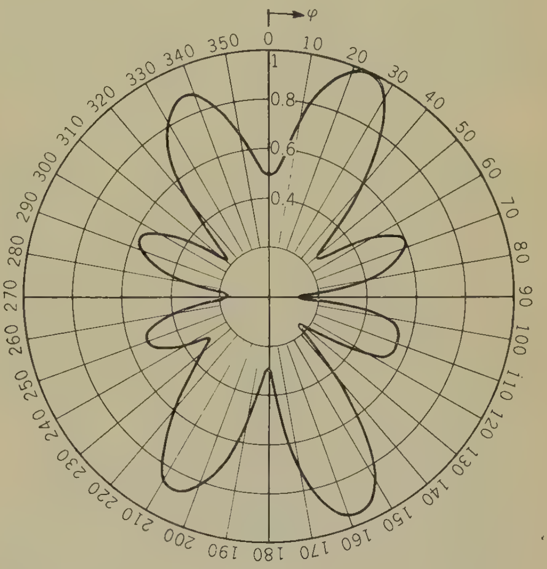

Fig. 12—Measured H_φ φ direction distribution at 24 Gc/s. The amplitude is the relative value proportional to the magnetic field strength.

H_z at the guide wall of higher order mode is, in general, much stronger than that of lower order; for this reason, H_z pattern is not much disturbed if lower mode is mixed to some extent. Even if this is taken into consideration, the fact that H_z pattern is pretty and field distribution pattern photograph is very clear as will be shown later, makes us believe that the mode purity is very high. The impedance frequency characteristics will be shown latter.

8. TE_{12} Mode Exciter

This mode is a very important one for low-loss waveguide transmission because it is liable to be generated at a tilt or an offset of a junction. Consequently, when experimental study about low-loss transmission is intended, an exciter of this mode is indispensable.

This exciter has a structure as shown in Fig. 13. The side wall of the rectangular waveguide is connected with the circular guide by the common plate on which three resonant slots are located at a distance of one half of the guide wavelength. The most important question sbout this exciter is the matter of the TE_{31} mode. The TE_{11}, TM_{11} etc. do not come up to a high value for the reason that excitation of the slot at the center and excitation of slots at both extremeties are anti-phase and cancel each other. The dimensions of the slots at both ends are the same, and the combination of the dimensions of these slots and that at the center should be decided experimentally with the purpose of making the contents of the TE_{11} and TM_{11} modes and the reflection minimum at the same time.

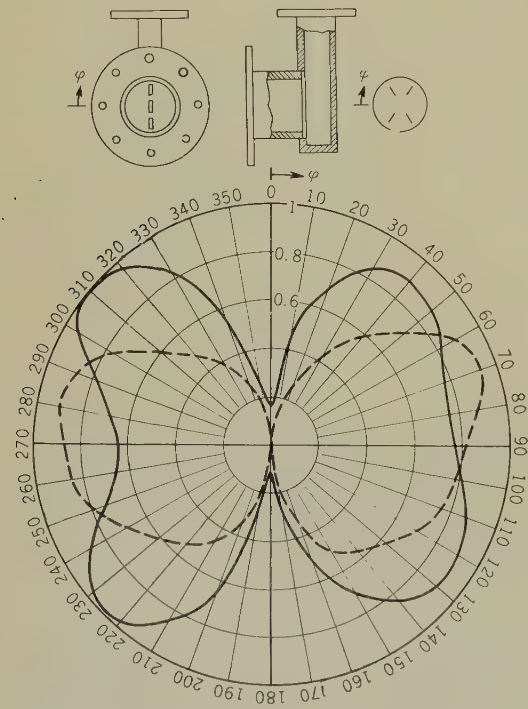

Fig. 13—The structures of the TE_{12} mode exciter and the mode filter for the TE_{12} mode and the measured H_z φ direction distribution at 24 Gc/s. The solid curve is measured without the mode filter, and the dotted curve is measured with it. The amplitude is the relative value proportional to the magnetic field strength.

There are no ways, in principle, to prevent the TE_{31} mode from appearing. However, as the efficiency of excitation for the TE_{31} mode is low, its amplitude is low.

A mode filter containing four pieces of radial resistive sheets attenuates the impure modes selectively, while this permits the TE_{12} mode to pass without considerable additional attenuation. The solid line of Fig. 13 is measured for φ direction distribution of H_z of the output when the mode filter is not used, and the mode, if pure, ought to have the shape of a horizontal "8" but actually it projects out in the vicinities of 30°, 150°, 210° and 330°; on the contrary, it is convex in the vicinity of 90° and 270°, and has the shape of butterfly wings. When the same measurement is done at half the distance of the beat wavelength between the TE_{12} and TE_{31} modes in the z direction, it projects out at the positions of 90° and 270°. Apparently the TE_{31} mode is superposed. By inserting the mode filter as shown at the upper right corner of Fig. 13, the field distribution has changed as the dotted line. It is clear that the mode has been purified, though not perfectly. The frequency characteristics of the impedance will be discussed later.

9. TM_{21} and TM_{02} Mode Exciters

The standard circular waveguide with a diameter of 22.2 mm allows ten modes propagate at a frequency of 24 Gc/s. Among them the TM_{21} and TM_{02} modes are not very important and at the same time it is hard to excite these modes with high purities. The only structures of the exciters made experimentally are shown in Fig. 14. In case of such difficult modes, extreme efforts for preventing the appearance of other modes are not made, but the desired mode output is experimentally adjusted to be as high as possible. There is no other meaus than to purify the modes by using a mode filter. In this meaning, in the case of TM modes, there is a filter as explained before which absorbs all TE, and thus it is advantageous. Moreover, in case of TM_{02}, it is possible in principle, to make a perfect mode filter by inserting concentric cylindrical resistive sheets into the waveguide.

10. Impedance and Field Distribution Photographs

Fig. 15 shows the input voltage standing wave ratio frequency characteristics of each exciter. The TE_{01} mode exciter characteristics already published(8) for comparison are also shown. If cobalt chlorite impregnated paper is inserted into the exciter output waveguide in front of a reflectionless termination perpendicular to guide axis, and, further, output power of the magnetron is incident, it is possible to take photographs of field distribution pattern,(7) Only strong portion of tangential electric field is heated and dried. Therefore, the color changes to blue, whereas the color of the portion not dried remains in light pink. Fig. 16 shows photographs of output field distribution patterns of exciters of each of the modes, TE_{11}, TE_{31}, TE_{01}, TM_{11}, TE_{41} and TE_{12}.

Conclusion

Resonant iris type exciters have been developed for several kinds of modes. The resonant iris type mode exciter has advantages of being small in size and weight, but, it has the defect that its frequency characteristics are narrow. In regard to the mode purity and frequency characteristics, by repeating many experiments, it is possible to find suitable size and good construction; and farther improvement is expected on the insertion loss by application of electroforming in the course of production.

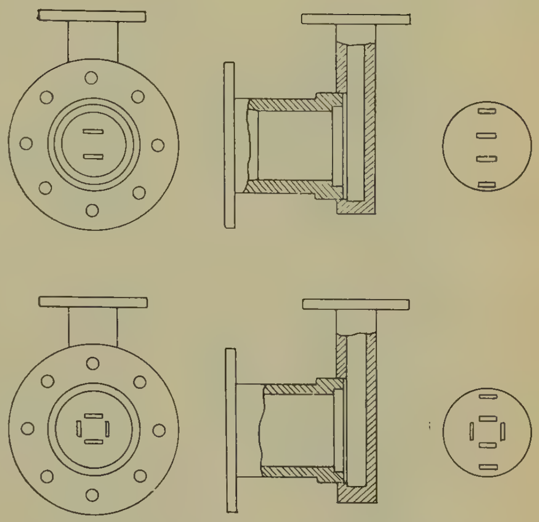

Fig. 14—The structures of TM_{21} (upper part) and TM_{02} (lower part) mode exciters.

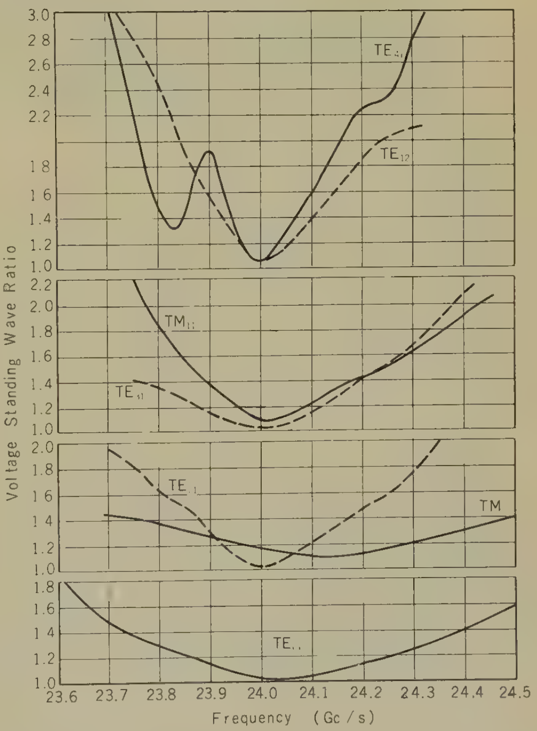

Fig. 15—The frequency characteristics of the voltage standing wave ratio of the mode exciters.

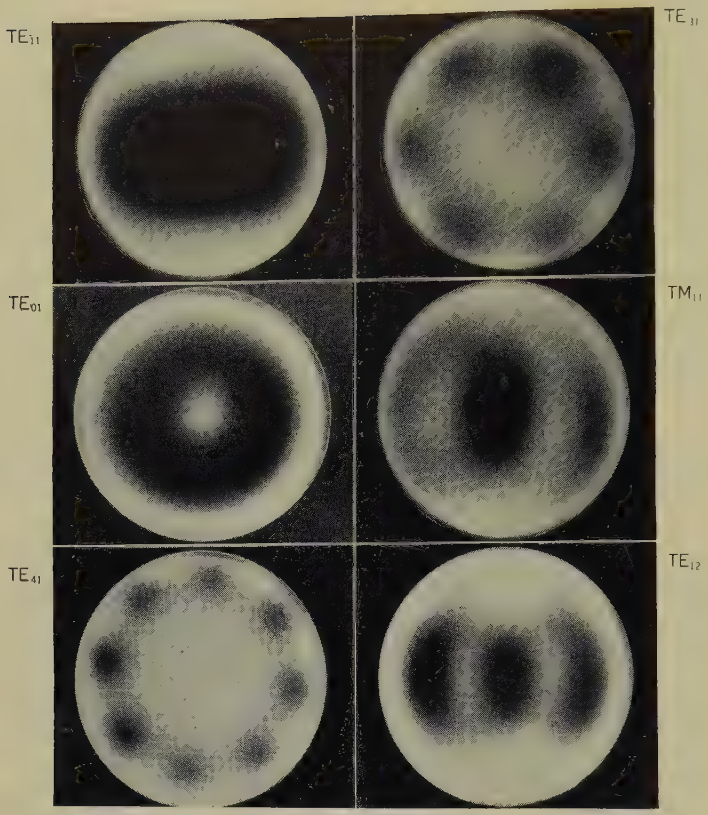

Fig. 16—Photograph of the field distributions of the mode exciter outputs.

Acknowledgment

The author wishes to express his gratitude to Mr- Y. Matsuura for performing a part of the experiments. He also wishes to thank Mr. Y. Nakamura, Mr. T. Miwa, and Dr. B. Oguchi for many for many helpful discussions and suggestions.

References

(1) S. E. Miller, "Coupled Wave Theory and Waveguide Applications," *B.S.T.J.*, **33**. 3, p. 661, 1954.

(2) G. L. Ragan et al, "*Microwave Transmission Circuits*," McGraw-Hill Book Co., New York, p. 385, 1948.

(3) C. G. Montgomery et al, "*Principles of Microwave Circuits*," McGraw-Hill Book Co.. New York, p. 340, 1948.

(4) D. A. Lanciani, "H_{01} Mode Circular Waveguide Components," *Trans. I.R.E.*, *MTT*-**2**, 2, p. 45, 1954.

(5) B. Oguchi and K. Yamaguchi, "Centre-excited Type of Rectangular TE_{10} to Circular TE_{01} Mode Transducer," *Proc. I.R.E.*,**106**, Part B, Supplement, 13, p. 132, 1959.

(6) J. E. Storer. L. S. Sheingold and S. Stein, "A Simple Graphical Analysis of a Two-Port Waveguide Junction," *Proc. IR.E.*, **41**, 8, p. 1004, 1953.

(7) H. Sakamoto and T. Hasegawa, "A New Method of Observing Electromagnetic Fields at Microwave Frequencies by the Use of Test Paper," *Report of the Microwave Communication Research Committee in Japan*, December, 1955.

(8) S. Iiguchi and K. Yamaguchi, "Resonant Slots Type TE_{01} Mode Exciter," *Annual Convention of the Institution of Electrical Communication Engineers of Japan*, p. 592, 1956.

* * * *

REVIEW OF THE ELECTRICAL COMMUNICATION LABORATORY
VOLUME 8, NUMBERS 9-10, SEPTEMBER-OCTOBER, 1960

U.D.C. 621. 395. 623. 001

The Design of a New Telephone Receiver*

Kenro MASUZAWA† and **Kiyoshi TAJIMA**†

The specific response of a receiver is formulated in terms of parameters suitable for design purposes, and general considerations are given to increase the response. A simulator is useful to determine each element in the equivalent circuit so that the required frequency response may be obtained.

Non-linear displacement, leakage path performance, stability factor, etc. of a formed vibrating diaphragm are analyzed.

The receiver newly designed according to these methods is remarkably improved in performance and in simplicity of manufacture.

1. Introduction

In 1950 the No. 4 telephone set presently used in Japan was first announced. However, during the last ten years, the manufacturing techniques in Japan have progressed greatly. In addition, it has become necessary to produce a new telephone set with better performance in order to be able to use small gauge local cable.

For these reasons the development of a new telephone receiver is now being planned.

The response of the new telephone receiver is about 5 dB better than that of the old one, and the transmission frequency band has been extended up to 3600 c/s. The structure of the new telephone receiver has been designed so as to be suitable for massproduction.

2. Design

The equivalent circuit of a telephone receiver whose construction is as shown in Fig. 1 can be represented as shown in Fig. 2 (a). Simplified equivalent circuits are shown in Fig. 2 (b) and in Fig. 2 (c).

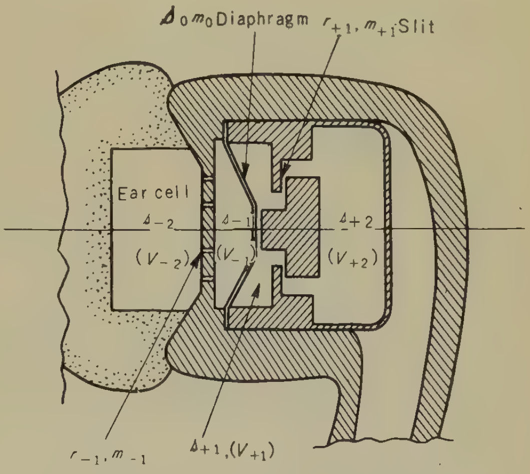

Fig. 1—The structure of telephone receiver.

The *s*, *m*, *r*, *z* and *Q* in the figure represent stiffness, mass, mechanical resistance, mechanical impedance and displacement respectively. The relationships between the elements of the equivalent circuit are as follows:

$$\left.\begin{aligned} p_{\pm}&=\frac{s_{\pm1}}{s_{\pm1}+s_{\pm2}}, & s_{\pm}&=p_{\pm}s_{\pm1} \\ m_{\pm}&=p_{\pm}^{2}m_{\pm1}, & r_{\pm}&=p_{\pm}^{2}r_{\pm1} \end{aligned}\right\} \qquad (1)$$

---

* MS in Japanese received by the Electrical Communication Laboratory, Feb. 15, 1959. Originally published in the *Kenkyû Zituyôka Hôkoku* (*Electrical Communication Laboratory Technical Journal*), N.T.T., Vol. 9, No. 5, pp. 447–474, 1960.

† Station Apparatus Research Sect.on.

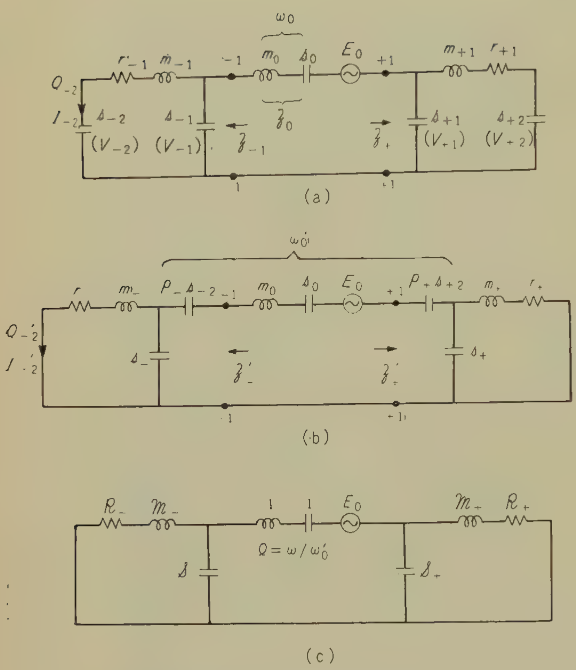
ω_0
r_{-1} m_{-1} -1 m_0 s_0 E_0 $+1$ m_{+1} r_{+1}
Q_{-2}
I_{-2} s_{-2} s_{-1} z_0 s_{+1} s_{+2}
(V_{-2}) (V_{-1}) z_{-1} z_+ (V_{+1}) (V_{+2})
1 +1
(a)
ω_0'
r m_- p_-s_{-2} -1 m_0 s_0 E_0 $+1$ p_+s_{+2} m_+ r_+
Q'_{-2}
I'_{-2}
s_- z'_- z'_+ s_+
1 +1
(b)
R_- $\mathcal{M}_-$ 1 1 E_0 $\mathcal{M}_+$ R_+
$\Omega=\omega/\omega_0'$
S S_+
(c)

Fig. 2—Equivalent circuits.

$$\left.\begin{aligned}S_\pm&=\frac{s_\pm}{s_0+p_-s_{-2}+p_+s_{+2}}\\ M_\pm&=\frac{m_\pm}{m_0}\\ R_\pm&=\frac{r_\pm}{\omega_0' m_0}\\ \omega_0'&=\frac{s_0+p_-s_{-2}+p_+s_{+2}}{m_0}.\end{aligned}\right\}\qquad(2)$$

Using the symbols of the equivalent circuit, the specific response q of the telephone receiver can be represented as follows:

$$q=\frac{P}{I\sqrt{Z}}=\frac{Qs_{-2}}{I\sqrt{Z}S_0}$$

$$=\frac{A}{S_0\sqrt{Z}}\,\frac{1}{\omega^2(z_0+z_-+z_+)}$$

$$\times\frac{s_-}{r_-+j\omega\{m_--(s_-/\omega^2)\}}p_-s_{-2}\qquad(3)$$

where

$q=$Specific response ($\mu b/\sqrt{\text{watt}}$)
$P=$Sound pressure developed in coupler or ear cavity (dynes/cm^2)
$I=$Receiver current (Amperes)
$Z=$Electric free impedance of receiver (Ohms)
$S_0=$Effective area of receiver diaphragm (cm^2)
$A=$Force factor (dynes/Ampere)
$s_{-2}=$Stiffness of coupler.

2.1. Response in the Low Frequency Region

In Eq. (3), putting, $r+j\omega m\ll s/j\omega$, we obtain:

$$q_0=\frac{A}{S_0\sqrt{Z}}\,\frac{p_-s_{-2}}{s_0+p_-s_{-2}+p_+s_{+2}}.\qquad(4)$$

From Eq. (1) and (2),

$$s_{-1}=S_-(s_0+p_-s_{-2}+p_+s_{+2})$$

$$\times\frac{1+\sqrt{1+\dfrac{4s_{-2}}{S_-(s_0+p_-s_{-2}+p_+s_{+2})}}}{2}.\qquad(5)$$

On the other hand,

$$s_{-2}=\frac{\kappa S_0^2}{V_{-2}}$$

where κ is the modulus of volume elasticity of air. Substituting Eqs. (5) and (6) into Eq. (4)

$$q_0=\frac{A}{\sqrt{Z}}\,\frac{\kappa S_0}{V_{-2}}\,\frac{1}{s_0+p_-s_{-2}+p_+s_{+2}}$$

$$\times\frac{2}{1+\sqrt{1+\dfrac{4s_{-2}}{S_-(s_0+p_-s_{-2}+p_+s_{+2})}}}.\qquad(7)$$

The free impedance Z of the receiver is represented by the sum of the damped impedance $R+j\omega L$ and the motional impedance. In the low frequency region, the free impedance Z can be expressed as follows:

$$Z=R+j\omega L\left(1+\frac{A^2}{\omega_0'^2 m_0 L}\right) \tag{8}$$

then, putting

$$k^2=\frac{A^2}{\omega_0'^2 m_0 L} \tag{9}$$

where m_0 is the mass of the vibrating diaphragm including the armature mass m_a and

$$\beta^2=\frac{\kappa S_0^2}{V_{-2}}\,\frac{1}{\omega_0'^2 m_0}. \tag{10}$$

We obtain the low-frequency specific response as follows:

$$q_0=\sqrt{\frac{\kappa}{\omega V_{-2}}}\,\frac{2\beta}{1+\sqrt{1+\{(2\beta)^2/S_-\}}}$$

$$\times\frac{k}{\sqrt[4]{(R/\omega L)^2+(1+k^2)^2}}. \tag{11}$$

When k, β, and S_- are given in the design of the driving system and the vibrating system, the response can be obtained from Eq. (11).

The values of the 2nd and 3rd terms of

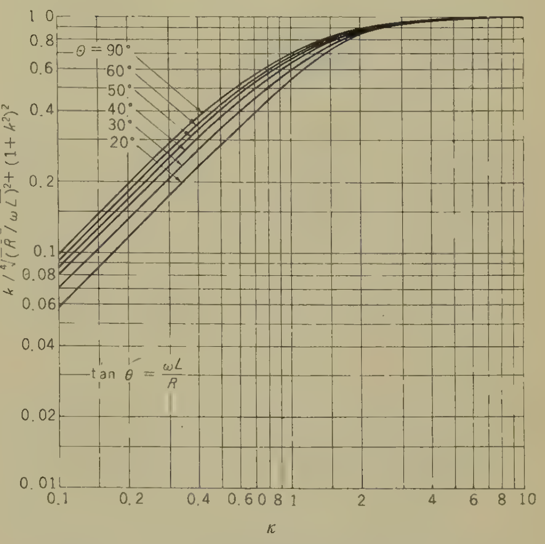

Fig. 3 (b)—$k/\sqrt[4]{(R/\omega L)^2+(1+k^2)^2}$ vs. k.

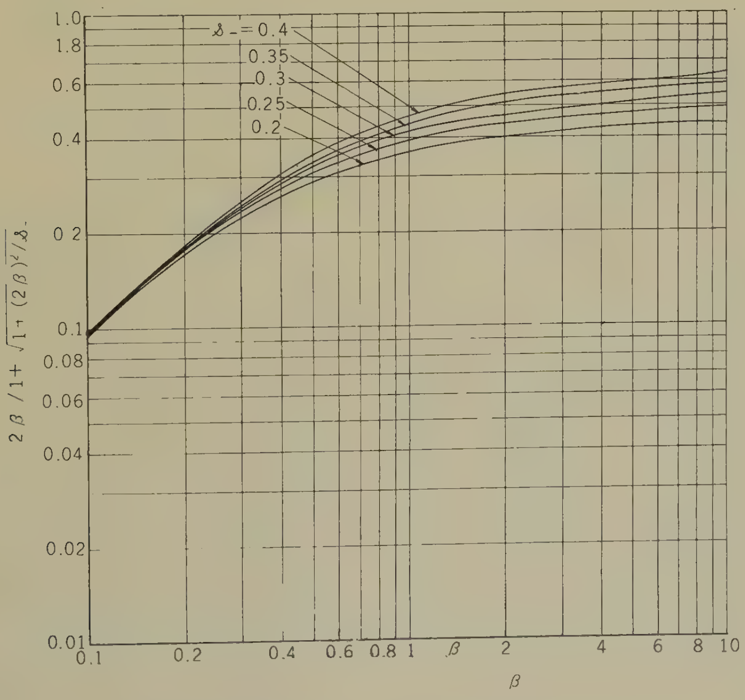

Fig. 3 (a)—$2\beta/1+\sqrt{1+(2\beta)^2/S_-}$ vs. β.

Eq. (11) are shown in Fig. 3 (a) and (b). As they do not exceed 1, the maximum value of the response is given by:

$$q_0=\sqrt{\frac{\kappa}{\omega V_{-2}}}^{(1)} \tag{12}$$

2.2. Response vs. Frequency Characteristics

Because S_0, s_-, s_{-2}, and p_- in Eq. (3) are independent of frequency, the terms relating to the frequency characteristics are given by

$$\frac{A}{\sqrt{Z}}\ \frac{1}{\omega^2(z_0+z_-+z_+)}\ \frac{s_-}{r_-+j\omega\{m_- -(s_-/\omega^2)\}} \tag{13}$$

where $|A/\sqrt{Z}|$ is determined by the magnetic circuit design only.

The measured values of $|A/\sqrt{Z}|$ of two typical samples are shown in Fig. 4 (a) and (b). These values are approximately proportional to $1/\sqrt{\omega}$ over the frequency range from 300 to 3600 c/s. Therefore, to obtain a flat response each element in the equivalent circuit must be so determined that the remaining term

$$\left|\frac{1}{\omega^2(z_0+z_-+z_+)}\ \frac{s_-}{r_-+j\omega\{m_- -(s_-/\omega^2)\}}\right.$$

is proportional to $\sqrt{\omega}$.

The two sets of examples, which are shown in Fig. 5 (a) and (b), have been obtained by use of the equivalent circuit shown in Fig. 2 (c).

The right-hand side of Fig. 5 shows the value of each element, while the left-hand side shows the characteristics of the receiver using these elements. Sometimes the value of $|A/\sqrt{Z}|$ deviates from the ratio of $|1/\sqrt{\omega}|$, owing to the construction of the magnetic circuit. In such cases, the value of each element should be changed slightly during the final adjustment.

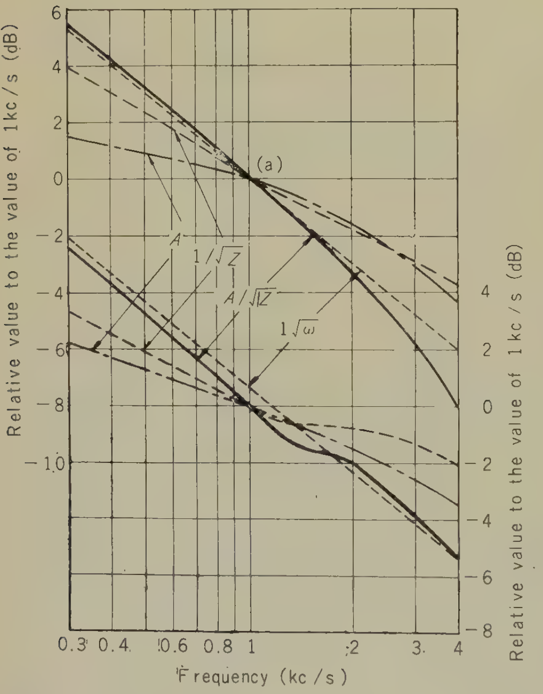

Fig. 4—Tow typical curves of $20\log_{10} A/\sqrt{Z}$ frequency characteristics.

2.3. Practical Design

The inner and outer pole pieces are arranged concentrically in the magnetic circuit. The dimensions of the magnetic circuit were determined aftcr a series of experiments made for a study of the effects of various dimensions.

The construction decided upon is shown in Fig. 6. The inner pole piece is made of an alloy of 45% Ni and 55% Fe, and has a diameter of 6 mm. The outer pole piece is made of magnetic iron. The central portion of the outer pole piece is raised in a power press, permitting the use of a small armature without decreasing the space for the voice coil.(2) The armature is made of an alloy of 49% Co, 2% V, and 49% Fe, and has a thickness of 0 4 mm.

The dimensions of the pole piece and the armature are determined so as to be suitable for production, and to make $A/\sqrt{Lm_a}$ large. The magnet is made of Barium Ferrite, and a protection ring surrounds it to prevent mechanical shock.

The rating of the magnetic circuit was

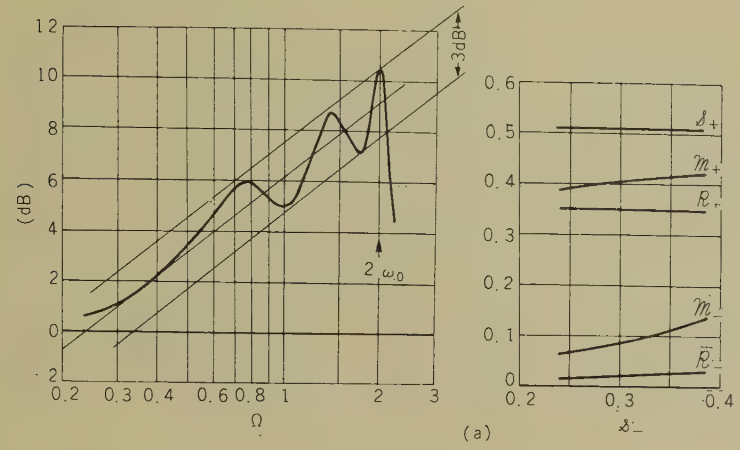

Fig. 5 (a)—Frequency characteristics for design.

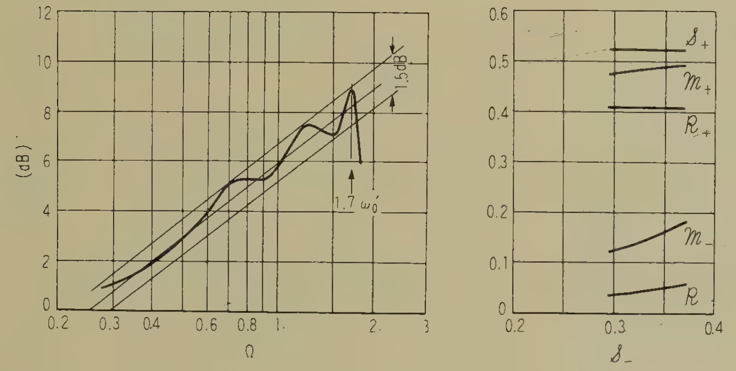

Fig. 5 (b)—Frequency characteristics for design.

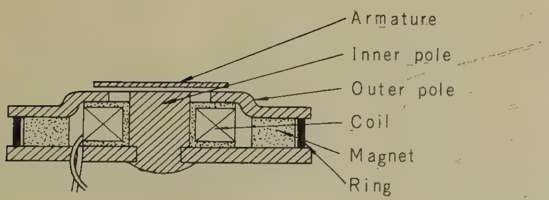

Fig. 6—The construction of magnetic circuit.

determined as follows from experimental results.

$A/\sqrt{L}=3.5\times10^3$ C.G.S.

$s_n=0.32\times10^8$ dyne/cm (negative field stiffness)

$m_a=0.38$ g (mass of armature)

and the impedance angle of the coil is equal to 60°.

The design of the vibrating system and the calculation of the response shall now be explained for an example using the following assumptions: diameter of the diaphragm is 40 mm, f_0' is 1700 c/s, and S_- is equal to 0.3.

The effective area, stiffness, and effective mass of the formed diaphragm are given approximately as follows:

$$S_0=\pi a^2\left\{\frac{1}{4}\;\frac{1-\nu^4+4\nu^2\log_e\nu}{1-\nu^2-\dfrac{4\nu^2}{1-\nu^2}(\log_e\nu)^2}\right\} \tag{14}$$

$$s_{00}=\frac{4\pi E h^3}{3(1-\sigma^2)a^2}\;\frac{1}{1-\nu^2-\dfrac{4\nu^2}{1-\nu^2}(\log_e\nu)^2} \tag{15}$$

$$m_0=m_a+\pi a^2 h\rho(1.22\nu-0.22) \tag{16}$$

where

E=Young's modulus

σ=Poisson's ratio
ρ=density
$\nu=b/a$, b is inner diameter of diaphragm
h=thickness of diaphragm.

By using Eqs. (14), (16), (9), (10), and (11), q_0 can be obtained as a function of h and ν.

If it is assumed that fhe stability factor $\mu=s_{00}/s_n$ should not be less than 2, the combination of h and ν is confined within a definite region. In the region where μ is less than 2 and f_0' is higher than 1700 c/s, a receiver suitable for practical production can not be designed. By making use of Fig. 7 (a) and (b), ν, h, and q_0 can be determined.

A diaphragm of the same type construction as that of the No. 4 telephone set is considered suitable. The authors recommend the diaphragm structure shown in Fig. 8 after studying the results of research on the form and the method of supporting the armature. The authors have ascertained that the diaphragm can be made almost creep-free against the magnetic attractive force.

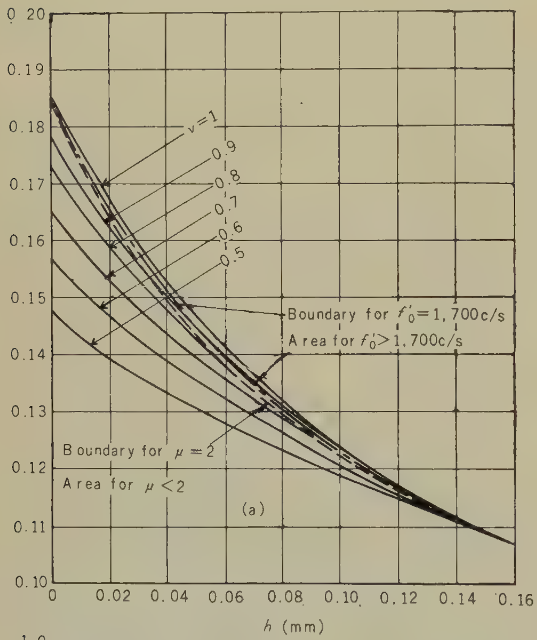

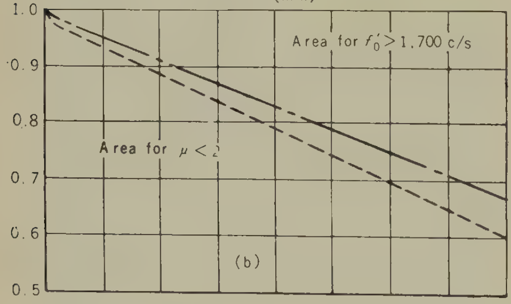

Fig. 7 (a)— $\dfrac{2\beta}{1+\sqrt{1+\dfrac{(2\beta)^2}{S_-}}}\;\dfrac{k}{\sqrt[4]{\left(\dfrac{R}{\omega L}\right)^2+(1+k^2)^2}}$ vs. ν & h.

Fig. 7 (b)—ν vs. h.

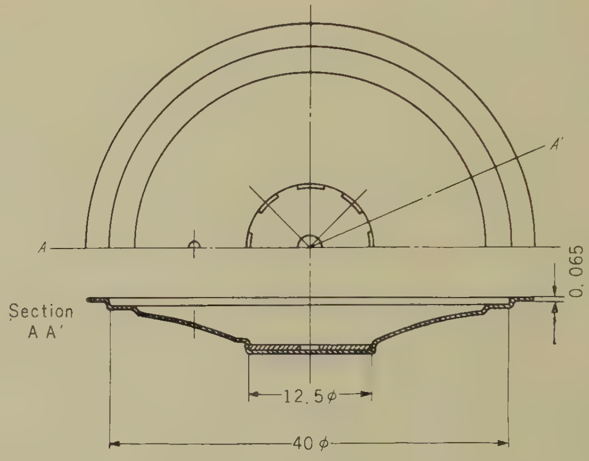

Fig. 8—The construction of diaphragm.

3. Stability Factor*

When a force is axially applied to a formed diaphragm, if the force is small, the displacement increases linearly.

As the applied force becomes large enough, the displacement becomes non-linear.

Fig. 9 shows the displacement of the diaphragm of the new telephone receiver with an axially applied force. Force vs. displacement characteristics obtained for the like diaphragms generally proves dissymmetry of the displacement in both sides of the rest

---

* Stability factor μ is defined as:

$$\mu=\frac{\text{stiffness of diaphragm}}{\text{negative field stiffness}}.$$

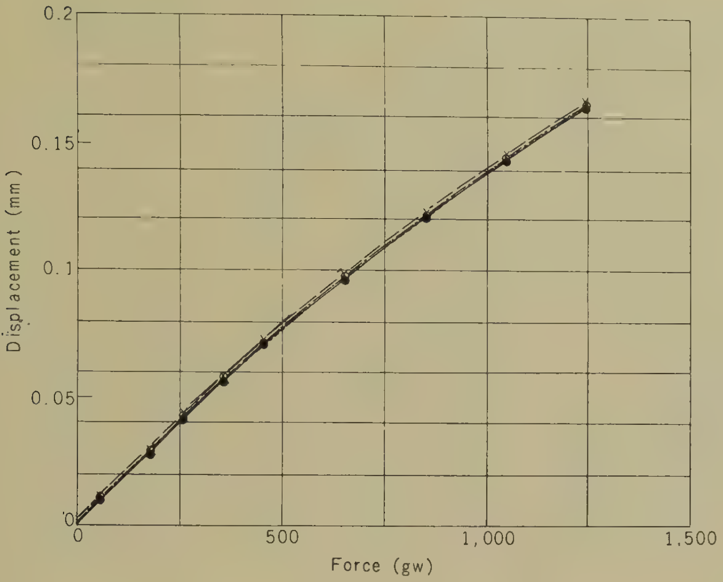

Fig. 9—Displacement vs. force characteristics of diaphragm (1).

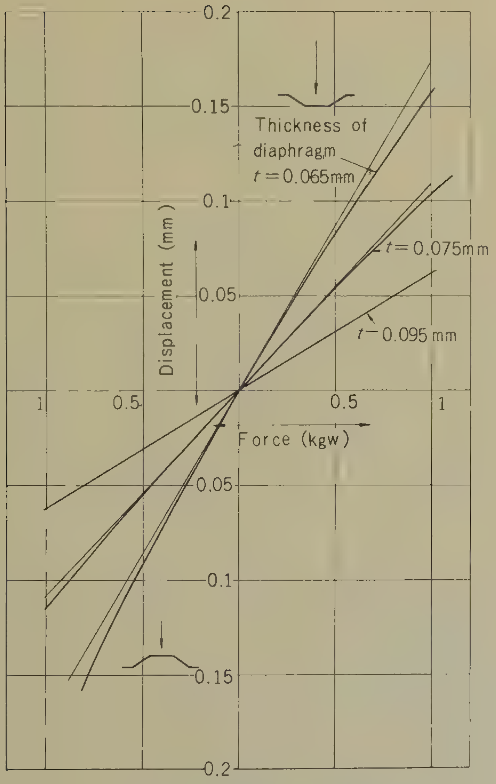

Displacement vs Force

Fig. 10—Displacement vs. force characteristics of diaphragm (2).

position. Fig. 10 presents an example actually measured.

The attractive force vs. gap distance characteristics of the magnetic circuit are shown by the solid curve in Fig. 11. For the magnetic circuit in combination with the diaphragm, the restoring force of the diaphragm is shown as a dashed curve. "B" shows the diaphragm rest position before the magnet core is magnetized.

The magnetic gap can never become less than the thickness of the non-magnetic diaphragm which is 0.065 mm.

If the dashed curve occupies a higher position than the solid curve in the figure for the magnetic gap distance between the $g=0.065$ mm and the abscissa of "A," the receiver operates stably.

The mechanical stiffness of the diaphragm is calculated from the tangent of the dashed curve at point A. We obtain the value of $s_{00}=0.73\times10^8$ dyne/cm.

The negative field stiffness is similarly obtained from the tangent of the solid curve at point A, $s_n=0.32\times10^8$ dyne/cm.

Stability factor μ is given by:

$$\mu=\frac{s_{00}}{s_n}\doteqdot 2.3$$

In this receiver, by utilizing the non-lineari-

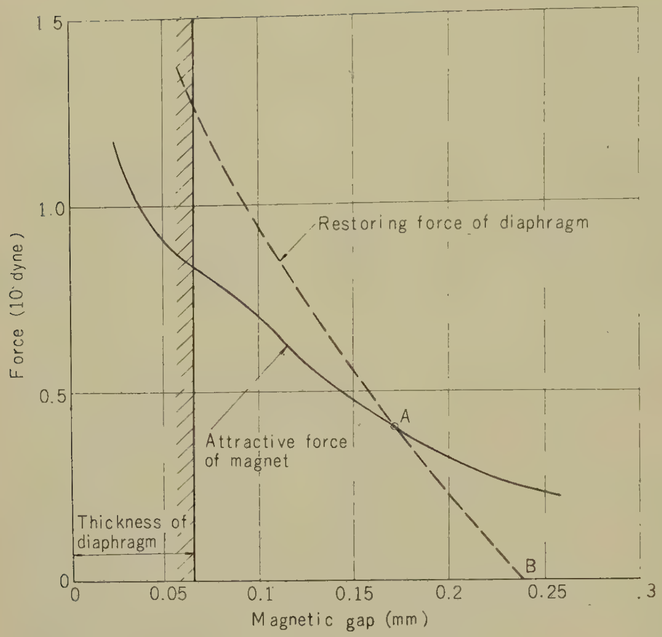

Fig. 11—Force vs. magnetic gap.

ty of diaphragm displacement and the existence of non-magnetic diaphragm materials near the pole piece, the operation of the receiver could be made quite stable despite of the low value of μ.

4. Leakage Hole for Pressure Balance

The accoustic impedance of a small hole located on the diaphragm has a non-linear characteristic. For example, (a) and (b) of Fig. 12 show the response vs. frequency characteristics when small holes with diameters of 0.8 mm and 0.5 mm respectively are located on the diaphragm.

In both cases, the response vs. frequency characteristics vary with the electric power applied to the telephone receiver. This change of characteristics is not attributed to the non-linear magnetic characteristics, but to the effect of the hole.

However, this change of characteristics is desirable when the receiver is actually used for communication, this effect is weakened by the existence of leakage between the ear and the ear piece. From the standpoint of production control of the telephone receiver, curve (b) is preferable because it does not vary. In our telephone receiver a hole diameter of 0.5 mm was adopted.

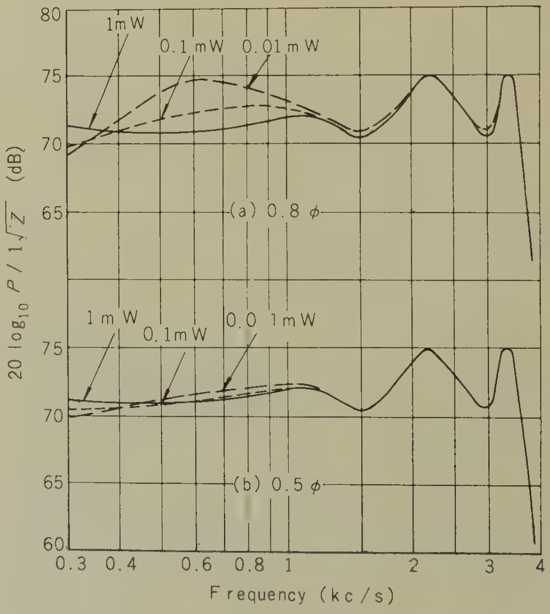

Fig. 12—Response vs. frequency characteristics of receiver with leakage hole.

5. Temperature Characteristics of the Response

It is known that the magnetic characteristics of barium ferrite varies with temperature more than those of the usual magnet alloys. Telephone receivers using this kind of magnet should be affected by temperature as little as possible.

In order to minimize the variation of polarizing magnetic flux due to temperature, the dimension of the magnet should be such that the operating field H of the magnet is approximately 60% of the coersive force H_c. We can satisfy this condition by demagnetizing the magnet. It is necessary to fix the sensitivity lower than the value of maximum sensitivity by 1 to 2 dB. The curves in Fig. 13 (a) and (b) suggest this method of adjustment.

By the treatment mentioned above, the change of specific response $20\log_{10} P/I\sqrt{Z}$, and the impedance $|Z|$ are kept approximately within 4 dB and 10 Ohms respectively over a temperature range of −20 to 50° C.

6. Construction and Performance of the New Telephone Receiver

The construction of the new telephone receiver is shown in Fig. 14. It is of the enclosed moisture-and-dust-proof type. Slits are

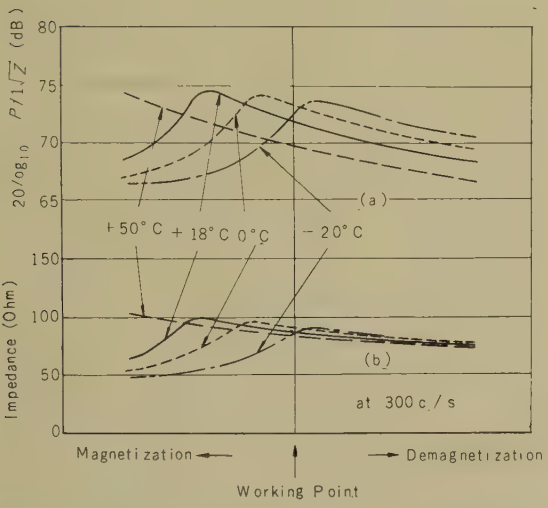

Fig. 13—Response and impedance vs. superimposed direct current characteristics.

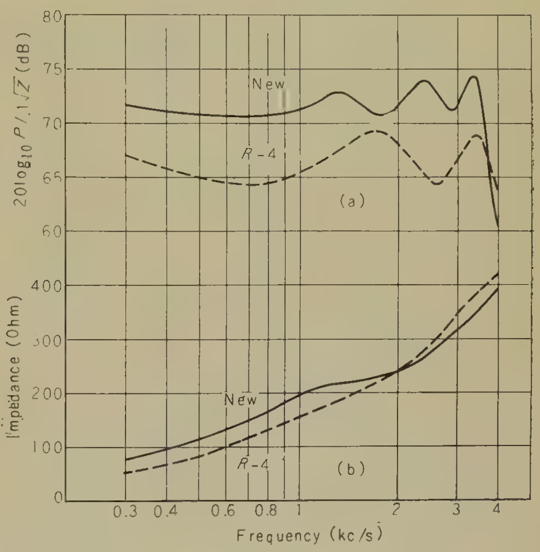

Fig. 15—Response and impedance vs. frequency characteristics of new telephone receiver (with R-4 receiver).

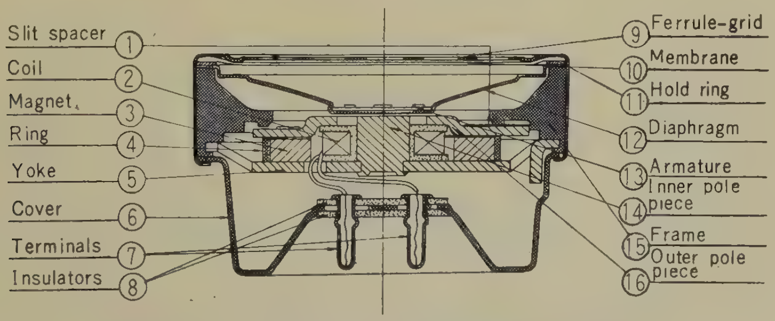

Fig. 14—The structure of new telephone receiver.

used as damping elements. The thickness of the slit spacer is 0.12 mm.

A typical example of the frequency characteristics of the specific response and the impedance are shown by a solid curve in Fig. 15 (a) and (b).

For the purpose of comparison, the characteristics of the Present Standard R-4 Receiver are indicated by a dashed curve in the same figure.

7. Conclusion

In this paper the outline of method and the representative data of the design of the new telephone receiver are described.

The merits of this receiver may be summarized as follows:

1) The specific response has been improved by about 5 dB compared with that of R-4 receiver used to date.

2) During the design of this receiver the cost of the individual parts and the cost of the entire receiver were carefully considered. It is expected that the cost of this receiver will be about 10% less than the cost of the R-4 receiver.

8. Acknowledgement

This work was carried out under the supervision of Dr. Toshio Hayasaka. The anthors appreciate his valuable suggestions, they also wish to thank the Tokyo Shibaura Electric Co., Ltd. for experimental production of the receiver.

References

(1) E. E. Mott & R. C. Miner: The Ring Armature Telephone Receiver, *B.S.T.J.*, **30**, 110 (1951).

(2) H. Jacoby & H. Panzerbieter: Über moderne Mikrophone und Telephone, *Elektr. Nachr. Tech.*, **13**, 75 (1636).

* * * *

Papers Contributed to Scientific and Technical Journals by the Members of the Laboratory

Papers Published in Other Publications of the Electrical Communication Laboratory

U.D.C. 621.315.592 : 548.3]:536.21.083

Measurement of Thermal Conductivity in Semiconductors*
Riro NII
Kenkyû Zituyôka Hôkoku (Electr. Comm. Labor. Techn. Journ.), NTT, **9**, 7, pp. 817–825, July, 1960

A translation of this paper was published in the "Review of the Electrical Communication Laboratory," Vol. 8, Nos. 3–4, pp. 99–104, 1960.

U.D.C. 621.374.32 : 621.382.2

The Design of Germanium Diodes for use in Semiconductor Parametrons*
Yasuhiro HIYAMA
Kenkyû Zituyôka Hôkoku (Electr. Comm. Labor. Techn. Journ.), NTT, **9**, 8, pp. 915–928, Aug., 1960

A method of designing junction diodes for parametrons and the characteristics of the diodes which were experimentally manufactured are described.

U.D.C. 621.376.92 : 621.374

Triple Balanced Modulator Using Binocular-Type Magnetic Cores*
Takasi ITO
Kenkyû Zituyôka Hôkoku (Electr. Comm. Labor. Techn. Journ.), NTT, **9**, 7, pp. 739–752, July, 1960

Basic principles and the fundamental characteristics of the triple balanced modulator (T.B.M.) are described. Some considerations applicable when modulators constructed on binocular-type magnetic cores are used in parametron-control systems are discussed.

U.D.C. 621.382.3.029.62.001

High Frequency Alloy Type Transistor (ECL–1205)*
Susumu YOSHIDA
Kenkyû Zituyôka Hôkoku (Electr. Comm. Labor. Techn. Journ.), NTT, **9**, 8, pp. 829–862, Aug., 1960

The techniques for fabricating a high-frequency transistor are described. The required parallel-plane junctions and narrow base width are obtained by making use of the limiting actions of the (111) crystal plane and edge locations during alloying. The electrical characteristics of this transistor are discussed in detail.

---

* Reprints may be available upon your request to the author.

U.D.C. 621.385.632.14

A Spartial Harmonic Traveling-Wave Tube for 48 Gc Using a Comb-Type Structure*

Yoshio KATO and *Shisei MIYAZAKI* and *Ryosuke KOSHI* and *Toshio KOBAYASHI*
Kenkyû Zituyôka Hôkoku (Electr. Comm. Labor. Techn. Journ.),

The precise methods of milling a comb-type structure for 48 Gc are described. About 10 dB of gain and a saturated power output of 50 mW have been obtained with a demountable tube using this structure.

U.D.C. 621.391.833:621.376.56:621.395.64

Experimental Production of Ceramic Film Capacitors*

Saburo NAKAGAWA
Kenkyû Zituyôka Hôkoku (Electr. Comm. Labor. Techn. Journ.), NTT, **9**, 7, pp. 701–737, July, 1960

The formation of thin films of $B_aT_i0_3$ ceramics for capacitor dielectrics is discussed. Capacitors using these film dielectrics are smaller in size than those now available, and are especially suitable for transistor circuits.

U.D.C. 621.395.636.1.001.2:621.838.22

The Dial-Spring Clutch*

Akira YANAGI and *Syozi SAKAI* and *Tatuo KIGAWA*
Kenkyû Zituyôka Hôkoku (Electr. Comm. Labor. Techn. Journ.), NTT, **9**, 8, pp. 895–913, Aug., 1960

The dial-spring clutch is theoretically analyzed. Also, the experimental verification of basic design, production, and inspection techniques is reported.

U.D.C. 665.335.5.067:[621.315.615:621.319.4

Refining of Castor Oil for Capacitor Dielectrics*

Masaaki KATAGIRI and *Katunari KODATI*
Kenkyû Zituyôka Hôkoku (Electr. Comm. Labor. Techn. Journ.), NTT, **9**, 7, pp. 771–783, July, 1960

The authors developed a simple method of refining castor oil by using active clay and active alumina.

U.D.C. 667.782.011.9:[543.53:546.1′8

A Note on the Radioactivation Analysis of Arsenic in Pure Silicon*

Toshi KAWASHIMA
Kenkyû Zituyôka Hôkoku (Electr. Comm. Labor. Techn. Journ.), NTT, **9**, 7, pp. 827–828, July, 1960

Radioactivation analysis of arsenic in pure silicon was examined. It was found that an analysis based on treatment by $HF–HN0_3$ is not suitable to quantify arsenic in pure silicon.

U.D.C. 678.02:621.315.616.012

Electrical Properties of Rubber-Styrene Casting Resin*

Tsuneo TAMADA and *Tomio TADOKORO*
Kenkyû Zituyôka Hôkoku (Electr. Comm. Labor. Techn. Journ.), NTT, **9**, 8, pp. 929–934, August, 1960

In this paper the relation between the compositions of resins and their electrical properties is discussed.

Papers Published in Publications of Scientific and Technical Societies

U.D.C.

Zone Refinig of Pure Copper
Tomisaburo NARA and *Yoshito YAMADA*
Journ. Japan. Inst. Metals, **24,** 7, pp. 460–464, July, 1960

The zone refining process has been applied to vacuum-melted pure copper. The results of experiments on the distributions of various chemical elements those on electrical resistivity are discussed.

U.D.C. 621.372.81:538.566.5

Proof of the Completeness of a Set of Transverse Components of Normal Modes in a Waveguide
Shin-ichi IIGUCHI
Journ. Inst. Electr. Comm. Engr. Japan, **43,** 8, pp. 901–905, Aug., 1960

This paper proves that an arbitrary two-dimensional vector function whose square is integrable in region S can be expanded in the mean by a set of transverse components of normal mode in a conventional waveguide of cross section S, on the basis of the completeness theorem of scalar functions.

U.D.C. 621.374.32:511.1

The Circuit Detecting the Number of Bits
Noriyoshi KUROYANAGI
Journ. Inst. Electr. Comm. Engr. Japan, **43,** 7, pp. 794–800, July, 1960

A circuit that has sensing functions which enable it to sense the number of bits of logical value 1 (or 0) which continue from the least or most significant digit in one operation is described.

U.D.C. 621.375.9

Two-Phase Excitation of Parametrons Used in Logical Circuits
Masaru ONO
Journ. Inst. Electr. Comm. Engr. Japan, **43,** 7, pp. 822–825, July, 1960

Advantages and disadvantages of two-phase excitation of parametrons used in logical circuits are discussed. Preliminary experiments carried out with simple magnetic gates, which are necessary for building logical circuits, are also mentioned.

U.D.C. 621.395.623:621.318.3

The Magnetic Circuit of the Telephone Receiver
Ryozo ARAKI and *Tatsuo SHIMAMURA*
Journ. Inst. Electr. Comm. Engr. Japan, **43,** 8, pp. 894–900, Aug., 1960

The data necessary for the design of the driving system of a telephone receiver are obtained through systematic experiments on the concentric type magnetic circuit. A practical procedure for the design of a telephone receiver is described.

U.D.C. 621.395.636.1:621.552

Some Considerations on the Governor for Telephone Dials
Tetsuo KUDO
Journ. Inst. Electr. Comm. Engr. Japan, **43,** 7, pp. 800–806, Aug., 1960

A fly-bar type telephone-dial governor is preferable to a drive-bar type governor from the standpoints of low manufacturing cost and stable regulation. Several conditions of restraint occuring in the design of the governor are also discussed.

* * * *

Vol. 8 Nos. 9–10 SEPTEMBER–OCTOBER 1960

CONTENTS

The Analysis of Frame Vibrating Systems 397
Motonobu YONEKAWA

On Fundamental Qualities of Vowel Sounds in Speech Communication 410
Yosiyuki OCHIAI and *Teruo FUKUMURA*

Circular Electric Wave Transmission through Hybrid-Mode Waveguide........... 426
Ken-ichi NODA

Mode Exciters in Circular Waveguides 465
Ken-ichi NODA

The Design of a New Telephone Receiver 477
Kenrô MASUZAWA and *Kiyoshi TAJIMA*

Papers Contributed to Scientific and Technical Journals
by the Members of the Laboratory 487

Copyright 1960 by the Electrical Communication Laboratory, NTT